

Langevin simulation of the full QCD hadron mass spectrum on a lattice

M. Fukugita

Research Institute for Fundamental Physics, Kyoto University, Kyoto, 606 Japan

Y. Oyanagi

Institute for Information Sciences, University of Tsukuba, Ibaraki, 305 Japan

A. Ukawa

Institute of Physics, University of Tsukuba, Ibaraki, 305 Japan

(Received 29 December 1986)

Langevin simulation of quantum chromodynamics (QCD) on a lattice is carried out fully taking into account the effect of the quark vacuum polarization. It is shown that the Langevin method works well for full QCD and that simulation on a large lattice is practically feasible. A careful study is made of systematic errors arising from a finite Langevin time-step size. The magnitude of the error is found to be significant for light quarks, but the well-controlled extrapolation allows a separation of the values at the vanishing time-step size. As another important ingredient for the feasibility of Langevin simulation the advantage of the matrix inversion algorithm of the preconditioned conjugate residual method is described, as compared with various other algorithms. The results of a hadron-mass-spectrum calculation on a $9^3 \times 18$ lattice at $\beta=5.5$ with the Wilson quark action having two flavors are presented. It is shown that the contribution of vacuum quark loops significantly modifies the hadron masses in lattice units, but that the dominant part can be absorbed into a shift of the gauge coupling constant at least for the ground-state hadrons. Some suggestion is also presented for the physical effect of vacuum quark loops for excited hadrons.

I. INTRODUCTION

One of the ultimate goals of numerical simulations of lattice quantum chromodynamics¹ is an explicit calculation of strong-interaction physical observables from first principles. A full incorporation of the quark-vacuum-polarization effect, however, necessitates evaluation of the quark determinant arising from the Gaussian integral over the quark field, which is an extremely time-consuming procedure. Because of this technical reason the hadron-spectrum calculations made so far have employed the quenched approximation² in which the dynamical quark loop effect is ignored without proper justification.

Recent developments in fast computer technology and significant progress made in the last few years in simulation techniques, however, have made it possible to attempt a full QCD simulation including the quark-vacuum-polarization effect and to examine the validity of the quenched approximation. The continuous progress being made in this direction leads us to hope that a full-scale calculation of hadron dynamics could become possible within the next few years.

The inclusion of dynamical quarks has of course been a major problem from the early periods of lattice QCD simulations and the proposals for this purpose are quite numerous.³⁻⁸ Among them the methods^{5,6} based on stochastic quantization⁹ of the system with the Langevin equation have recently gained popularity for two good reasons. In these methods the cost of including quark loops is reduced to solving a linear equation of the form $Dx = \xi$ with D the lattice Dirac operator once or twice per

update of the entire lattice. This is in contrast with the variants of the Metropolis method such as the pseudofermion algorithm^{10,3} which requires evaluation of the nonlocal quantity $\text{tr}(D^{-1}\delta D/\delta U)$ for each link update. (In this respect the Langevin procedure is similar to the microcanonical simulation.⁴) Another important advantage of the Langevin simulation is that the property of systematic errors is relatively well understood and the errors seem controllable. In fact the only source of the systematic bias in practical applications is the finiteness of the Langevin time step in solving the stochastic evolution equation and the magnitude of such biases can be examined theoretically with the aid of the Fokker-Planck equation. In the microcanonical method⁴ it is in general a difficult problem to control systematic biases that arise from the lack of sufficient coverage of the energy surface in a short time interval. In any case this method has to rely on the (unproven) ergodicity assumption for its validity. In order to remove this difficulty some authors⁷ devised a hybrid approach, where the stochastic noise is applied to the microcanonical system to ensure the ergodicity. In practical applications, however, the method is quite close to microcanonical simulation in its nature, and hence the issue of ergodicity still remains.¹¹ In the pseudofermion method³ the ratio of the quark determinant is approximated by the leading term in the variation of the gauge variables. In practical applications error also arises from the violation of the detailed balance caused by the fact that the pseudofermion variable is often not refreshed till all the gauge link variables are updated. A finite acceptance of the hitting may also be a source of systematic bias, especially

when the system is close to critical.¹²

The Langevin equation for the gauge system is extensively discussed in Ref. 9 and has been applied for numerical simulations.¹³ The extension to full QCD including quarks uses an effective action¹⁰ given by

$$S_{\text{eff}}(U, Y) = S_{\text{gauge}}(U) + Y^\dagger \frac{1}{D^\dagger(U)D(U)} Y,$$

with Y the pseudofermion variable.^{5,6} The derivation of the Langevin equation is then straightforward.

The numerical implementation of the Langevin equation requires a discretization of the fictitious time.¹⁴ Alternatively one may try to set up, from the start, a discrete-time stochastic process which simulates full QCD with the effective action given above. In either approach, the Langevin equation with a finite time step $\Delta\tau$ leads to a limiting distribution of the form

$$\rho_\infty = \exp[-S_{\text{eff}} + \Delta\tau S_1 + (\Delta\tau)^2 S_2 + \dots],$$

that differs from the desired form $\exp(-S_{\text{eff}})$ by the term $O(\Delta\tau)$. It may seem advantageous at first glance to remove the $O(\Delta\tau)$ term by some higher-order discretization of the Langevin equation. For the pure gauge system one can in fact do so by a second-order formalism,^{15,5,6} or by a redefinition of the gauge variables.⁶ In the presence of quarks one can still remove the term $O(\Delta\tau)$ for a certain discretization of the quark sector.⁵ We note, however, that the second-order discretization is not quite advantageous for light quarks. An analysis of the Fokker-Planck equation shows that the residual error in ρ_∞ from $\exp(-S_{\text{eff}})$ is of order $\Delta\tau/\lambda^2$ or $(\Delta\tau/\lambda^2)^2$ with λ the eigenvalue of the Dirac operator $\gamma_5 D$. At small quark masses, the minimum eigenvalue decreases and the ratio $\Delta\tau/\lambda^2$ may exceed unity. In such a case the long-distance modes that satisfy $\Delta\tau/\lambda^2 \gtrsim 1$ may be seriously distorted and the second-order formalism obviously does not improve the situation. (For the gauge sector the finite-time step suppresses ultraviolet modes. This seems to be practically harmless, because the ultraviolet modes shorter than the lattice spacing are irrelevant quantities on the lattice. This is why the second-order formalism works well for the pure gauge sector.³) Under these circumstances the best way to control the systematic error is to make simulations with the first-order formalism at several values of $\Delta\tau$ and carry out extrapolations in $\Delta\tau$ using the behavior of physical quantities $F = F_0 + \Delta\tau F_1$ expected at sufficiently small $\Delta\tau$.

Another issue concerning the systematic error is the dependence of their magnitude on the discretization schemes of the quark part of the Langevin equation. There is a continuous set of possibilities, and one extreme is naive discretization⁵ in which a simple white noise is added to Y at each time step. In the other extreme⁶ the Y variable is made proportional to the white noise and hence eliminated from the equations. All these schemes have errors of order $\Delta\tau/\lambda^2$ in the first-order formalism, and it is not *a priori* clear which scheme has less problems with systematic errors. After some trial runs we found that the latter method⁶ has smaller systematic errors for small quark masses and used it for our production runs.

A very important ingredient for the feasibility of the simulation is an efficient algorithm for solving the linear equation $Dx = \xi$, on which the bulk of computer time is spent. A standard solver for such equations is the conjugate-gradient (CG) algorithm.¹⁶ However, this algorithm is not fast enough for full QCD simulations, especially for light quarks, because the speed of convergence of the CG method is controlled by the minimum eigenvalues of D . A general strategy to alleviate this problem is the preconditioning of the equation which promotes the minimum eigenvalues. One such method is the Fourier acceleration technique.⁶ Our method is based on an incomplete LU decomposition¹⁷ making use of the γ -matrix structure of the Wilson quark action.¹⁸ For the solver we adopted the conjugate residual algorithm,¹⁹ a variant of the CG method. Further improvement was achieved by a trick similar to successive-over-relaxation- (SOR) type acceleration. Altogether an improvement factor of about 15 was attained in computer time over the standard CG method.

In addition to the technical problems discussed above there also appear some physical problems which are not encountered in the quenched simulation. The problem of the finite-size effect arising from fake quark loop contributions becomes much more severe in the presence of the dynamical quarks. This is not only due to the fact that quark loops render the gauge configurations more ordered and the lattice size effectively shrinks toward a light-quark mass, but also by the fact²⁰ characteristic of the Wilson quark action that the fake loop contribution continuously increases for any value of the coupling constant when the hopping parameter approaches the critical value. Therefore, for a given lattice size, a careful choice of the coupling parameter is necessary to avoid the fake loop effect even at the largest hopping parameter to be used in the simulation.

Another interesting physical problem is that excited states of hadrons are generally not stable in the presence of dynamical quarks and hence their propagators should be qualitatively modified by the continuum contributions. The extraction of hadron masses would not be a trivial problem in this situation. Unfortunately the efficiency of our algorithm is not quite enough to explore this interesting region and the quantitative study of the effects of decay will be left for future investigations.

In this paper we present a full account of our attempt at Langevin simulation of full QCD with the Wilson fermion, expounding on our earlier report already published elsewhere.²¹ The technical problem which arose in our attempt and various checks which have been carried out to ensure the reliability of the result are discussed in detail. We study the hadron spectrum^{22,23} for two quark flavors with the same hopping parameter. The gauge group is SU(3). We made a simulation with various sizes of lattice from $4^3 \times 8$ to $9^3 \times 18$. For production runs we employed a $9^3 \times 18$ lattice and chose the gauge coupling $\beta = 6/g^2 = 5.5$. Our lattice size $9^3 \times 18$ is probably not large enough to extract quantitative predictions for the hadron mass spectrum, especially for baryons. Nevertheless semiquantitative trends of the quark-vacuum-polarization effect are already apparent in our calculation.

The numerical calculation was carried out on HITAC S810/10 vector computer at KEK with the central memory of 128MB and the peak speed of 315Mflops.

In Sec. II we present the formulation of Langevin simulation and discuss the systematic errors characteristic of the formalisms. The method for solving the linear equation $Dx = \xi$ is given in this section with some additional discussions deferred to the Appendix. Our simulation is described in Sec. III. We discuss in detail the checks which we have made to ensure the reliability of the simulation. The result is presented in Sec. IV and its physical implication is discussed in Sec. V. Section VI is devoted to conclusions.

II. FORMALISM AND METHOD OF COMPUTATION

A. Langevin equation and systematic errors

The effective QCD action is given by

$$S_{\text{eff}}(U, Y) = S_{\text{gauge}}(U) + \sum Y_n^\dagger M^{-1}(U)_{nn'} Y_{n'}, \quad (1)$$

where U is the gauge link variable, $M(U)$ some lattice Dirac operator, and the complex scalar field Y_n denotes the pseudofermion variable on site n . In our present analysis we take the single-plaquette action for the gauge field

$$S_{\text{gauge}}(U) = -\frac{\beta}{6} \sum_p \text{tr}(U_p + U_p^\dagger). \quad (2)$$

The fermion determinant is generated by the Gaussian integral over the pseudofermion variable Y which is well defined if the operator M is positive Hermitian. This is ensured if one doubles the number of flavors and writes

$$M = D^\dagger D \quad (3)$$

with

$$D = 1 - K \sum [(1 - \gamma_\mu) U_l + (1 + \gamma_\mu) U_l^\dagger], \quad (4)$$

the Wilson quark action satisfying $\det D^\dagger = \det D$. The Langevin equation is given by

$$\begin{aligned} -iU_l(\tau)^{-1} \frac{d}{d\tau} U_l(\tau) &= -i \frac{\delta}{\delta U_l(\tau)} S_{\text{eff}}(U(\tau), Y(\tau)) \\ &+ \eta_l(\tau), \end{aligned} \quad (5)$$

$$\frac{d}{d\tau} Y_n(\tau) = -M^{-1}(U(\tau))_{nn'} Y_{n'}(\tau) + \xi_n(\tau), \quad (6)$$

where τ denotes the fictitious time and $\delta/\delta U_l(\tau)$ is the derivative over $\text{SU}(3)$. The white noise $\eta_l(\tau) = \eta_l^a t^a$ is $\text{SU}(3)$ -algebra valued with t^a , $a = 1-8$ the generators of $\text{SU}(3)$ ($\text{tr} t^a t^b = \delta^{ab}$) and $\xi_n = (\xi_n^\alpha)$ has Dirac index $\alpha = 1-4$ as well as color index $i = 1-3$. They are normalized as

$$\begin{aligned} \langle \eta_l^a(\tau) \eta_{l'}^b(\tau') \rangle &= 2\delta^{ab} \delta_{ll'} \delta(\tau - \tau'), \\ \langle \xi_n^{\alpha i}(\tau) \xi_{n'}^{\beta j}(\tau')^\dagger \rangle &= 2\delta^{\alpha\beta} \delta_{ij} \delta_{nn'} \delta(\tau - \tau'). \end{aligned} \quad (7)$$

Equations (5) and (6) may be discretized in steps of $\Delta\tau$ as

$$U(\tau_{n+1}) = U(\tau_n) e^{i\Delta\tau X^{(n)}}; \quad (8)$$

$$X^{(n)} = -i \frac{\delta}{\delta U(\tau_n)} S_{\text{eff}} + \Delta\tau^{-1/2} \eta^{(n)}, \quad (9)$$

$$\begin{aligned} Y(\tau_{n+1}) &= [1 - \Delta\tau B(U(\tau_n))] Y(\tau_n) \\ &+ \Delta\tau^{1/2} C(U(\tau_n)) \xi^{(n)}, \end{aligned}$$

where the indices referring to the site n or link l are suppressed, and $\eta^{(n)}$ and $\xi^{(n)}$ are the Gaussian noise of width 2. The functions B and C in Eq. (9) represent the freedom in discretizing the Langevin equation, and they are subject to the condition

$$BM + MB^\dagger - 2CC^\dagger = 0 \quad (10)$$

to ensure the correct distribution for the quark sector at $\Delta\tau \rightarrow 0$.

The simplest choice of B and C is

$$(A) \quad B = M^{-1}, \quad C = 1, \quad (11)$$

which corresponds to the naive discretization^{5,6} of the Langevin equation (6). Another extreme choice is

$$(B) \quad B = \Delta\tau^{-1}, \quad C = \Delta\tau^{-1/2} M^{1/2}, \quad (12)$$

proposed in Ref. 6. In this case Y does not evolve and is written directly in terms of the white noise. As a result the Langevin equations reduce to a single equation for the gauge variable with a bilinear noise term. We call the schemes (A) and (B) pseudofermionic and bilinear noise schemes, respectively.

The distribution of field variables generated by the Langevin equation satisfies the Fokker-Planck equation. Using a generic notation $\phi^{(n)}$ for field variables with n the time step and i the site and other indices, the distribution function $\rho^{(n)}(\phi)$ for the Langevin equation of the form

$$\phi_i^{(n+1)} = \phi_i^{(n)} + \Delta_i^{(n)}$$

satisfies

$$\begin{aligned} \rho^{(n+1)}(\phi) - \rho^{(n)}(\phi) &= \sum_{l=1}^{\infty} \sum_{i_1 \dots i_l} \frac{1}{l!} \partial_{i_1} \dots \partial_{i_l} \langle \Delta_{i_1} \dots \Delta_{i_l} \rangle \rho^{(n)}, \end{aligned} \quad (13)$$

where the angular brackets denote the average over the noise. Since the right-hand side is a power series in $\Delta\tau$, the limiting ($n \rightarrow \infty$) distribution ρ_∞ should behave with respect to $\Delta\tau$ as

$$\rho_\infty = \exp(-S_{\text{eff}} - \Delta\tau S_1 - \dots). \quad (14)$$

In the pseudofermion scheme the $O(\Delta\tau)$ deviation S_1 is local and the part depending on Y is given by

$$S_1 = -\frac{1}{4} Y^\dagger M^{-2}(U) Y + 2 \text{tr} M^{-1}(U). \quad (15)$$

Hence the magnitude of the $O(\Delta\tau)$ term^{21,24} relative to S_{eff} is $\Delta\tau/\lambda^2$ with λ the eigenvalue of the Hermitized Dirac operator $\gamma_5 D$. One can remove the S_1 term using a second-order Runge-Kutta formalism.⁵ An analysis of the Fokker-Planck equation (13) shows that the residual error is of order $(\Delta\tau/\lambda^2)^2$ relative to S_{eff} .

With the bilinear noise scheme it can easily be shown that the residual error is also $O(\Delta\tau/\lambda^2)$. The removal of

the $O(\Delta\tau)$ term is not straightforward. Particularly troublesome is the so-called nonintegrable term, which arises from the nontrivial contraction of the bilinear noise terms in (13) and cannot be integrated by a local function of fields. As was shown in Ref. 25 the removal of this term requires a modification of the gauge white noise in (8) of the form

$$\eta_l^a \rightarrow \eta_l^a + \Delta\tau H_{ll}^{ab} \eta_l^b \quad (16)$$

with

$$H_{ll}^{ab} = \frac{1}{8} \xi_1^\dagger D^{-1} \nabla_l^a D \xi_2 \xi_2^\dagger D^{-1} \nabla_l^b D \xi_1 + (a \leftrightarrow b), \quad (17)$$

where the white noise ξ_1 and ξ_2 are independent and $\nabla_l = \delta/\delta U_l$. One can easily check that the square of the second term on the right-hand side of (16), after averaging over ξ_1, ξ_2 , and η , is of order $(\Delta\tau/\lambda^2)^2 V$, where the lattice volume V arises from the sum over l' . For V reasonably large, unless one takes an unfeasibly small $\Delta\tau$, this term substantially widens the total width of the noise term (16) and hence effectively reduces the gauge coupling β in an uncontrollable manner. We have checked these points by trial runs on $4^3 \times 8$ lattice with $\Delta\tau=0.01$ at $\beta=5.0$. We found that the width of (16) is increased in some cases in excess of 50% and the Wilson loops decreased by 15–40%. The second-order formalism therefore does not work in practice.

The integrable local terms of $O(\Delta\tau)$ in the bilinear noise scheme can be removed by a second-order Runge-Kutta algorithm, which was originally devised for the pure gauge sector,⁵ without introducing the problem discussed. Since the integrable terms give rise to a significant systematic deviation even in the pure gauge sector and hence also at a small value of K (see below), it is worthwhile to remove at least these terms. The partial second-order formalism for N_f dynamical quark flavors is given by

$$U^{(n+1/2)} = U^{(n)} e^{iX_0}, \quad (18)$$

$$X_0 = -i\Delta\tau [\nabla S_{\text{gauge}}(U^{(n)}) - N_f \nabla \xi_1^\dagger \ln D(U^{(n)}) \xi_1] + \Delta\tau^{1/2} \eta,$$

$$U^{(n+1)} = U^{(n)} e^{i(\beta X_0 + \gamma X_1)},$$

$$X_1 = -i\Delta\tau [\nabla S_{\text{gauge}}(U^{(n+1/2)}) - N_f \nabla \xi_2^\dagger \ln D(U^{(n+1/2)}) \xi_2] + \Delta\tau^{1/2} \eta,$$

where the independent white noises ξ_1, ξ_2 , and $\eta = \eta^a t^a$ are normalized as

$$\langle \xi_1 \xi_1^\dagger \rangle = \langle \xi_2 \xi_2^\dagger \rangle = 2, \quad (19)$$

$$\langle \eta^a \eta^b \rangle = 2\delta^{ab} \left[1 - \frac{\Delta\tau}{2} c_2 \right], \quad (20)$$

and

$$\beta = \frac{1}{2} + \Delta\tau\beta_1, \quad \gamma = \frac{1}{2} + \Delta\tau\gamma_1, \quad (21)$$

where $\beta_1 + \gamma_1 = c_2/6$ with $c_2 = N$ the quadratic Casimir eigenvalue for $SU(N)$. (In our calculations we used $\beta_1 = \gamma_1 = c_2/12$.) The systematic error of this scheme is still of order $\Delta\tau$ due to the nonintegrable terms.

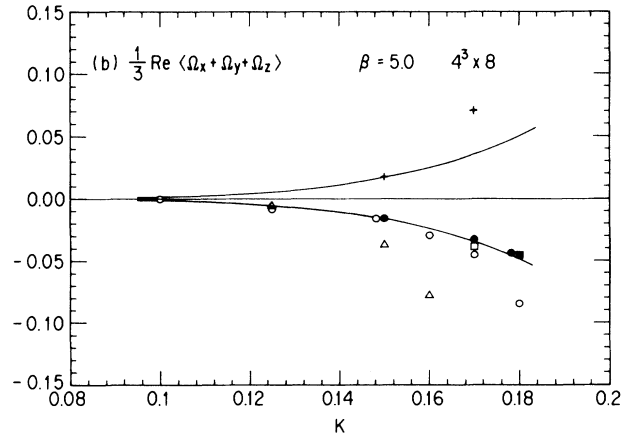
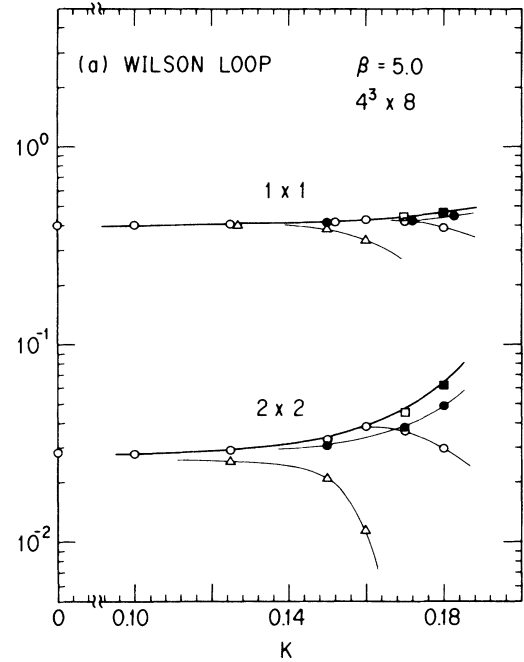


FIG. 1. Comparison of various Langevin schemes. Test runs are made at $\beta=5.0$ on a $4^3 \times 8$ lattice with $N_f=2$. About $3 \times 10^3 - 10 \times 10^3$ sweeps are made at each parameter set. (a) Wilson loop of the size 1×1 and 2×2 as a function of K . Solid points denote the bilinear noise scheme in a partial second-order formalism with $\Delta\tau=10^{-2}$ (circle) and $\Delta\tau=10^{-3}$ (square). Open points are for the second-order pseudofermion noise scheme with $\Delta\tau=10^{-2}$ (circle), $\Delta\tau=5 \times 10^{-2}$ (triangle), and $\Delta\tau=10^{-3}$ (square). The periodic boundary condition is imposed. The thick curve represents the Wilson loop expected for $\Delta\tau=0$. (b) Polyakov line averaged over the three spatial directions. The meaning of the symbols are the same as in (a) except for crosses which denote runs with pseudofermion scheme ($\Delta\tau=10^{-2}$) with the antiperiodic boundary condition. Curves are drawn to indicate the contribution by genuine finite-size effects.

The numerical implementation of the above formalism is straightforward, including vectorization of the code. The exponentiation of a 3×3 traceless Hermitian matrix $X \rightarrow e^{iX}$ was done with the analytic expressions for the eigenvalues and eigenvectors provided by the Cardano formula.

It is not *a priori* clear which fermionic scheme results in a smaller error for a given $\Delta\tau$. We then have made test runs with various schemes on a $4^3 \times 8$ lattice changing the values of $\Delta\tau$ and K ($\beta=5.0$). Figure 1(a) compares the Wilson loop obtained from the second-order pseudofermion scheme and the bilinear noise scheme in the partial second-order formalism. The solid curves represent the expected value with $\Delta\tau=0$. The deviation due to finite $\Delta\tau$ is apparent. It is more serious with the pseudofermion scheme than with the bilinear noise scheme; the Wilson loop with the former bends down for large values of K . On the other hand, the Wilson loop at least continues to increase with the bilinear noise scheme, though the deviation at our largest K is sizable with $\Delta\tau=0.01$. From several additional runs on $8^3 \times 16$ lattice we found that these trends are independent of the lattice size. In Fig. 1(b) we have shown the real part of the Polyakov line $\langle \Omega_\mu \rangle = \frac{1}{3} \text{tr}(\prod U_{n\mu})$ averaged over its transverse directions. It is apparent that the systematic bias in the pseudofermion scheme increases the value of the Polyakov line beyond the genuine finite-size effect represented by the solid curve. (We confirmed that the latter disappears on a $8^3 \times 16$ lattice.) This fake loop contribution leads to a significant difference in hadron propagators between different boundary conditions.

If one adopts the first order, instead of the partial second order, in the bilinear noise formalism there appears a significant systematic deviation even at small values of K , as is expected from the analysis for the pure gauge system.⁵ Based on the considerations given above we take the partial second-order bilinear noise scheme for our production runs.

B. Incomplete LU conjugate residual (ILUCR) method

The most time-consuming procedure in our simulation is the solution of $Dx=\xi$, which has to be carried out twice per gauge update. A standard procedure is to use iterative methods such as the conjugate gradient (CG), Gauss-Seidel, or successive-over-relaxation (SOR) methods. The last two algorithms, however, fail to converge when the hopping parameter is nearly critical. Therefore the CG method has been regarded as suitable. We used the ILUCR method in our simulation, which is a variant of CG improved by a preconditioning. The detailed description of the algorithm is given in Ref. 18, and here we only sketch the outline. The same algorithm is also used when we calculate quark propagators on a given gauge configuration. A comparison of various algorithms applied to our problem is discussed in the Appendix.

Let us consider an equation of the form

$$Dx = \xi . \quad (22)$$

We first make an incomplete block LU decomposition,

$$D = LU - R , \quad (23)$$

where L (U) is a lower (upper) triangular matrix in the lexicographic ordering of the site index i and R represents the error of the decomposition. For the Wilson fermion $D_{ii}=I$ (unit matrix with respect to Dirac and color indices) and D_{ij} ($i \neq j$) is nonvanishing only if i and j are adjacent. We now show that the triangular separation of D

$$\begin{aligned} L_{ij} &= D_{ij} \quad (i \geq j) , \\ U_{ij} &= D_{ij} \quad (i \leq j) , \end{aligned} \quad (24)$$

provides a desired incomplete LU decomposition. For an adjacent (i, j) pair with $i < j$, the relation

$$(LU)_{ij} = \sum_{k=1}^{i-1} L_{ik} U_{kj} + L_{ii} U_{ij} = D_{ij}$$

holds since three different sites (i, j, k) cannot be mutually adjacent at the same time. In a similar manner we have, for adjacent pair (i, j) with $i > j$,

$$(LU)_{ij} = D_{ij} .$$

For diagonal blocks

$$(LU)_{ii} = \sum_{k=1}^{i-1} L_{ik} U_{ki} + I = I ,$$

where the sum over k vanishes due to the projection operator $(1 \pm \gamma_\mu)$ in the Wilson fermion. The error R_{ij} has nonvanishing elements of $O(K^2)$ for next-nearest-neighbor pairs (i, j) .

Using this decomposition as a preconditioner we solve

$$(LU)^{-1} Dx = (LU)^{-1} \xi \quad (25)$$

instead of (22). The matrix $(LU)^{-1}D$ is close to diagonal and a rapid convergence of iterative solvers is ensured.

For the solver we adopted the conjugate residual (CR) algorithm,¹⁹ a variant of the CG method. In this algorithm the norm of the residual vector $\|Dx - \xi\|$ is minimized over the affine space $x_v + \langle p_v, p_{v-1}, \dots, p_{v-k} \rangle$ with p_v an appropriately chosen trial direction vector in the v th iteration. The algorithm consists of iterative steps starting with

$$r = Dx, \quad p = r , \quad (26)$$

and repeating

$$\begin{aligned} \alpha &= (r, Dp) / (Dp, Dp) , \\ x &= x + \alpha p , \\ r &= r - Dp, \quad \text{update } p , \end{aligned} \quad (27)$$

till convergence is achieved, where α is so determined as to minimize the norm of the new residual $\|r - \alpha Dp\|$. In principle the new p can be chosen to be fully orthogonal to all the previous p 's with respect to $D^\dagger D$ so that the algorithm gives the exact solution in finite steps, but here we choose p to be orthogonal to only the last k (≥ 0) direction vectors to save computer memory, viz.,

$$p_v = r_v + \beta_1 p_{v-1} + \dots + \beta_k p_{v-k} \quad (28)$$

with

$$\beta_j = -(Dr_v, Dp_{v-j}) / (Dp_{v-j}, Dp_{v-j}) \quad (29)$$

($j = 1, 2, \dots, k$).

The convergence of this algorithm is ensured if the Hermitian part of D is positive definite.²⁶

As can easily be seen in (29), the CR algorithm needs only one multiplication Dr , rather than two in the CG method for $D^\dagger D$. Therefore, if the number of iterations necessary for the required accuracy is the same for both methods, the CR method may give the computer time gain by a factor of 2.

We found that the convergence rate can be increased further by an SOR-type acceleration. This is a trick of replacing the hopping parameter K in the LU decomposition with cK with c chosen appropriately. (Since the preconditioner is in principle arbitrary, the hopping parameter in the LU decomposition need not be equal to K .) This acceleration can be considered as approximating cD by LU . The residual $R = LU - cD$ now has nonzero diagonal entries

$$R_{ii} = -(c - 1)I$$

as well as

$$R_{ij} = c^2 K^2 (1 - \gamma_\mu)(1 + \gamma_\nu) U_{i,\mu} U_{i+\hat{\mu},\nu}^\dagger$$

for next-nearest-neighbor sites i and $j = i + \hat{\mu} - \hat{\nu}$. When the gauge field U as well as the solution vector x are nearly aligned, the effect of those two errors tend to cancel with each other so that $(LU)^{-1}D$ is closer to a constant multiple of I .

We present in Fig. 2 a comparison of the convergence

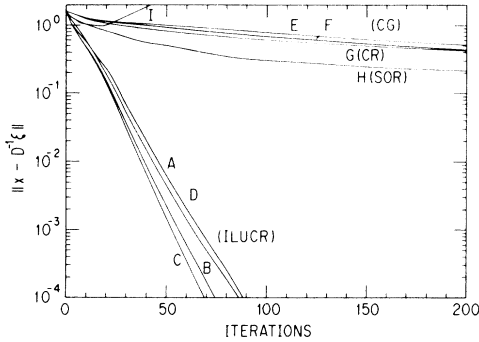


FIG. 2. Convergence of the iteration procedure with various matrix inversion algorithms. Comparison is made of the behavior of the deviation from the true solution as a function of the number of iterations. The gauge configuration is taken from a quenched simulation on $9^3 \times 18$ lattice with $\beta = 5.5$ ($K_c = 0.1844$) and the hopping parameter is chosen to be $K = 0.18$. The right-hand side ξ is a point source and the starting value x_0 is set equal to ξ . The symbols denote A–D: ILUCR (A: $c = 1.0$; B: $c = 1.1$; C: $c = 1.2$; D: $c = 1.3$). E and F: CG [E: least-square (LS) type; F: least-norm (LN) type]. G: CR. H and I: SOR [H: $\omega = 0.7$; I: $\omega = 1.0$ (Gauss-Seidel)]. For more explanations see the Appendix. The behavior of convergence with more iterations is shown in Fig. 27.

of various methods (see also Fig. 27 in the Appendix). This is an example with a point source $\xi_i = \delta_{i0}$ on a $9^3 \times 18$ lattice for a quenched gauge configuration with $\beta = 5.5$ and $K = 0.18$. (The number of elements in x is 157461.) The critical hopping parameter is $K_c = 0.1844$ and $m_\pi a \simeq 0.47$ at $K = 0.18$. The advantage of the preconditioning is apparent. The preconditioned conjugate residual (ILUCR) converges about 15 times faster than the standard CG or CR methods. The convergence of the latter is slow in the beginning and becomes faster at several hundred iterations when the correct direction vector is found by the solver (see Fig. 27 in the Appendix). In Fig. 2 one can also see a merit of the SOR-type acceleration; an extra 30% improvement was achieved with $c = 1.2$. We found that this acceleration is particularly efficient for the “bad” gauge configurations for which one needs a large number of iterations for convergence. We used the value $c = 1.2$ for our production runs.

C. Hadron propagators

To obtain hadron propagators, we first find the quark propagator $G_{nn'}$ on a given gauge configuration by solving

$$D_{nm} G_{mn'} = \delta_{nn'} \quad (30)$$

with the ILUCR method imposing the periodic or antiperiodic boundary condition. The quark propagators thus obtained are combined in a way appropriate for correlations of hadron operators $O_\pi = \bar{u}\gamma_5 d$, $O_\rho = \bar{u}\gamma d$, $O_S = \bar{u}d$, $O_A = \bar{u}\gamma\gamma_5 d$, $O_N = (\bar{u}C\gamma_5 d)u$, and $O_\Delta = (\bar{u}C\gamma u)u$. Here the summation over the color and Dirac indices, and also the color antisymmetrization for baryons with the factor $1/3!$ are understood implicitly. The average over the ensemble of gauge configurations then gives the hadron propagators

$$\begin{aligned} G_H(n, n') &= \frac{1}{Z} \int [dU] [dq d\bar{q}] O_H(n) O_H^\dagger(n') e^{-S_{\text{gauge}} - \bar{q}D(U)q} \\ &= \frac{1}{Z} \int [dU] \langle O_H(n) O_H^\dagger(n') \rangle_q \det D(U) e^{-S_{\text{gauge}}} \end{aligned} \quad (31)$$

with O_H ($H = \pi, \rho, S, A, N, \Delta$) the hadron operator defined above. The Green’s functions for the scalar- and axial-vector-meson propagators vanish in the nonrelativistic limit, for they pick up the interference between the large and small Dirac components. (A nonlocal operator is necessary to obtain a Green’s function nonvanishing in this limit.) All other Green’s functions have a nonvanishing nonrelativistic limit. To extract masses we project out the zero-momentum states by the summation over the spatial sites:

$$G_H(t) = \sum_{\mathbf{n}} G_H(\mathbf{n}, t, (0, 0)) \quad (32)$$

For baryons we use the positive-energy components projected out by $(1 + \gamma_0)/2$.

In the presence of dynamical quarks excited states of

hadrons are generally not stable and the hadron propagator should behave as

$$G_H(t) \simeq \sum_{m_i < m_0} e^{-m_i t} + \int_{m_0}^{\infty} dm \sigma_H(m) e^{-m t} \\ + (\text{contributions from } t \rightarrow N_t - t). \quad (33)$$

In the region of the hopping parameter that we could explore in our simulation, however, we always find $m_\rho < 2m_\pi$ and $m_\Delta < m_N + m_\pi$. We therefore have ignored the continuum contribution when extracting hadron masses.

The chiral order parameters $\langle \bar{\psi}\psi \rangle$ and $\langle \bar{\psi}\gamma_5\psi \rangle$ were calculated from the expectation values of $\text{tr}G_{nn}$ and $\text{tr}(G_{nn}\gamma_5)$. One can of course use the explicit evaluation of $G_{nn'}$ made for hadron propagators. An alternative is to use the relation

$$\frac{1}{V} \sum_{n,n'} \xi_n^\dagger D^{-1}_{nn'} \xi_{n'} = 2 \text{tr} D^{-1} \quad (34)$$

valid for large V and recall that $D^{-1}\xi$ is calculated at each Langevin update. We confirmed that the results of the two calculations agree very well.

The latter method can also be used for hadron propagators except for the wrong relative sign (“Bose” statistics) of contractions. The fluctuations, however, are large in actual simulations.

III. SIMULATION

A. Choice of parameters

We employed a lattice of size $9^3 \times 18$ with the periodic boundary condition for both gauge and quark variables. We have also made some runs with the antiperiodic boundary condition in the spatial directions imposed for the quark variables to check the finite-size effect. We study the case of two flavors $N_f=2$ with the same hopping parameter K [see Eq. (3)]. The bulk of our calculation is made at $\beta=6/g^2=5.5$. This value is above the near transition²⁷ of the pure gauge system. We generated gauge configurations at five values of the hopping parameters: $K=0.14, 0.15, 0.155, 0.16$, and 0.162 . (At the largest hopping parameter $K=0.162$, $m_\pi a \simeq 0.43$, and $m_\rho/m_\pi \simeq 1.5$.)

The Langevin time step is chosen to be $\Delta\tau=0.01, 0.02$, and 0.005 . The starting configurations were generated by making matrix Gaussian random numbers $\eta=\eta^a t^a$ of appropriate width and exponentiating them to obtain the gauge link variables $U=e^{i\eta}$. We made 5000 iterations at each K with $\Delta\tau=0.01$ ($\tau=0-50$), followed by 1500 and 6000 iterations with $\Delta\tau=0.02$ and 0.005 ($\tau=50-80$), respectively, starting from the last configurations of the $\Delta\tau=0.01$ runs. [For $K=0.16$, we made an additional 1000 sweeps with $\Delta\tau=0.01$ ($\tau=50-60$) for checks of thermalization and round-off errors.] The Wilson loop $W(L \times L)$ and the Polyakov line $\langle \Omega_\mu \rangle$ ($\mu=1-4$) are calculated at every $\delta\tau=0.5$ and $\delta\tau=0.05$, respectively, and the hadronic quantities at every $\delta\tau=1$. The thermalization is checked by inspecting both Wilson loops and had-

ron propagators. We see in Fig. 3 that about 1500 iterations are sufficient for equilibration when started with our initial configuration and discarded the initial 2000 iterations. As a further check, averages of physical quantities over the interval $\delta\tau=10$ were calculated to detect a systematic drift with long periods and we did not find any such drift. For successive runs with $\Delta\tau=0.02$ and 0.005 similar analyses led us to discard the first one-third of sweeps. We have analyzed then 30–20 configurations per parameter set as summarized in Table I.

We also made 5000–6000 Langevin sweeps with $\Delta\tau=0.01$ using the pure gauge action at $\beta=5.5$ and at some other required β 's (see Sec. V) to compare the result of full QCD with the quenched case (see Table I). Some physical quantities calculated on these gauge configurations are compared with those on the gauge configurations generated by the standard Monte Carlo procedure to confirm the absence of systematic biases in the Langevin results.

Simulations are also made at $\beta=4.0$ and 5.0 on a smaller lattice $6^3 \times 12$ to study the behavior of the critical hopping parameter $K_c(\beta)$ for $N_f=2$ and 4 .

Throughout our work the whole calculations are made with the 64-bit precision, including storage of the gauge configurations, to avoid round-off errors. With the purpose to extend our calculation to a larger lattice we have

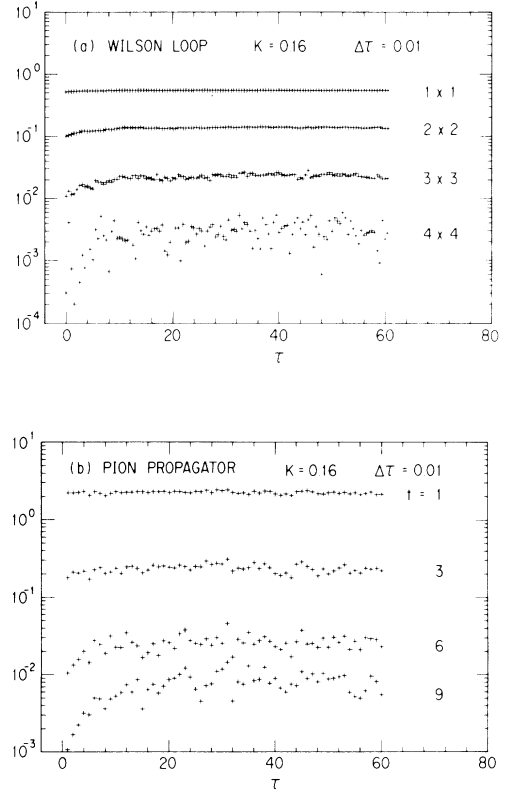


FIG. 3. Thermalization of the Wilson loop (a) and the pion propagator (b) at $K=0.160$ with $\Delta\tau=0.01$. (τ is the Langevin time.) In our simulation average is taken from $\tau=20$ for physical quantities.

TABLE I. Number of gauge configurations analyzed in our Langevin simulation at $\beta=5.5$. The numbers in parentheses are the range of τ where configurations are collected. In the last column, p (ap) stands for the periodic (antiperiodic) boundary condition imposed on the quark field in the spatial directions. The runs with $\Delta\tau=0.02, 0.005$, and those with the antiperiodic boundary condition are started from the configurations at $\tau=50$ of the $\Delta\tau=0.01$ (p) runs.

		(a) Full QCD			
		$\Delta\tau=0.01$	$\Delta\tau=0.02$	$\Delta\tau=0.005$	BC
$K=0.14$	30 ($\tau=20-50$)	20 ($\tau=60-80$)	20 ($\tau=60-80$)	20 ($\tau=60-80$)	p
$K=0.15$	30 ($\tau=20-50$)	20 ($\tau=60-80$)	20 ($\tau=60-80$)	20 ($\tau=60-80$)	p
$K=0.155$	30 ($\tau=20-50$)				p
$K=0.16$	40 ($\tau=20-60$)	20 ($\tau=60-80$)	20 ($\tau=60-80$)	20 ($\tau=60-80$)	p
$K=0.16$	20 ($\tau=60-80$)				ap
$K=0.162$	30 ($\tau=20-50$)				p

		(b) Quenched (QCD)				
β	5.5	5.62	5.65	5.73	5.75	5.79
	40	30	30	20	30	30
	($\tau=20-60$)	($\tau=20-50$)	($\tau=20-50$)	($\tau=10-30$)	($\tau=20-50$)	($\tau=20-50$)

examined the accuracy when the 32-bit precision is used for the storage. (Floating point vector operations always use the 64-bit arithmetic in HITAC S810/10.) We found that it is crucial to make reunitarization of the gauge link matrices in the course of Langevin sweeps; if the reunitarization is made, say, at every 25 sweeps, no systematic deviation is seen for physical quantities. For example, in the 32- and 64-bit test runs at $\beta=5.5$, $K=0.16$ with $\Delta\tau=0.01$, both runs starting from the same configuration at $\tau=50$, $\beta=5.5$, $K=0.16$, and extended over 1000 sweeps, the change of Wilson loop averages and hadron masses are smaller than the statistical error by a factor of 10–50.

B. Pseudorandom-number generation

The Langevin simulation uses a fixed number N_R of random numbers at each time step, e.g., $N_R=80$ times the lattice volume for the partial second-order bilinear noise scheme. Hence this method might be quite sensitive to the (quasi)periods of the random-number sequence generated by a recursive algorithm. For our simulation we used the multiplicative congruence method based on $x_{n+1}=5^{11}x_n \pmod{2^{31}}$. In order to avoid the influence of a relatively short quasiperiod 2^{14} (generally $2^{[(m-3)/2]}$ for modulus 2^m) characteristic of this algorithm, we generated several random numbers in addition to those needed per sweep and discarded them. We have checked the reliability of this procedure by comparing Wilson loops in the pure gauge sector with those from the standard Monte Carlo simulations. We also made runs with the pseudorandom numbers generated by the M sequence²⁸ based on the primitive polynomial $x^{607}+x^{273}+1$ whose period is $2^{607}-1$. We found good agreement among the three runs when the above procedure was used for the multiplicative congruence method, whereas the result of runs without it did not agree at all.

In order to convert the uniform random numbers to the Gaussian noise, we used the Box-Muller method²⁹ since it is bias-free and can be easily vectorized.

C. Convergence of ILUCR

We adopted the version ILUCR ($k=1$) with $c=1.2$. The convergence is monitored by the norm of the residual vector $\|r\|=\|Dx-\xi\|$. In Figs. 4(a) and 4(b) we show an example of the convergence of ILUCR in our gauge sweeps at $\beta=5.5$ and $K=0.16$ in the $\Delta\tau=0.01$ run. The convergence is quite smooth, and any desired accuracy can be attained by continuing the iteration till an appropriate residual norm is realized.

In the production runs we made the iteration until $\|Dx-\xi\|\leq 1.0$ which corresponds to 1% accuracy in each element of the vector x . We have confirmed that a more severe stopping condition on the residual norm does not modify hadron propagators beyond statistics. We show in Table II an approximate number of iterations N_{CR} necessary to satisfy the condition $\|Dx-\xi\|\leq 1$.

TABLE II. Numbers of ILUCR iterations (N_{CR}) necessary to satisfy the requirement $\|Dx-\xi\|<1.0$, and numbers of gauge sweeps (N_G) per one CPU hour on HITAC S810/10. CPU time necessary for the evaluation of observables is not included.

K	N_{CR}	N_G (sweeps/h)
pure gauge		810
0.14	6	150
0.15	8	127
0.155	10	105
0.16	20	65
0.162	55	27

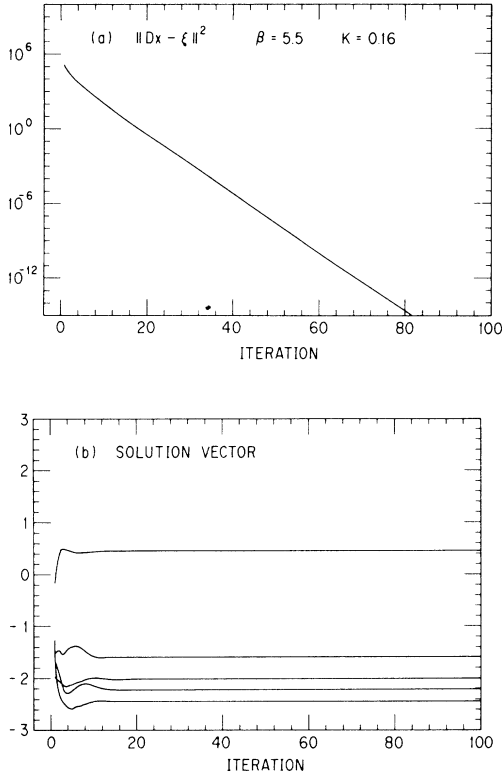


FIG. 4. Convergence of ILUCR in the gauge sweep ($K=0.16$, $\Delta\tau=0.01$) as a function of ILUCR iterations. (a) Residual norm vector squared $\|Dx - \xi\|^2$, (b) behavior of several elements of the solution vector.

[The numbers of iterations necessary for the two inversions in (18) are approximately the same.] If one defines the quark mass by $m_q = (1/2a)(K^{-1} - K_c^{-1})$, the number of iterations N_{CR} increases as

$$N_{CR} \sim m_q^{-\alpha}, \quad \alpha = 0.8 - 1.0, \quad (35)$$

for small m_q ($K \gtrsim 0.155$ or $m_q \lesssim 0.17a^{-1} \simeq 250$ MeV for the value $a^{-1} \simeq 1.6$ GeV found in our analysis). This m_q dependence agrees with the estimate given in Ref. 30. For a larger m_q the index becomes smaller ($\alpha \sim 0.3$).

Naturally we set a more severe condition $\|Dx - b\| \lesssim 10^{-5}$ when ILUCR is used to find the quark propagator with a point source b . This corresponds to 0.1% accuracy even for the small elements of x at sites far from the location of the point source.

On our $9^3 \times 18$ lattice a single ILUCR iteration with the ILU preconditioning vectorized by a hyperplane method^{31,18} takes 1.23 sec on HITAC S810/10. This may be compared with 0.66 sec for the standard CG and 0.39 sec for CR.

D. Eigenvalue analysis

It is important to know the magnitude of the minimum eigenvalue λ_{\min} of the Hermitized Dirac operator $\gamma_5 D$,

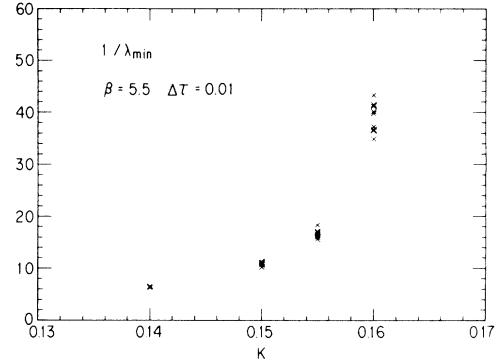


FIG. 5. Inverse minimum eigenvalues of the Dirac operator $\gamma_5 D$ as a function of the hopping parameter K on ten gauge configurations in the interval $\tau=40-50$ of the $\Delta\tau=0.01$ sweeps.

since $\Delta\tau/\lambda_{\min}^2$ controls the dominant part of the systematic error at large distance.

To estimate λ_{\min} we used a simpler power method and occasionally the Lanczos method.³² In Fig. 5 we show λ_{\min}^{-1} as a function of K with $\Delta\tau=0.01$. We see that $\Delta\tau/\lambda_{\min}^2 \gtrsim 1$ already at $K=0.155$, and hence expect some distortion of gauge configurations due to the finite $\Delta\tau$ beyond this value of K . Indeed this is clearly seen in Fig. 6, which exhibits λ_{\min}^{-1} as a function of $\Delta\tau$ at $K=0.15$ and $K=0.16$. For $K=0.15$, $1/\lambda_{\min}$ does not change appreciably when we decrease $\Delta\tau$. On the other hand, for $K=0.16$, $1/\lambda_{\min}$ increases rapidly toward a smaller value of $\Delta\tau$. This means that infrared modes, which have small eigenvalues $\lambda^2 \leq \Delta\tau$, become gradually fledged with decreasing $\Delta\tau$. We will observe in Sec. IV A that large-size Wilson loop suffers strongly from this suppression of the infrared modes.

E. Finite-size effect

Finite-size effects are divided into two classes. The first one concerns the gauge configurations and arises from

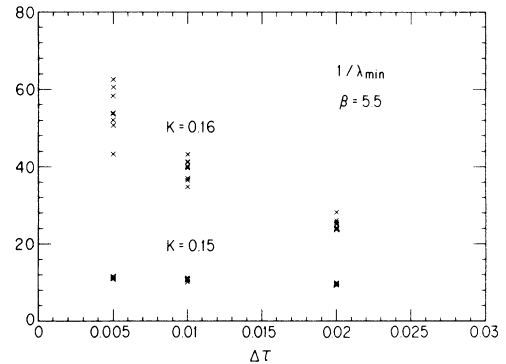


FIG. 6. Inverse minimum eigenvalues of the Dirac operator $\gamma_5 D$ at $K=0.15$ and $K=0.16$ as a function of the Langevin time step $\Delta\tau$.

fake dynamical quark loops wrapping around the lattice in spatial directions. A large contribution of such loops implies that the gauge field fluctuations more resemble those at finite temperature rather than those at zero temperature required for spectroscopic studies. This problem seems more severe with the Wilson fermion²⁰ and hence has to be checked carefully.

In our work two kinds of checks have been made. We examined whether the distribution of the Polyakov line in the spatial direction $\Omega_{x,y,z}$ accumulates around the origin on the complex plane. As seen in Figs. 7(a) and 7(c) no signature is observed for the deviation which signals the effect of fake loop contributions. A more precise and quantitative check is to measure physical quantities on the gauge configurations generated with the antiperiodic

boundary condition for quarks in the spatial directions.³³ The contribution of spatial fake loops changes sign [e.g., positive values of Ω are now favored as compared to negative for the periodic boundary condition as is easily seen from the hopping-parameter expansion, which gives an effective action for Ω of the form

$$\det D = \exp(-\gamma K^{L_s} \Omega + \dots)$$

with L_s the spatial lattice size and γ a positive constant for the periodic boundary condition; see Fig. 1(b) in this connection]. Hence the fake loop effect appears most clearly as the difference in physical quantities between the two boundary conditions. Since the gauge sweep is a time-consuming procedure, we generated the

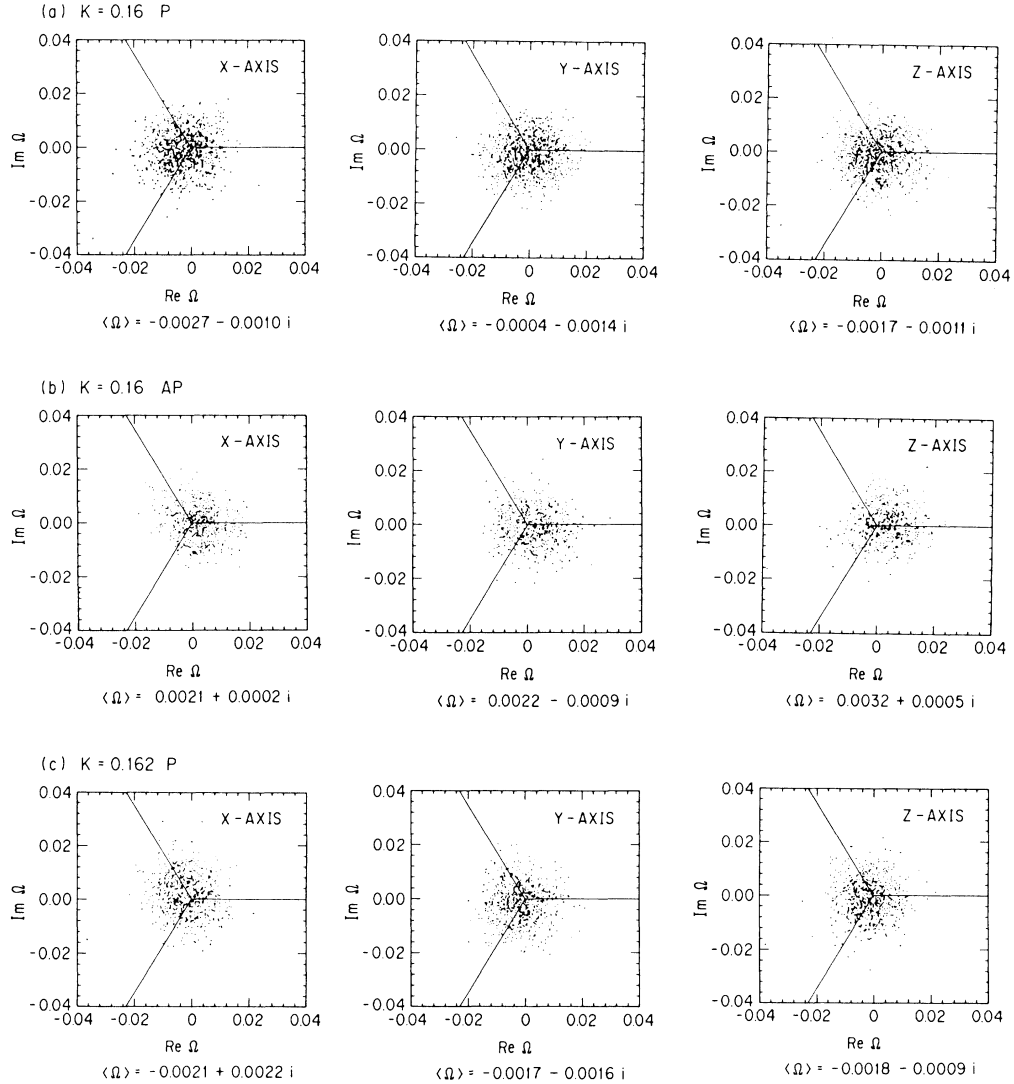


FIG. 7. Distribution of Polyakov lines in the spatial direction averaged over its transverse directions during the course of gauge sweeps ($\beta=5.5$, $\Delta\tau=0.01$, $9^3 \times 18$ lattice). (a) $K=0.16$ with the periodic boundary condition for quarks ($20 \leq \tau \leq 60$). (b) $K=0.16$ with the antiperiodic boundary condition ($60 \leq \tau \leq 80$). (c) $K=0.162$ with the periodic boundary condition ($20 \leq \tau \leq 50$).

configurations with the antiperiodic boundary condition only at $K=0.16$ with $\Delta\tau=0.01$. As shown in Table III the averages from the periodic and antiperiodic runs are consistent within statistical errors. We also plotted $\Omega_{x,y,z}$ for the antiperiodic run in Fig. 7(b).

The second kind of finite-size effect arises from the possibility that the spatial extent of the lattice is not large enough compared to the size of hadrons. Our analyses will show that the lattice spacing is $a=0.12\text{--}0.16$ fm in our simulation, and our spatial size of $L_s a/2=4.5a=0.54\text{--}0.68$ fm might not be large enough to contain hadrons inside the lattice. Such a finite-size effect can be checked by calculating the hadron propagators and masses with different spatial boundary conditions for quark propagators on a given gauge configuration. The difference arises from the process in which the trajectory of one of the quarks forming hadrons (but not two) wraps around the lattice in the spatial direction. A care should be made, however, with baryon propagators which receive nonzero-momentum contributions when the procedure (32) is applied to the case of antiperiodic boundary condition. For this case we pick out the state with the minimum momentum $p_{\min}=\pi/L_s$ by the weighted sum given by

$$G_H(t) = \sum_{\mathbf{n}} G_H((\mathbf{n}, t), (\mathbf{0}, 0)) \cos(n_x \cdot p_{\min}) \\ \times \cos(n_y \cdot p_{\min}) \cos(n_z \cdot p_{\min}) \quad (36)$$

instead of (32). The result will be given in Sec. IV when hadron propagators are presented.

TABLE III. Physical quantities obtained for the gauge sweep at $K=0.16$ with $\Delta\tau=0.01$ with the periodic and antiperiodic boundary conditions imposed on quarks in the spatial directions. The same boundary conditions are also used to solve hadron propagators.

	Periodic	Antiperiodic
$W(1\times 1)$	0.548 32 $\pm 0.000 51$	0.548 13 $\pm 0.000 87$
$W(2\times 2)$	0.137 74 $\pm 0.000 71$	0.137 94 $\pm 0.001 10$
$W(3\times 3)$	0.022 96 $\pm 0.000 40$	0.023 20 $\pm 0.000 72$
$W(4\times 4)$	0.003 14 $\pm 0.000 27$	0.002 98 $\pm 0.000 35$
m_π	0.631 ± 0.023	0.622 ± 0.036
m_ρ	0.767 ± 0.022	0.747 ± 0.045
m_N	1.256 ± 0.108	1.467 ± 0.170
m_Δ	1.348 ± 0.104	1.471 ± 0.165
$\langle \bar{\psi}\psi \rangle$	0.9158 ± 0.0030	0.9124 ± 0.0033

F. Error analysis

Consecutive gauge configurations generated in the Langevin sweeps are more strongly correlated than those in the conventional Monte Carlo procedure. In order to estimate statistical errors, it is important to know the correlation of physical quantities over the successive gauge configurations, and to estimate how many data samples can be regarded as statistically independent. For this purpose we have calculated the Langevin time autocorrelation $\omega(\tau)$ of measured quantity $f(\tau)$,

$$\omega(\tau) = \overline{\delta(\tau + \tau') \delta(\tau')} / \overline{\delta(\tau')^2}, \quad (37)$$

normalized as $\omega(0)=1$ with $\delta(\tau)=f(\tau)-\overline{f(\tau)}$. Some examples of ω for the Wilson loop and hadron propagator are depicted in Fig. 8. The correlation rapidly falls off with the Langevin time. Clearly the number of our data samples (20–30) are not sufficient to give a reliable estimate of the relaxation time. If we operationally define two successive data samples to be uncorrelated when the autocorrelation becomes smaller than 0.1, we estimate that the relaxation time τ_r is of the order of $\tau_r \sim 1\text{--}5$. This means that gauge configurations over the consecutive 100–500 sweeps are correlated for $\Delta\tau=0.01$.

The relaxation time, of course, depends on the coupling parameters and the length scale of measured physical quantities. The change observed in our parameter range, however, was rather mild, perhaps by a factor of 2. In view of the smallness of our data samples, we used $\tau_r=4$ throughout, rather than estimating τ_r for each $(\beta, K, \Delta\tau)$. The error quoted in this paper is given by $\sqrt{\sigma/N}$ with σ the standard deviation for the entire sample and $N=\tau/\tau_r$ with τ the interval used for the average and $\tau_r=4$.

IV. RESULT

A. Wilson loop

We show the Wilson loop in Figs. 9(a)–9(d) as a function of $\Delta\tau$. The average of the space- and timelike Wilson loop is taken here. The $\Delta\tau$ dependence is rather modest for $W(1\times 1)$ even at $K=0.16$ [Fig. 9(a)]. The extrapolation to $\Delta\tau=0$ modifies the value at $\Delta\tau=0.01$ only by 2% at $K=0.16$. On the other hand, for $W(4\times 4)$ the $\Delta\tau$ dependence is quite significant and the modification reaches almost a factor 2 [Fig. 9(d)]. This reflects the fact mentioned in Sec. III C that the infrared modes are strongly affected at large values of K for a finite $\Delta\tau$. Fortunately the dependence with respect to $\Delta\tau$ is almost linear over the range $\Delta\tau=0.005\text{--}0.02$ and the extrapolation procedure well applies to find the value at $\Delta\tau=0$. Figure 10 shows the Wilson loop extrapolated to $\Delta\tau=0$ as a function of K (see Ref. 34). The numerical values are presented more extensively in Table IV. Errors shown are statistical only.

B. Hadron propagators and masses

Examples of hadron propagators are shown in Fig. 11 at $K=0.16$. (Selected numerical data are tabulated in Table V.) As has been known in simulations for

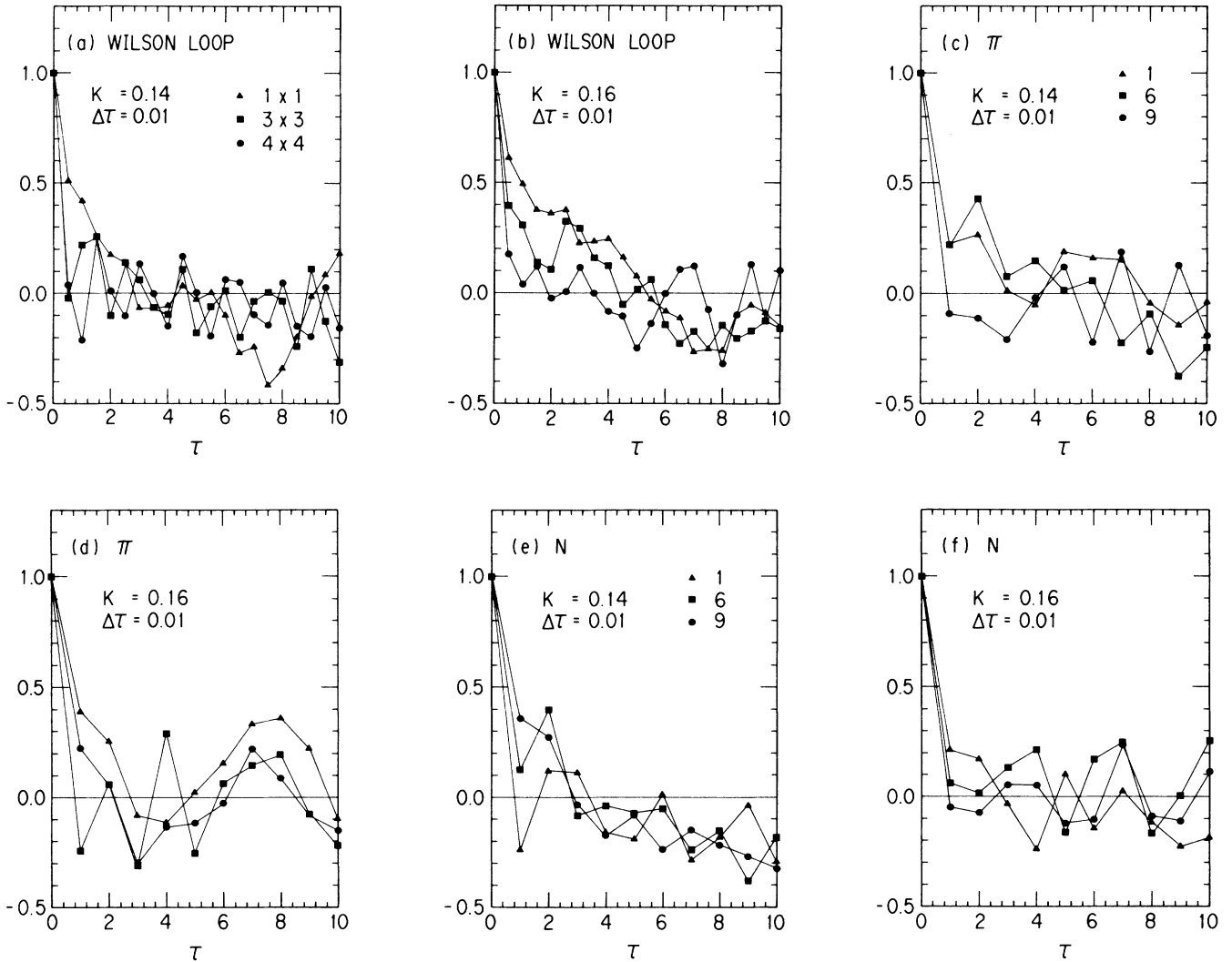


FIG. 8. Autocorrelation (37) of physical observables as a function of the relative time difference τ . (a), (b) Wilson loop for $K=0.14$ and $K=0.16$; (c), (d) pion propagator for $K=0.14$ and $K=0.16$; (e), (f) nucleon propagator for $K=0.14$ and $K=0.16$.

quenched QCD hadron masses, the hadron propagator with the Wilson action shows a concave curve for a small t and then starts to follow the exponential falloff. We have fitted the propagator data by a single hyperbolic cosine for mesons over the temporal separation $t=5-13$ and by a single exponential for baryons over $t=6-9$. We did not dare to fit the data by a more elaborate function such as two exponentials, because we feel that our temporal lattice size is not sufficient to separate excited hadron masses reliably. Therefore our mass data might contain some contamination from the excited states. Our procedure, however, should be enough for our purpose of finding the effects of quark vacuum polarization. We applied the same procedure of extracting masses in a consistent manner to both full QCD and the quenched data. The quality of the fit was generally excellent, and was equally good for full QCD and the quenched case.

Let us first discuss the spectrum of π , ρ , N , and Δ for

which the Green's functions have a nonrelativistic limit. We tabulated their masses in Table VI, where errors shown are purely statistical. (The errors arising from the fitting range in t and $\Delta\tau$ is within the statistical ones shown except for those for the $\Delta\tau$ extrapolation at $K=0.16$ for which the $\Delta\tau=0$ value is reduced by about one standard deviation.) These data are also exhibited in Figs. 12(a)–12(d) as a function of $\Delta\tau$. The linear dependence with respect to $\Delta\tau$ is clearly visible, and it validates a linear extrapolation to $\Delta\tau=0$. In Fig. 13 we plotted (a) m_π^2 , (b) m_ρ , (c) m_N , and (d) m_Δ as a function of $1/K$ at fixed values of $\Delta\tau$, together with the data given by the extrapolation to $\Delta\tau=0$. In the same figure we also presented values obtained in the quenched approximation at $\beta=5.5$ for comparison. The masses for ρ , N , and Δ at $\Delta\tau=0$ are recapitulated in Fig. 14. The contribution of vacuum quark loops is quite clear. It pushes down the hadron mass for lighter quark masses and hence shifts

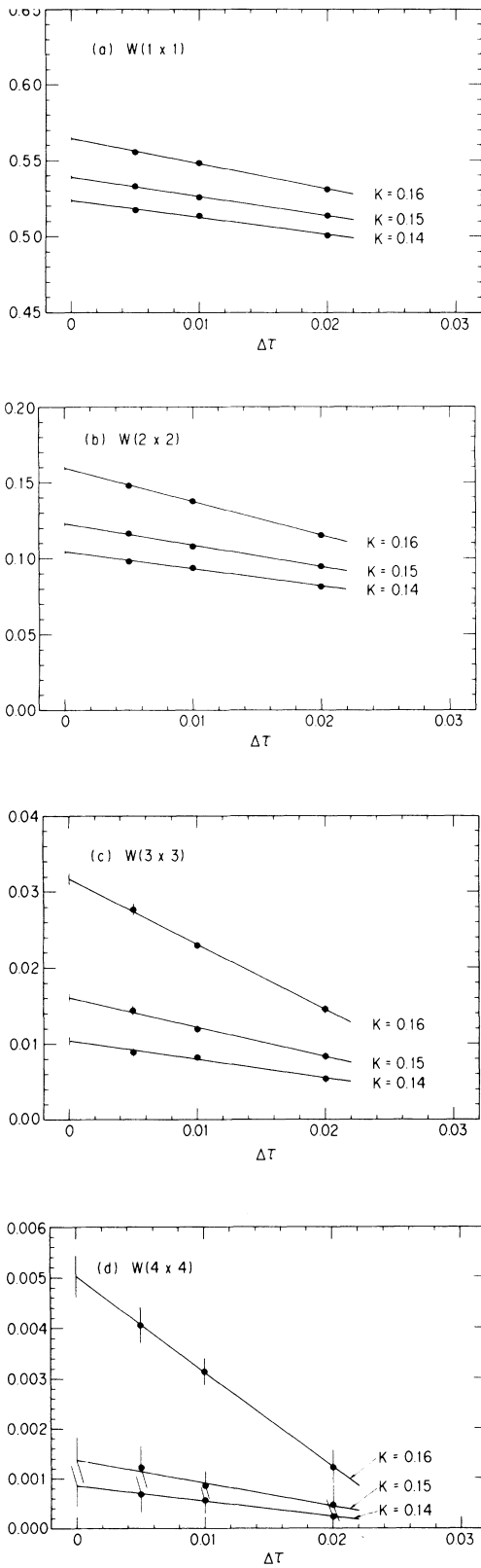


FIG. 9. Wilson loop for full QCD $W(L \times L)$ as a function of the Langevin time step $\Delta\tau$. Average of the spacelike and time-like Wilson loops is taken. Lines show the $\Delta\tau$ extrapolation.

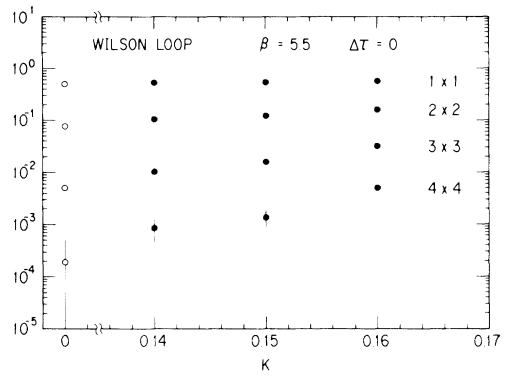


FIG. 10. Wilson loop as a function of K at $\Delta\tau=0$. Open circles at $K=0$ show the value for the pure gauge system.

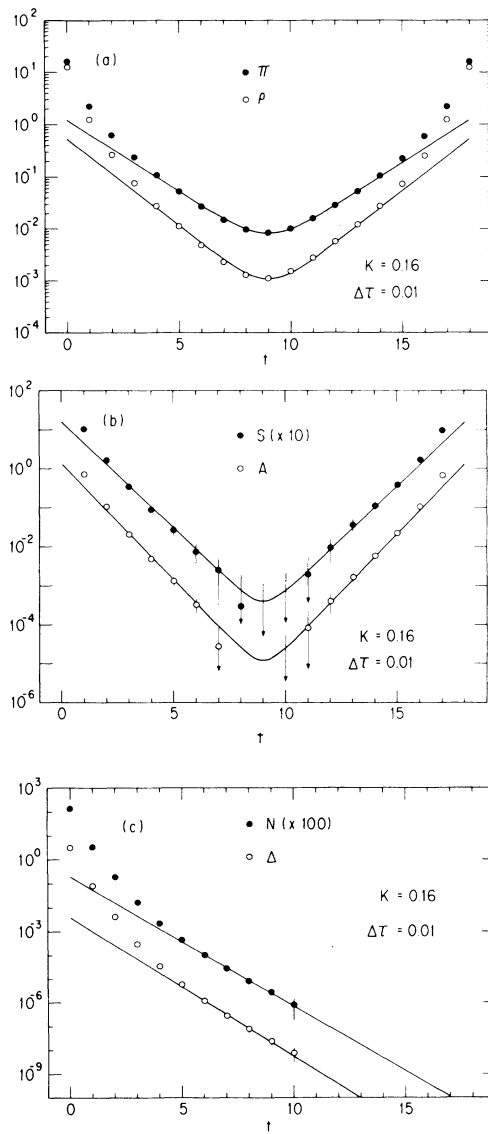


FIG. 11. Examples of hadron propagators ($K=0.16$, $\Delta\tau=0.01$). (a) π and ρ ; (b) scalar (S) and axial vector (A); (c) nucleon (N) and Δ . The scalar and nucleon propagators are scaled by a factor shown. Curves show the fit used in the text.

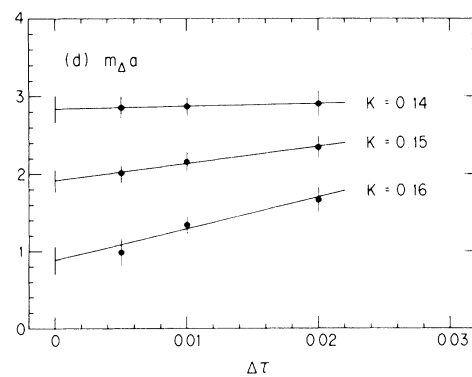
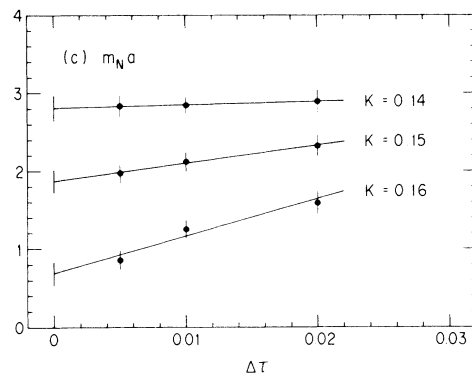
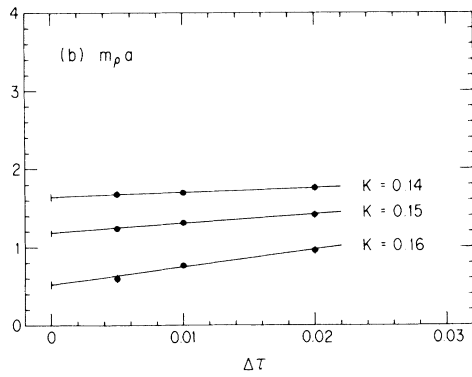
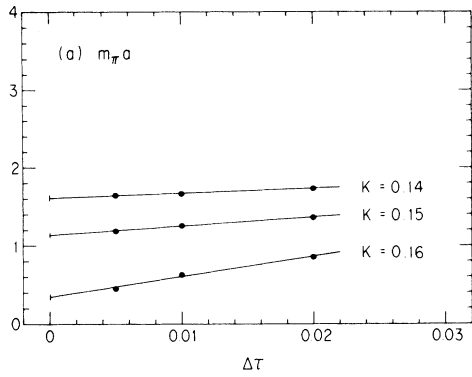


FIG. 12. Hadron masses as a function of $\Delta\tau$ with lines of extrapolation. (a) π ; (b) ρ ; (c) N ; (d) Δ . Propagator data for $t=5-13$ are used for mesons and $t=6-9$ for baryons.

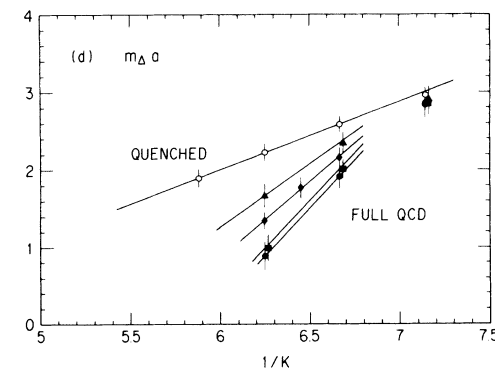
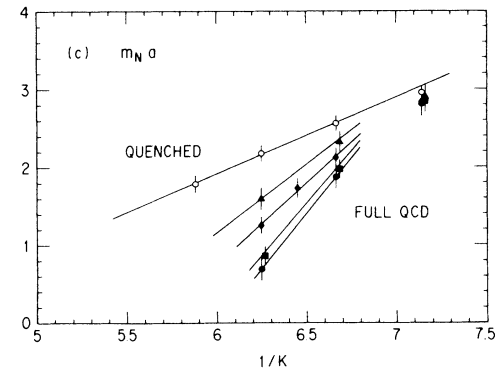
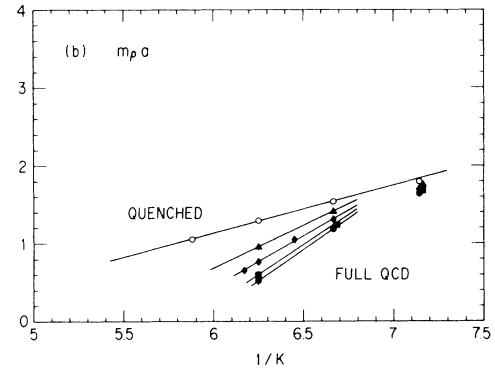
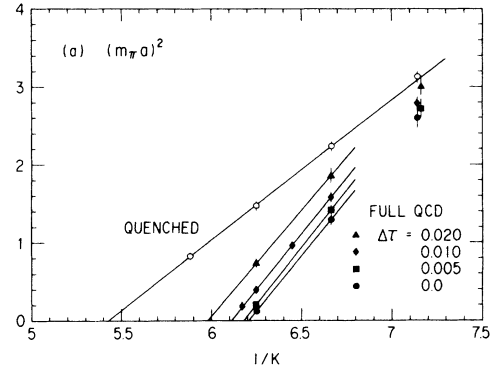


FIG. 13. Hadron masses (squared) for full QCD as a function of $1/K$ for various values of $\Delta\tau$, as compared with those for quenched QCD. (a) $(m_\pi a)^2$; (b) $m_\rho a$; (c) $m_N a$; (d) $m_\Delta a$. Errors shown are statistical only.

TABLE IV. Average value of the Wilson loop $W(L \times L)$ at $\beta=5.5$. The value for $\Delta\tau=0$ is obtained by a linear extrapolation in $\Delta\tau$. For the Wilson loop up to 4×4 , the spacelike and timelike loops are averaged before the extrapolation.

	$K=0.14$						
	$\Delta\tau=0.02$	Spacelike 0.01	0.005	$\Delta\tau=0.02$	Timelike 0.01	0.005	0
$W(1 \times 1)$	0.500 72 $\pm 0.000 86$	0.513 58 $\pm 0.000 74$	0.517 27 $\pm 0.000 72$	0.500 67 $\pm 0.000 83$	0.513 41 $\pm 0.000 62$	0.517 45 $\pm 0.000 67$	0.523 67 $\pm 0.000 80$
$W(1 \times 2)$	0.263 49 $\pm 0.000 71$	0.279 79 $\pm 0.000 71$	0.284 92 $\pm 0.000 70$	0.263 46 $\pm 0.000 75$	0.279 72 $\pm 0.000 57$	0.284 71 $\pm 0.000 64$	0.292 97 $\pm 0.001 02$
$W(1 \times 3)$	0.140 32 $\pm 0.000 63$	0.154 58 $\pm 0.000 67$	0.158 97 $\pm 0.000 77$	0.140 22 $\pm 0.000 70$	0.154 43 $\pm 0.000 56$	0.158 66 $\pm 0.000 74$	0.166 24 $\pm 0.001 01$
$W(1 \times 4)$	0.074 88 $\pm 0.000 51$	0.085 60 $\pm 0.000 61$	0.088 87 $\pm 0.000 67$	0.074 62 $\pm 0.000 58$	0.085 50 $\pm 0.000 53$	0.088 53 $\pm 0.000 66$	0.094 38 $\pm 0.000 82$
$W(1 \times 5)$				0.039 92 $\pm 0.000 75$	0.047 52 $\pm 0.000 67$	0.049 36 $\pm 0.000 86$	0.013 36 $\pm 0.000 24$
$W(1 \times 6)$				0.021 50 $\pm 0.000 73$	0.026 60 $\pm 0.000 65$	0.027 59 $\pm 0.000 65$	0.007 53 $\pm 0.000 20$
$W(2 \times 2)$	0.081 50 $\pm 0.000 80$	0.093 89 $\pm 0.000 88$	0.098 35 $\pm 0.000 95$	0.081 55 $\pm 0.000 80$	0.093 85 $\pm 0.000 69$	0.097 81 $\pm 0.001 00$	0.104 48 $\pm 0.000 94$
$W(2 \times 3)$	0.026 36 $\pm 0.000 43$	0.033 43 $\pm 0.000 49$	0.036 04 $\pm 0.000 52$	0.026 44 $\pm 0.000 50$	0.033 23 $\pm 0.000 40$	0.035 54 $\pm 0.000 59$	0.039 37 $\pm 0.000 63$
$W(2 \times 4)$	0.008 49 $\pm 0.000 46$	0.012 09 $\pm 0.000 33$	0.013 36 $\pm 0.000 41$	0.008 52 $\pm 0.000 50$	0.012 09 $\pm 0.000 36$	0.013 02 $\pm 0.000 42$	0.015 05 $\pm 0.000 43$
$W(2 \times 5)$				0.002 55 $\pm 0.000 71$	0.004 25 $\pm 0.000 46$	0.004 63 $\pm 0.000 63$	0.001 38 $\pm 0.000 19$
$W(2 \times 6)$				0.001 04 $\pm 0.000 62$	0.001 47 $\pm 0.000 44$	0.001 42 $\pm 0.000 74$	0.000 43 $\pm 0.000 19$
$W(3 \times 3)$	0.005 32 $\pm 0.000 54$	0.008 39 $\pm 0.000 55$	0.009 12 $\pm 0.000 55$	0.005 41 $\pm 0.000 57$	0.008 09 $\pm 0.000 40$	0.008 68 $\pm 0.000 60$	0.010 44 $\pm 0.000 50$
$W(3 \times 4)$	0.001 33 $\pm 0.000 40$	0.002 32 $\pm 0.000 32$	0.002 24 $\pm 0.000 35$	0.000 86 $\pm 0.000 41$	0.002 04 $\pm 0.000 29$	0.002 38 $\pm 0.000 45$	0.002 94 $\pm 0.000 35$
$W(3 \times 5)$				0.000 38 $\pm 0.000 57$	0.000 43 $\pm 0.000 44$	0.000 65 $\pm 0.000 51$	0.000 17 $\pm 0.000 15$
$W(4 \times 4)$	0.000 38 $\pm 0.000 52$	0.000 43 $\pm 0.000 40$	0.000 73 $\pm 0.000 48$	0.000 08 $\pm 0.000 54$	0.000 69 $\pm 0.000 42$	0.000 64 $\pm 0.000 49$	0.000 86 $\pm 0.000 40$

$K=0.15$							
$W(1 \times 1)$	0.513 60 $\pm 0.000 90$	0.525 67 $\pm 0.000 79$	0.533 13 $\pm 0.000 92$	0.513 87 $\pm 0.000 86$	0.525 78 $\pm 0.000 70$	0.532 93 $\pm 0.000 85$	0.538 93 $\pm 0.000 96$
$W(1 \times 2)$	0.279 77 $\pm 0.000 82$	0.295 78 $\pm 0.000 73$	0.305 54 $\pm 0.000 88$	0.280 12 $\pm 0.000 77$	0.295 81 $\pm 0.000 62$	0.305 14 $\pm 0.000 86$	0.313 05 $\pm 0.001 25$
$W(1 \times 3)$	0.154 50 $\pm 0.000 83$	0.168 88 $\pm 0.000 72$	0.178 19 $\pm 0.000 82$	0.155 02 $\pm 0.000 75$	0.168 92 $\pm 0.000 63$	0.177 66 $\pm 0.000 87$	0.184 78 $\pm 0.001 13$
$W(1 \times 4)$	0.085 42 $\pm 0.000 75$	0.096 62 $\pm 0.000 63$	0.104 47 $\pm 0.000 75$	0.085 83 $\pm 0.000 70$	0.096 61 $\pm 0.000 56$	0.103 72 $\pm 0.000 76$	0.109 42 $\pm 0.000 91$
$W(1 \times 5)$				0.047 76 $\pm 0.000 88$	0.055 17 $\pm 0.000 62$	0.060 32 $\pm 0.001 00$	0.015 92 $\pm 0.000 27$
$W(1 \times 6)$				0.026 54 $\pm 0.000 78$	0.031 48 $\pm 0.000 61$	0.035 29 $\pm 0.000 93$	0.009 36 $\pm 0.000 25$
$W(2 \times 2)$	0.094 35 $\pm 0.001 05$	0.108 02 $\pm 0.000 98$	0.116 73 $\pm 0.001 23$	0.094 97 $\pm 0.000 85$	0.108 01 $\pm 0.000 80$	0.116 33 $\pm 0.001 24$	0.122 79 $\pm 0.001 21$
$W(2 \times 3)$	0.033 54 $\pm 0.000 56$	0.041 80 $\pm 0.000 50$	0.047 82 $\pm 0.000 66$	0.034 19 $\pm 0.000 50$	0.042 00 $\pm 0.000 50$	0.047 07 $\pm 0.000 67$	0.051 14 $\pm 0.000 81$
$W(2 \times 4)$	0.011 92 $\pm 0.000 48$	0.016 28 $\pm 0.000 39$	0.019 92 $\pm 0.000 50$	0.012 72 $\pm 0.000 39$	0.016 57 $\pm 0.000 41$	0.019 33 $\pm 0.000 47$	0.021 47 $\pm 0.000 50$
$W(2 \times 5)$				0.004 78 $\pm 0.000 64$	0.006 67 $\pm 0.000 49$	0.007 73 $\pm 0.000 53$	0.002 17 $\pm 0.000 17$
$W(2 \times 6)$				0.002 00 $\pm 0.000 68$	0.002 92 $\pm 0.000 38$	0.003 15 $\pm 0.000 65$	0.000 92 $\pm 0.000 18$
$W(3 \times 3)$	0.007 93 $\pm 0.000 56$	0.011 62 $\pm 0.000 46$	0.014 59 $\pm 0.000 68$	0.008 84 $\pm 0.000 55$	0.012 28 $\pm 0.000 54$	0.014 27 $\pm 0.000 66$	0.016 06 $\pm 0.000 59$

TABLE IV. (Continued).

	$K = 0.15$						
	$\Delta\tau=0.02$	Spacelike 0.01	0.005	$\Delta\tau=0.02$	Timelike 0.01	0.005	0
$W(3\times 4)$	0.001 76 $\pm 0.000 37$	0.003 34 $\pm 0.000 33$	0.004 95 $\pm 0.000 39$	0.002 62 $\pm 0.000 40$	0.003 74 $\pm 0.000 28$	0.004 42 $\pm 0.000 47$	0.005 18 $\pm 0.000 38$
$W(3\times 5)$				0.000 94 $\pm 0.000 58$	0.001 16 $\pm 0.000 39$	0.000 95 $\pm 0.000 51$	0.000 27 $\pm 0.000 15$
$W(4\times 4)$	0.000 30 $\pm 0.000 60$	0.000 58 $\pm 0.000 46$	0.001 33 $\pm 0.000 67$	0.000 66 $\pm 0.000 50$	0.001 12 $\pm 0.000 36$	0.001 11 $\pm 0.000 49$	0.001 37 $\pm 0.000 47$
$K = 0.16$							
$W(1\times 1)$	0.530 78 $\pm 0.000 72$	0.548 25 $\pm 0.000 54$	0.555 45 $\pm 0.000 79$	0.530 85 $\pm 0.000 61$	0.548 40 $\pm 0.000 57$	0.555 54 $\pm 0.000 79$	0.564 54 $\pm 0.000 77$
$W(1\times 2)$	0.302 77 $\pm 0.000 71$	0.326 46 $\pm 0.000 55$	0.336 64 $\pm 0.000 79$	0.302 81 $\pm 0.000 61$	0.326 78 $\pm 0.000 57$	0.336 59 $\pm 0.000 79$	0.348 91 $\pm 0.001 03$
$W(1\times 3)$	0.175 74 $\pm 0.000 72$	0.198 31 $\pm 0.000 57$	0.208 04 $\pm 0.000 83$	0.175 82 $\pm 0.000 71$	0.198 55 $\pm 0.000 61$	0.207 97 $\pm 0.000 86$	0.219 73 $\pm 0.001 03$
$W(1\times 4)$	0.102 45 $\pm 0.000 68$	0.121 00 $\pm 0.000 53$	0.129 23 $\pm 0.000 75$	0.102 40 $\pm 0.000 75$	0.121 16 $\pm 0.000 54$	0.129 13 $\pm 0.000 77$	0.138 77 $\pm 0.000 91$
$W(1\times 5)$				0.059 72 $\pm 0.001 11$	0.073 80 $\pm 0.000 74$	0.080 27 $\pm 0.001 07$	0.021 85 $\pm 0.000 31$
$W(1\times 6)$				0.034 57 $\pm 0.001 02$	0.044 91 $\pm 0.000 70$	0.049 81 $\pm 0.000 97$	0.013 75 $\pm 0.000 28$
$W(2\times 2)$	0.115 37 $\pm 0.000 87$	0.137 58 $\pm 0.000 76$	0.147 86 $\pm 0.001 20$	0.114 94 $\pm 0.000 79$	0.137 91 $\pm 0.000 85$	0.147 89 $\pm 0.001 13$	0.159 49 $\pm 0.001 09$
$W(2\times 3)$	0.047 07 $\pm 0.000 43$	0.062 45 $\pm 0.000 44$	0.070 16 $\pm 0.000 71$	0.046 81 $\pm 0.000 53$	0.062 87 $\pm 0.000 48$	0.070 18 $\pm 0.000 77$	0.078 16 $\pm 0.000 86$
$W(2\times 4)$	0.019 50 $\pm 0.000 41$	0.029 10 $\pm 0.000 35$	0.034 22 $\pm 0.000 58$	0.019 30 $\pm 0.000 42$	0.029 21 $\pm 0.000 36$	0.033 96 $\pm 0.000 60$	0.038 94 $\pm 0.000 62$
$W(2\times 5)$				0.007 88 $\pm 0.000 41$	0.013 64 $\pm 0.000 52$	0.016 85 $\pm 0.000 72$	0.004 91 $\pm 0.000 19$
$W(2\times 6)$				0.003 32 $\pm 0.000 40$	0.006 25 $\pm 0.000 45$	0.008 51 $\pm 0.000 59$	0.002 46 $\pm 0.000 16$
$W(3\times 3)$	0.014 60 $\pm 0.000 52$	0.022 91 $\pm 0.000 48$	0.027 45 $\pm 0.000 85$	0.014 52 $\pm 0.000 67$	0.023 01 $\pm 0.000 53$	0.027 96 $\pm 0.000 88$	0.031 69 $\pm 0.000 71$
$W(3\times 4)$	0.004 61 $\pm 0.000 40$	0.009 00 $\pm 0.000 27$	0.011 35 $\pm 0.000 38$	0.004 79 $\pm 0.000 41$	0.008 92 $\pm 0.000 33$	0.011 59 $\pm 0.000 54$	0.013 48 $\pm 0.000 47$
$W(3\times 5)$				0.001 12 $\pm 0.000 51$	0.003 44 $\pm 0.000 39$	0.005 09 $\pm 0.000 63$	0.001 53 $\pm 0.000 17$
$W(3\times 6)$				0.000 54 $\pm 0.000 53$	0.001 24 $\pm 0.000 44$	0.002 35 $\pm 0.000 51$	0.000 66 $\pm 0.000 15$
$W(4\times 4)$	0.001 33 $\pm 0.000 48$	0.003 16 $\pm 0.000 40$	0.004 04 $\pm 0.000 45$	0.001 11 $\pm 0.000 49$	0.003 12 $\pm 0.000 34$	0.004 08 $\pm 0.000 55$	0.005 03 $\pm 0.000 41$
$W(4\times 5)$				-0.000 16 $\pm 0.000 43$	0.001 11 $\pm 0.000 37$	0.001 64 $\pm 0.000 50$	0.000 57 $\pm 0.000 14$
$W(4\times 6)$				0.000 11 $\pm 0.000 52$	0.000 28 $\pm 0.000 38$	0.000 85 $\pm 0.000 64$	0.000 20 $\pm 0.000 17$
$K = 0.162$							
$W(1\times 1)$		0.554 69 $\pm 0.000 64$			0.554 77 $\pm 0.000 61$		
$W(1\times 2)$		0.335 79 $\pm 0.000 65$			0.335 83 $\pm 0.000 62$		
$W(1\times 3)$		0.207 51 $\pm 0.000 71$			0.207 42 $\pm 0.000 64$		
$W(1\times 4)$		0.128 69 $\pm 0.000 69$			0.128 77 $\pm 0.000 65$		
$W(1\times 5)$					0.080 21 $\pm 0.001 00$		

TABLE IV. (Continued).

	$\Delta\tau=0.02$	$K=0.162$				0
		Spacelike 0.01	0.005	$\Delta\tau=0.02$	Timelike 0.01	
$W(1\times 6)$					0.049 74 $\pm 0.000 96$	
$W(2\times 2)$		0.147 65 $\pm 0.000 90$			0.147 60 $\pm 0.000 90$	
$W(2\times 3)$		0.070 42 $\pm 0.000 52$			0.070 35 $\pm 0.000 57$	
$W(2\times 4)$		0.034 43 $\pm 0.000 44$			0.034 18 $\pm 0.000 48$	
$W(2\times 5)$					0.016 60 $\pm 0.000 53$	
$W(2\times 6)$					0.008 17 $\pm 0.000 52$	
$W(3\times 3)$		0.028 02 $\pm 0.000 61$			0.028 20 $\pm 0.000 62$	
$W(3\times 4)$		0.011 89 $\pm 0.000 33$			0.011 81 $\pm 0.000 40$	
$W(3\times 5)$					0.004 92 $\pm 0.000 47$	
$W(3\times 6)$					0.001 96 $\pm 0.000 41$	
$W(4\times 4)$		0.004 48 $\pm 0.000 51$			0.004 39 $\pm 0.000 53$	
$W(4\times 5)$					0.001 79 $\pm 0.000 46$	
$W(4\times 6)$					0.000 89 $\pm 0.000 52$	

also the critical hopping parameter to a smaller value. The amount of decrease of masses is larger for a smaller quark mass. Therefore, while the quenched data lie nearly on a straight line with respect to $1/K$, the masses in full QCD bend downward toward the critical hopping parameter.

We fitted the hadron mass data for $K \gtrsim 0.15$ with the form

$$(m_\pi a)^2 = A_\pi \left[\frac{1}{K} - \frac{1}{K_c} \right],$$

$$m_i a = A_i \left[\frac{1}{K} - \frac{1}{K_c} \right] + B_i, \quad i = \rho, N, \Delta \quad (38)$$

and the spectroscopic parameters in (38) are tabulated in Table VII (errors shown are statistical except for those for the mass ratios for which errors due to the fitting procedures are also taken into account). Here we fixed the physical mass scale using $m_\rho^{\text{expt}} = 770$ MeV and $m_\pi^{\text{expt}} = 140$ MeV. The lattice constant a shrinks from

$$a^{-1} = 0.98 \pm 0.04 \text{ GeV}$$

$$= (0.20 \text{ fm})^{-1} \quad (N_f = 0)$$

to

$$a^{-1} = 1.64 \pm 0.16 \text{ GeV}$$

$$= (0.12 \text{ fm})^{-1} \quad (N_f = 2) \quad (39)$$

by the inclusion of vacuum quark loops. If we assume scaling, these lattice constants are translated into the QCD scale parameter on the lattice

$$\Lambda_L = 4.0 \pm 0.2 \text{ MeV} \quad (N_f = 0)$$

and

$$\Lambda_L = 2.8 \pm 0.3 \text{ MeV} \quad (N_f = 2), \quad (40)$$

where we used

$$a \Lambda_L = \left[\frac{8\pi^2}{33 - 2N_f} \beta \right]^{(51 - 19N_f/3)/(11 - 2N_f/3)^2}$$

$$\times \exp \left[- \frac{4\pi^2}{33 - 2N_f} \beta \right]. \quad (41)$$

With the aid of

$$\Lambda_{\text{MOM}} / \Lambda_L = 83.5 \quad (N_f = 0) \text{ (Refs. 35-37)}$$

$$= 97 \quad (N_f = 2) \text{ (Ref. 37)}, \quad (42)$$

we obtain

TABLE V. Selected data of hadron propagators for full QCD at $\beta=5.5$.

$K=0.14$						
	π			ρ		
	$\Delta\tau=0.02$	0.01	0.005	$\Delta\tau=0.02$	0.01	0.005
$t=0$	1.556×10 $\pm 0.003 \times 10$	1.553×10 $\pm 0.003 \times 10$	1.551×10 $\pm 0.004 \times 10$	1.354×10 $\pm 0.005 \times 10$	1.349×10 $\pm 0.005 \times 10$	1.347×10 $\pm 0.005 \times 10$
$t=1$	1.129 ± 0.014	1.138 ± 0.014	1.145 ± 0.013	8.372×10^{-1} $\pm 0.115 \times 10^{-1}$	8.402×10^{-1} $\pm 0.094 \times 10^{-1}$	8.439×10^{-1} $\pm 0.105 \times 10^{-1}$
$t=2$	1.630×10^{-1} $\pm 0.045 \times 10^{-1}$	1.681×10^{-1} $\pm 0.039 \times 10^{-1}$	1.704×10^{-1} $\pm 0.041 \times 10^{-1}$	1.152×10^{-1} $\pm 0.034 \times 10^{-1}$	1.178×10^{-1} $\pm 0.027 \times 10^{-1}$	1.186×10^{-1} $\pm 0.034 \times 10^{-1}$
$t=3$	2.613×10^{-2} $\pm 0.112 \times 10^{-2}$	2.839×10^{-2} $\pm 0.105 \times 10^{-2}$	2.910×10^{-2} $\pm 0.122 \times 10^{-2}$	1.778×10^{-2} $\pm 0.082 \times 10^{-2}$	1.908×10^{-2} $\pm 0.072 \times 10^{-2}$	1.942×10^{-2} $\pm 0.096 \times 10^{-2}$
$t=4$	4.442×10^{-3} $\pm 0.307 \times 10^{-3}$	5.175×10^{-3} $\pm 0.251 \times 10^{-3}$	5.393×10^{-3} $\pm 0.315 \times 10^{-3}$	2.932×10^{-3} $\pm 0.226 \times 10^{-3}$	3.369×10^{-3} $\pm 0.174 \times 10^{-3}$	3.471×10^{-3} $\pm 0.233 \times 10^{-3}$
$t=5$	7.723×10^{-4} $\pm 0.671 \times 10^{-4}$	9.615×10^{-4} $\pm 0.534 \times 10^{-4}$	1.027×10^{-3} $\pm 0.079 \times 10^{-3}$	4.955×10^{-4} $\pm 0.495 \times 10^{-4}$	6.067×10^{-4} $\pm 0.358 \times 10^{-4}$	6.413×10^{-4} $\pm 0.567 \times 10^{-4}$
$t=6$	1.360×10^{-4} $\pm 0.131 \times 10^{-4}$	1.813×10^{-4} $\pm 0.107 \times 10^{-4}$	1.980×10^{-4} $\pm 0.181 \times 10^{-4}$	8.487×10^{-5} $\pm 0.956 \times 10^{-5}$	1.111×10^{-4} $\pm 0.070 \times 10^{-4}$	1.204×10^{-4} $\pm 0.126 \times 10^{-4}$
$t=7$	2.396×10^{-5} $\pm 0.239 \times 10^{-5}$	3.399×10^{-5} $\pm 0.201 \times 10^{-5}$	3.808×10^{-5} $\pm 0.395 \times 10^{-5}$	1.454×10^{-5} $\pm 0.170 \times 10^{-5}$	2.021×10^{-5} $\pm 0.127 \times 10^{-5}$	2.249×10^{-5} $\pm 0.268 \times 10^{-5}$
$t=8$	4.355×10^{-6} $\pm 0.435 \times 10^{-6}$	6.647×10^{-6} $\pm 0.400 \times 10^{-6}$	7.544×10^{-6} $\pm 0.828 \times 10^{-6}$	2.567×10^{-6} $\pm 0.299 \times 10^{-6}$	3.851×10^{-6} $\pm 0.253 \times 10^{-6}$	4.320×10^{-6} $\pm 0.533 \times 10^{-6}$
$t=9$	1.490×10^{-6} $\pm 0.150 \times 10^{-6}$	2.417×10^{-6} $\pm 0.148 \times 10^{-6}$	2.802×10^{-6} $\pm 0.321 \times 10^{-6}$	8.559×10^{-7} $\pm 0.992 \times 10^{-7}$	1.366×10^{-6} $\pm 0.094 \times 10^{-6}$	1.566×10^{-6} $\pm 0.200 \times 10^{-6}$
$\langle \bar{\psi}\psi \rangle$	0.9682 ± 0.0023	0.9668 ± 0.0023	0.9653 ± 0.0021			
	N			Δ		
	$\Delta\tau=0.02$	0.01	0.005	$\Delta\tau=0.02$	0.01	0.005
$t=0$	1.581 ± 0.011	1.572 ± 0.011	1.567 ± 0.010	3.744 ± 0.026	3.722 ± 0.027	3.710 ± 0.024
$t=1$	2.617×10^{-2} $\pm 0.047 \times 10^{-2}$	2.620×10^{-2} $\pm 0.038 \times 10^{-2}$	2.634×10^{-2} $\pm 0.056 \times 10^{-2}$	6.599×10^{-2} $\pm 0.110 \times 10^{-2}$	6.604×10^{-2} $\pm 0.092 \times 10^{-2}$	6.631×10^{-2} $\pm 0.136 \times 10^{-2}$
$t=2$	8.885×10^{-4} $\pm 0.457 \times 10^{-4}$	8.755×10^{-4} $\pm 0.349 \times 10^{-4}$	8.849×10^{-4} $\pm 0.509 \times 10^{-4}$	2.190×10^{-3} $\pm 0.109 \times 10^{-3}$	2.152×10^{-3} $\pm 0.083 \times 10^{-3}$	2.170×10^{-3} $\pm 0.122 \times 10^{-3}$
$t=3$	3.494×10^{-5} $\pm 0.291 \times 10^{-5}$	3.619×10^{-5} $\pm 0.267 \times 10^{-5}$	3.703×10^{-5} $\pm 0.370 \times 10^{-5}$	8.416×10^{-5} $\pm 0.689 \times 10^{-5}$	8.649×10^{-5} $\pm 0.615 \times 10^{-5}$	8.822×10^{-5} $\pm 0.873 \times 10^{-5}$
$t=4$	1.600×10^{-6} $\pm 0.224 \times 10^{-6}$	1.807×10^{-6} $\pm 0.199 \times 10^{-6}$	1.835×10^{-6} $\pm 0.254 \times 10^{-6}$	3.762×10^{-6} $\pm 0.519 \times 10^{-6}$	4.197×10^{-6} $\pm 0.453 \times 10^{-6}$	4.255×10^{-6} $\pm 0.599 \times 10^{-6}$
$t=5$	8.495×10^{-8} $\pm 1.925 \times 10^{-8}$	1.011×10^{-7} $\pm 0.159 \times 10^{-7}$	9.762×10^{-8} $\pm 1.837 \times 10^{-8}$	1.952×10^{-7} $\pm 0.444 \times 10^{-7}$	2.301×10^{-7} $\pm 0.360 \times 10^{-7}$	2.205×10^{-7} $\pm 0.427 \times 10^{-7}$
$t=6$	4.916×10^{-9} $\pm 1.396 \times 10^{-9}$	5.702×10^{-9} $\pm 1.081 \times 10^{-9}$	5.709×10^{-9} $\pm 1.332 \times 10^{-9}$	1.112×10^{-8} $\pm 0.321 \times 10^{-8}$	1.272×10^{-8} $\pm 0.243 \times 10^{-8}$	1.260×10^{-8} $\pm 0.303 \times 10^{-8}$
$t=7$	2.717×10^{-10} $\pm 0.783 \times 10^{-10}$	3.229×10^{-10} $\pm 0.682 \times 10^{-10}$	3.443×10^{-10} $\pm 0.948 \times 10^{-10}$	6.072×10^{-10} $\pm 1.786 \times 10^{-10}$	7.053×10^{-10} $\pm 1.508 \times 10^{-10}$	7.437×10^{-10} $\pm 2.129 \times 10^{-10}$
$t=8$	1.510×10^{-11} $\pm 0.450 \times 10^{-11}$	1.860×10^{-11} $\pm 0.423 \times 10^{-11}$	1.991×10^{-11} $\pm 0.534 \times 10^{-11}$	3.341×10^{-11} $\pm 1.020 \times 10^{-11}$	3.978×10^{-11} $\pm 0.916 \times 10^{-11}$	4.197×10^{-11} $\pm 1.180 \times 10^{-11}$
$t=9$	8.210×10^{-13} $\pm 2.746 \times 10^{-13}$	1.114×10^{-12} $\pm 0.253 \times 10^{-12}$	1.150×10^{-12} $\pm 0.351 \times 10^{-12}$	1.808×10^{-12} $\pm 0.617 \times 10^{-12}$	2.313×10^{-12} $\pm 0.533 \times 10^{-12}$	2.396×10^{-12} $\pm 0.740 \times 10^{-12}$
$t=10$	2.955×10^{-14} $\pm 8.646 \times 10^{-14}$	4.02×10^{-13} $\pm 1.031 \times 10^{-13}$	-1.840×10^{-13} $\pm 2.568 \times 10^{-13}$	0.830×10^{-13} $\pm 1.410 \times 10^{-13}$	1.276×10^{-13} $\pm 1.519 \times 10^{-13}$	-2.048×10^{-13} $\pm 3.811 \times 10^{-13}$
$t=11$	-0.509×10^{-13} $\pm 6.946 \times 10^{-13}$	-2.126×10^{-12} $\pm 1.033 \times 10^{-12}$	-3.347×10^{-12} $\pm 2.350 \times 10^{-12}$	-0.426×10^{-13} $\pm 8.350 \times 10^{-13}$	-2.242×10^{-12} $\pm 1.261 \times 10^{-12}$	-3.966×10^{-12} $\pm 2.623 \times 10^{-12}$
$t=12$	-0.862×10^{-11} $\pm 1.333 \times 10^{-11}$	-3.994×10^{-11} $\pm 1.722 \times 10^{-11}$	-7.282×10^{-11} $\pm 5.169 \times 10^{-11}$	-0.986×10^{-11} $\pm 1.732 \times 10^{-11}$	-4.232×10^{-11} $\pm 2.103 \times 10^{-11}$	-8.494×10^{-11} $\pm 5.966 \times 10^{-11}$
$t=13$	-5.927×10^{-10} $\pm 3.713 \times 10^{-10}$	-1.101×10^{-9} $\pm 0.402 \times 10^{-9}$	-1.507×10^{-9} $\pm 0.843 \times 10^{-9}$	-7.654×10^{-10} $\pm 4.881 \times 10^{-10}$	-1.331×10^{-9} $\pm 0.517 \times 10^{-9}$	-1.726×10^{-9} $\pm 0.986 \times 10^{-9}$
$t=14$	-2.623×10^{-8} $\pm 0.920 \times 10^{-8}$	-3.971×10^{-8} $\pm 1.054 \times 10^{-8}$	-4.568×10^{-8} $\pm 1.849 \times 10^{-8}$	-3.364×10^{-8} $\pm 1.233 \times 10^{-8}$	-5.120×10^{-8} $\pm 1.389 \times 10^{-8}$	-5.657×10^{-8} $\pm 2.361 \times 10^{-8}$

TABLE V. (Continued).

$K=0.14$						
	$\Delta\tau=0.02$	N 0.01	0.005	$\Delta\tau=0.02$	Δ 0.01	0.005
$t=15$	-9.597×10^{-7} $\pm 2.476 \times 10^{-7}$	-1.243×10^{-6} $\pm 0.274 \times 10^{-6}$	-1.331×10^{-6} $\pm 0.350 \times 10^{-6}$	-1.304×10^{-6} $\pm 0.344 \times 10^{-6}$	-1.674×10^{-6} $\pm 0.388 \times 10^{-6}$	-1.776×10^{-6} $\pm 0.489 \times 10^{-6}$
$t=16$	-3.916×10^{-5} $\pm 0.706 \times 10^{-5}$	-4.654×10^{-5} $\pm 0.703 \times 10^{-5}$	-4.812×10^{-5} $\pm 0.694 \times 10^{-5}$	-5.763×10^{-5} $\pm 1.065 \times 10^{-5}$	-6.821×10^{-5} $\pm 1.058 \times 10^{-5}$	-6.999×10^{-5} $\pm 1.036 \times 10^{-5}$
$t=17$	-1.996×10^{-3} $\pm 0.189 \times 10^{-3}$	-2.184×10^{-3} $\pm 0.176 \times 10^{-3}$	-2.192×10^{-3} $\pm 0.208 \times 10^{-3}$	-3.221×10^{-3} $\pm 0.315 \times 10^{-3}$	-3.538×10^{-3} $\pm 0.287 \times 10^{-3}$	-3.534×10^{-3} $\pm 0.344 \times 10^{-3}$
$K=0.15$						
	$\Delta\tau=0.02$	π 0.01	0.005	$\Delta\tau=0.02$	ρ 0.01	0.005
$t=0$	1.620×10 $\pm 0.005 \times 10$	1.615×10 $\pm 0.004 \times 10$	1.606×10 $\pm 0.004 \times 10$	1.354×10 $\pm 0.007 \times 10$	1.344×10 $\pm 0.006 \times 10$	1.331×10 $\pm 0.006 \times 10$
$t=1$	1.535 ± 0.020	1.565 ± 0.013	1.585 ± 0.016	1.033 ± 0.013	1.044 ± 0.009	1.051 ± 0.009
$t=2$	2.892×10^{-1} $\pm 0.064 \times 10^{-1}$	3.019×10^{-1} $\pm 0.051 \times 10^{-1}$	3.153×10^{-1} $\pm 0.067 \times 10^{-1}$	1.768×10^{-1} $\pm 0.037 \times 10^{-1}$	1.816×10^{-1} $\pm 0.031 \times 10^{-1}$	1.874×10^{-1} $\pm 0.040 \times 10^{-1}$
$t=3$	6.352×10^{-2} $\pm 0.214 \times 10^{-2}$	6.896×10^{-2} $\pm 0.182 \times 10^{-2}$	7.615×10^{-2} $\pm 0.224 \times 10^{-2}$	3.595×10^{-2} $\pm 0.131 \times 10^{-2}$	3.801×10^{-2} $\pm 0.110 \times 10^{-2}$	4.139×10^{-2} $\pm 0.115 \times 10^{-2}$
$t=4$	1.530×10^{-2} $\pm 0.075 \times 10^{-2}$	1.740×10^{-2} $\pm 0.063 \times 10^{-2}$	2.079×10^{-2} $\pm 0.084 \times 10^{-2}$	8.123×10^{-3} $\pm 0.443 \times 10^{-3}$	8.894×10^{-3} $\pm 0.379 \times 10^{-3}$	1.054×10^{-2} $\pm 0.044 \times 10^{-2}$
$t=5$	3.827×10^{-3} $\pm 0.250 \times 10^{-3}$	4.665×10^{-3} $\pm 0.212 \times 10^{-3}$	6.002×10^{-3} $\pm 0.282 \times 10^{-3}$	1.921×10^{-3} $\pm 0.137 \times 10^{-3}$	2.246×10^{-3} $\pm 0.119 \times 10^{-3}$	2.867×10^{-3} $\pm 0.149 \times 10^{-3}$
$t=6$	9.588×10^{-4} $\pm 0.789 \times 10^{-4}$	1.290×10^{-3} $\pm 0.070 \times 10^{-3}$	1.762×10^{-3} $\pm 0.091 \times 10^{-3}$	4.543×10^{-4} $\pm 0.419 \times 10^{-4}$	5.872×10^{-4} $\pm 0.370 \times 10^{-4}$	7.960×10^{-4} $\pm 0.477 \times 10^{-4}$
$t=7$	2.447×10^{-4} $\pm 0.229 \times 10^{-4}$	3.687×10^{-4} $\pm 0.242 \times 10^{-4}$	5.332×10^{-4} $\pm 0.331 \times 10^{-4}$	1.096×10^{-4} $\pm 0.118 \times 10^{-4}$	1.591×10^{-4} $\pm 0.118 \times 10^{-4}$	$\pm 2.292 \times 10^{-4}$ $\pm 0.166 \times 10^{-4}$
$t=8$	6.693×10^{-5} $\pm 0.651 \times 10^{-5}$	1.138×10^{-4} $\pm 0.088 \times 10^{-4}$	1.793×10^{-4} $\pm 0.137 \times 10^{-4}$	2.837×10^{-5} $\pm 0.325 \times 10^{-5}$	4.634×10^{-5} $\pm 0.403 \times 10^{-5}$	7.328×10^{-5} $\pm 0.629 \times 10^{-5}$
$t=9$	3.265×10^{-5} $\pm 0.320 \times 10^{-5}$	6.060×10^{-5} $\pm 0.493 \times 10^{-5}$	1.027×10^{-4} $\pm 0.089 \times 10^{-4}$	1.330×10^{-5} $\pm 0.155 \times 10^{-5}$	2.365×10^{-5} $\pm 0.217 \times 10^{-5}$	4.035×10^{-5} $\pm 0.391 \times 10^{-5}$
$\langle \bar{\psi}\psi \rangle$	0.9540 ± 0.0028	0.9506 ± 0.0023	0.9466 ± 0.0023			
$K=0.15$						
	$\Delta\tau=0.02$	N 0.01	0.005	$\Delta\tau=0.02$	Δ 0.01	0.005
$t=0$	1.527 ± 0.013	1.511 ± 0.011	1.491 ± 0.011	3.603 ± 0.032	3.564 ± 0.026	3.516 ± 0.026
$t=1$	3.176×10^{-2} $\pm 0.081 \times 10^{-2}$	3.209×10^{-2} $\pm 0.058 \times 10^{-2}$	3.159×10^{-2} $\pm 0.063 \times 10^{-2}$	7.858×10^{-2} $\pm 0.188 \times 10^{-2}$	7.915×10^{-2} $\pm 0.142 \times 10^{-2}$	7.770×10^{-2} $\pm 0.151 \times 10^{-2}$
$t=2$	1.355×10^{-3} $\pm 0.059 \times 10^{-3}$	1.395×10^{-3} $\pm 0.045 \times 10^{-3}$	1.449×10^{-3} $\pm 0.077 \times 10^{-3}$	3.231×10^{-3} $\pm 0.137 \times 10^{-3}$	3.297×10^{-3} $\pm 0.101 \times 10^{-3}$	3.401×10^{-3} $\pm 0.176 \times 10^{-3}$
$t=3$	7.543×10^{-5} $\pm 0.700 \times 10^{-5}$	7.888×10^{-5} $\pm 0.468 \times 10^{-5}$	8.608×10^{-5} $\pm 0.521 \times 10^{-5}$	1.720×10^{-4} $\pm 0.163 \times 10^{-4}$	1.760×10^{-4} $\pm 0.101 \times 10^{-4}$	1.889×10^{-4} $\pm 0.112 \times 10^{-4}$
$t=4$	5.352×10^{-6} $\pm 0.697 \times 10^{-6}$	5.934×10^{-6} $\pm 0.650 \times 10^{-6}$	7.180×10^{-6} $\pm 0.755 \times 10^{-6}$	1.164×10^{-5} $\pm 0.155 \times 10^{-5}$	1.243×10^{-5} $\pm 0.135 \times 10^{-5}$	1.461×10^{-5} $\pm 0.151 \times 10^{-5}$
$t=5$	4.247×10^{-7} $\pm 0.709 \times 10^{-7}$	5.415×10^{-7} $\pm 0.868 \times 10^{-7}$	7.410×10^{-7} $\pm 0.978 \times 10^{-7}$	8.846×10^{-7} $\pm 1.495 \times 10^{-7}$	1.072×10^{-6} $\pm 0.173 \times 10^{-6}$	1.411×10^{-6} $\pm 0.185 \times 10^{-6}$
$t=6$	3.438×10^{-8} $\pm 0.714 \times 10^{-8}$	5.687×10^{-8} $\pm 1.118 \times 10^{-8}$	8.515×10^{-8} $\pm 1.402 \times 10^{-8}$	6.857×10^{-8} $\pm 1.414 \times 10^{-8}$	1.069×10^{-7} $\pm 0.213 \times 10^{-7}$	1.542×10^{-7} $\pm 0.255 \times 10^{-7}$
$t=7$	3.192×10^{-9} $\pm 0.856 \times 10^{-9}$	6.590×10^{-9} $\pm 1.558 \times 10^{-9}$	1.106×10^{-8} $\pm 0.245 \times 10^{-8}$	6.147×10^{-9} $\pm 1.642 \times 10^{-9}$	1.178×10^{-8} $\pm 0.278 \times 10^{-8}$	1.935×10^{-8} $\pm 0.433 \times 10^{-8}$
$t=8$	3.218×10^{-10} $\pm 0.998 \times 10^{-10}$	8.105×10^{-10} $\pm 2.247 \times 10^{-10}$	1.574×10^{-9} $\pm 0.439 \times 10^{-9}$	6.053×10^{-10} $\pm 1.932 \times 10^{-10}$	1.399×10^{-9} $\pm 0.386 \times 10^{-9}$	2.650×10^{-9} $\pm 0.742 \times 10^{-9}$
$t=9$	3.210×10^{-11} $\pm 1.075 \times 10^{-11}$	9.693×10^{-11} $\pm 3.060 \times 10^{-11}$	2.320×10^{-10} $\pm 0.724 \times 10^{-10}$	6.008×10^{-11} $\pm 2.124 \times 10^{-11}$	1.624×10^{-10} $\pm 0.517 \times 10^{-10}$	3.770×10^{-10} $\pm 1.188 \times 10^{-10}$
$t=10$	0.698×10^{-12} $\pm 4.022 \times 10^{-12}$	7.010×10^{-12} $\pm 8.908 \times 10^{-12}$	2.971×10^{-11} $\pm 1.933 \times 10^{-11}$	3.681×10^{-12} $\pm 5.756 \times 10^{-12}$	1.387×10^{-11} $\pm 1.267 \times 10^{-11}$	5.280×10^{-11} $\pm 2.864 \times 10^{-11}$

TABLE V. (Continued).

$K=0.15$						
	N		Δ			
	$\Delta\tau=0.02$	0.01	0.005	$\Delta\tau=0.02$	0.01	0.005
$t=11$	-1.850×10^{-11}	-3.321×10^{-11}	-9.008×10^{-11}	-2.054×10^{-11}	-3.526×10^{-11}	-7.149×10^{-11}
	$\pm 2.205 \times 10^{-11}$	$\pm 2.917 \times 10^{-11}$	$\pm 7.629 \times 10^{-11}$	$\pm 2.456 \times 10^{-11}$	$\pm 3.634 \times 10^{-11}$	$\pm 9.059 \times 10^{-11}$
$t=12$	-2.420×10^{-10}	-4.099×10^{-10}	-1.078×10^{-9}	-2.283×10^{-10}	-4.528×10^{-10}	-1.010×10^{-9}
	$\pm 1.845 \times 10^{-10}$	$\pm 2.307 \times 10^{-10}$	$\pm 0.501 \times 10^{-9}$	$\pm 2.009 \times 10^{-10}$	$\pm 2.474 \times 10^{-10}$	$\pm 0.567 \times 10^{-9}$
$t=13$	-5.326×10^{-9}	-7.536×10^{-9}	-1.768×10^{-8}	-5.745×10^{-9}	-8.575×10^{-9}	-1.879×10^{-8}
	$\pm 2.948 \times 10^{-9}$	$\pm 2.850 \times 10^{-9}$	$\pm 0.468 \times 10^{-8}$	$\pm 3.712 \times 10^{-9}$	$\pm 3.195 \times 10^{-9}$	$\pm 0.489 \times 10^{-8}$
$t=14$	-1.333×10^{-7}	-1.563×10^{-7}	-3.001×10^{-7}	-1.567×10^{-7}	-1.802×10^{-7}	-3.465×10^{-7}
	$\pm 0.473 \times 10^{-7}$	$\pm 0.393 \times 10^{-7}$	$\pm 0.818 \times 10^{-7}$	$\pm 0.606 \times 10^{-7}$	$\pm 0.469 \times 10^{-7}$	$\pm 0.996 \times 10^{-7}$
$t=15$	-3.174×10^{-6}	-3.674×10^{-6}	-5.366×10^{-6}	-4.008×10^{-6}	-4.712×10^{-6}	-6.737×10^{-6}
	$\pm 0.679 \times 10^{-6}$	$\pm 0.593 \times 10^{-6}$	$\pm 0.871 \times 10^{-6}$	$\pm 0.911 \times 10^{-6}$	$\pm 0.785 \times 10^{-6}$	$\pm 1.140 \times 10^{-6}$
$t=16$	-9.300×10^{-5}	-1.009×10^{-4}	-1.271×10^{-4}	-1.303×10^{-4}	-1.426×10^{-4}	-1.789×10^{-4}
	$\pm 1.040 \times 10^{-5}$	$\pm 0.118 \times 10^{-4}$	$\pm 0.122 \times 10^{-4}$	$\pm 0.154 \times 10^{-4}$	$\pm 0.178 \times 10^{-4}$	$\pm 0.183 \times 10^{-4}$
$t=17$	-3.378×10^{-3}	-3.593×10^{-3}	-4.173×10^{-3}	-5.341×10^{-3}	-5.693×10^{-3}	-6.625×10^{-3}
	$\pm 0.272 \times 10^{-3}$	$\pm 0.255 \times 10^{-3}$	$\pm 0.243 \times 10^{-3}$	$\pm 0.446 \times 10^{-3}$	$\pm 0.420 \times 10^{-3}$	$\pm 0.408 \times 10^{-3}$
$K=0.16$						
	π		ρ			
	$\Delta\tau=0.02$	0.01	0.005	$\Delta\tau=0.02$	0.01	0.005
$t=0$	1.661×10	1.642×10	1.631×10	1.296×10	1.271×10	1.260×10
	$\pm 0.008 \times 10$	$\pm 0.008 \times 10$	$\pm 0.014 \times 10$	$\pm 0.010 \times 10$	$\pm 0.008 \times 10$	$\pm 0.014 \times 10$
$t=1$	2.187	2.231	2.230	1.248	1.244	1.233
	± 0.021	± 0.024	± 0.025	± 0.013	± 0.008	± 0.010
$t=2$	5.732×10^{-1}	6.156×10^{-1}	6.160×10^{-1}	2.619×10^{-1}	2.597×10^{-1}	2.505×10^{-1}
	$\pm 0.124 \times 10^{-1}$	$\pm 0.153 \times 10^{-1}$	$\pm 0.188 \times 10^{-1}$	$\pm 0.057 \times 10^{-1}$	$\pm 0.041 \times 10^{-1}$	$\pm 0.040 \times 10^{-1}$
$t=3$	1.905×10^{-1}	2.321×10^{-1}	2.420×10^{-1}	7.143×10^{-2}	7.502×10^{-2}	7.309×10^{-2}
	$\pm 0.070 \times 10^{-1}$	$\pm 0.088 \times 10^{-1}$	$\pm 0.113 \times 10^{-1}$	$\pm 0.294 \times 10^{-2}$	$\pm 0.200 \times 10^{-2}$	$\pm 0.160 \times 10^{-2}$
$t=4$	7.332×10^{-2}	1.058×10^{-1}	1.216×10^{-1}	2.360×10^{-2}	2.782×10^{-2}	2.841×10^{-2}
	$\pm 0.329 \times 10^{-2}$	$\pm 0.050 \times 10^{-1}$	$\pm 0.064 \times 10^{-1}$	$\pm 0.117 \times 10^{-2}$	$\pm 0.099 \times 10^{-2}$	$\pm 0.117 \times 10^{-2}$
$t=5$	3.070×10^{-2}	5.308×10^{-2}	7.049×10^{-2}	8.791×10^{-3}	1.187×10^{-2}	1.335×10^{-2}
	$\pm 0.165 \times 10^{-2}$	$\pm 0.298 \times 10^{-2}$	$\pm 0.407 \times 10^{-2}$	$\pm 0.535 \times 10^{-3}$	$\pm 0.050 \times 10^{-2}$	$\pm 0.101 \times 10^{-2}$
$t=6$	1.307×10^{-2}	2.798×10^{-2}	4.452×10^{-2}	3.363×10^{-3}	5.352×10^{-3}	7.114×10^{-3}
	$\pm 0.077 \times 10^{-2}$	$\pm 0.177 \times 10^{-2}$	$\pm 0.290 \times 10^{-2}$	$\pm 0.237 \times 10^{-3}$	$\pm 0.265 \times 10^{-3}$	$\pm 0.762 \times 10^{-3}$
$t=7$	5.712×10^{-3}	1.560×10^{-2}	3.084×10^{-2}	1.314×10^{-3}	2.555×10^{-3}	4.169×10^{-3}
	$\pm 0.390 \times 10^{-3}$	$\pm 0.109 \times 10^{-2}$	$\pm 0.234 \times 10^{-2}$	$\pm 0.117 \times 10^{-3}$	$\pm 0.156 \times 10^{-3}$	$\pm 0.576 \times 10^{-3}$
$t=8$	2.776×10^{-3}	1.007×10^{-2}	2.427×10^{-2}	5.691×10^{-4}	1.432×10^{-3}	2.849×10^{-3}
	$\pm 0.222 \times 10^{-3}$	$\pm 0.081 \times 10^{-2}$	$\pm 0.215 \times 10^{-2}$	$\pm 0.661 \times 10^{-4}$	$\pm 0.114 \times 10^{-3}$	$\pm 0.480 \times 10^{-3}$
$t=9$	1.992×10^{-3}	8.532×10^{-3}	2.221×10^{-2}	3.786×10^{-4}	1.130×10^{-3}	2.434×10^{-3}
	$\pm 0.175 \times 10^{-3}$	$\pm 0.739 \times 10^{-3}$	$\pm 0.217 \times 10^{-2}$	$\pm 0.502 \times 10^{-4}$	$\pm 0.104 \times 10^{-3}$	$\pm 0.454 \times 10^{-3}$
$\langle \bar{\psi}\psi \rangle$	0.9221	0.9158	0.9135			
	± 0.0038	± 0.0030	± 0.0048			
$K=0.16$						
	N		Δ			
	$\Delta\tau=0.02$	0.01	0.005	$\Delta\tau=0.02$	0.01	0.005
$t=0$	1.388	1.356	1.344	3.264	3.191	3.164
	± 0.017	± 0.014	± 0.022	± 0.041	± 0.032	± 0.052
$t=1$	3.500×10^{-2}	3.412×10^{-2}	3.229×10^{-2}	8.406×10^{-2}	8.148×10^{-2}	7.747×10^{-2}
	$\pm 0.098 \times 10^{-2}$	$\pm 0.063 \times 10^{-2}$	$\pm 0.089 \times 10^{-2}$	$\pm 0.232 \times 10^{-2}$	$\pm 0.150 \times 10^{-2}$	$\pm 0.219 \times 10^{-2}$
$t=2$	1.912×10^{-3}	1.907×10^{-3}	1.701×10^{-3}	4.248×10^{-3}	4.189×10^{-3}	3.765×10^{-3}
	$\pm 0.118 \times 10^{-3}$	$\pm 0.065 \times 10^{-3}$	$\pm 0.116 \times 10^{-3}$	$\pm 0.254 \times 10^{-3}$	$\pm 0.145 \times 10^{-3}$	$\pm 0.258 \times 10^{-3}$
$t=3$	1.553×10^{-4}	1.630×10^{-4}	1.431×10^{-4}	3.058×10^{-4}	3.061×10^{-4}	2.733×10^{-4}
	$\pm 0.177 \times 10^{-4}$	$\pm 0.072 \times 10^{-4}$	$\pm 0.125 \times 10^{-4}$	$\pm 0.334 \times 10^{-4}$	$\pm 0.135 \times 10^{-4}$	$\pm 0.241 \times 10^{-4}$
$t=4$	1.914×10^{-5}	2.304×10^{-5}	2.073×10^{-5}	3.260×10^{-5}	3.571×10^{-5}	3.195×10^{-5}
	$\pm 0.292 \times 10^{-5}$	$\pm 0.137 \times 10^{-5}$	$\pm 0.257 \times 10^{-5}$	$\pm 0.504 \times 10^{-5}$	$\pm 0.211 \times 10^{-5}$	$\pm 0.398 \times 10^{-5}$
$t=5$	3.306×10^{-6}	4.555×10^{-6}	5.120×10^{-6}	4.909×10^{-6}	6.017×10^{-6}	6.417×10^{-6}
	$\pm 0.567 \times 10^{-6}$	$\pm 0.394 \times 10^{-6}$	$\pm 0.825 \times 10^{-6}$	$\pm 0.832 \times 10^{-6}$	$\pm 0.535 \times 10^{-6}$	$\pm 1.125 \times 10^{-6}$
$t=6$	6.420×10^{-7}	1.061×10^{-6}	1.813×10^{-6}	8.560×10^{-7}	1.236×10^{-6}	1.985×10^{-6}
	$\pm 1.262 \times 10^{-7}$	$\pm 0.125 \times 10^{-6}$	$\pm 0.335 \times 10^{-6}$	$\pm 1.675 \times 10^{-7}$	$\pm 0.156 \times 10^{-6}$	$\pm 0.453 \times 10^{-6}$

TABLE V. (Continued).

$K = 0.16$						
	$\Delta\tau = 0.02$	N 0.01	0.05	$\Delta\tau = 0.02$	Δ 0.01	0.005
$t = 7$	1.308×10^{-7} $\pm 0.301 \times 10^{-7}$	2.745×10^{-7} $\pm 0.428 \times 10^{-7}$	7.506×10^{-7} $\pm 1.457 \times 10^{-7}$	1.585×10^{-7} $\pm 0.371 \times 10^{-7}$	2.854×10^{-7} $\pm 0.491 \times 10^{-7}$	7.181×10^{-7} $\pm 1.801 \times 10^{-7}$
$t = 8$	2.683×10^{-8} $\pm 0.886 \times 10^{-8}$	8.197×10^{-8} $\pm 1.691 \times 10^{-8}$	3.304×10^{-7} $\pm 0.703 \times 10^{-7}$	3.053×10^{-8} $\pm 1.105 \times 10^{-8}$	7.793×10^{-8} $\pm 1.800 \times 10^{-8}$	2.782×10^{-7} $\pm 0.844 \times 10^{-7}$
$t = 9$	5.270×10^{-9} $\pm 2.312 \times 10^{-9}$	2.832×10^{-8} $\pm 0.914 \times 10^{-8}$	1.325×10^{-7} $\pm 0.409 \times 10^{-7}$	5.690×10^{-9} $\pm 2.712 \times 10^{-9}$	2.449×10^{-8} $\pm 0.731 \times 10^{-8}$	9.780×10^{-8} $\pm 4.327 \times 10^{-8}$
$t = 10$	6.972×10^{-10} $\pm 9.448 \times 10^{-10}$	8.220×10^{-9} $\pm 6.331 \times 10^{-9}$	4.208×10^{-8} $\pm 3.374 \times 10^{-8}$	0.895×10^{-9} $\pm 1.033 \times 10^{-9}$	7.632×10^{-9} $\pm 4.491 \times 10^{-9}$	2.761×10^{-8} $\pm 2.316 \times 10^{-8}$
$t = 11$	-2.090×10^{-9} $\pm 1.995 \times 10^{-9}$	-8.585×10^{-9} $\pm 9.021 \times 10^{-9}$	-1.388×10^{-8} $\pm 4.143 \times 10^{-8}$	-1.424×10^{-9} $\pm 1.816 \times 10^{-9}$	-5.551×10^{-9} $\pm 5.574 \times 10^{-9}$	-1.396×10^{-8} $\pm 2.365 \times 10^{-8}$
$t = 12$	-1.611×10^{-8} $\pm 0.978 \times 10^{-8}$	-7.505×10^{-8} $\pm 1.953 \times 10^{-8}$	-1.419×10^{-7} $\pm 0.635 \times 10^{-7}$	-1.299×10^{-8} $\pm 0.898 \times 10^{-8}$	-5.647×10^{-8} $\pm 1.343 \times 10^{-8}$	-1.009×10^{-7} $\pm 0.433 \times 10^{-7}$
$t = 13$	-1.174×10^{-7} $\pm 0.509 \times 10^{-7}$	-4.948×10^{-7} $\pm 0.720 \times 10^{-7}$	-7.475×10^{-7} $\pm 1.831 \times 10^{-7}$	-9.933×10^{-8} $\pm 4.535 \times 10^{-8}$	-4.191×10^{-7} $\pm 0.566 \times 10^{-7}$	-5.481×10^{-7} $\pm 1.500 \times 10^{-7}$
$t = 14$	-1.192×10^{-6} $\pm 0.262 \times 10^{-6}$	-3.185×10^{-6} $\pm 0.334 \times 10^{-6}$	-4.280×10^{-6} $\pm 0.730 \times 10^{-6}$	-1.134×10^{-6} $\pm 0.265 \times 10^{-6}$	-3.057×10^{-6} $\pm 0.361 \times 10^{-6}$	-3.856×10^{-6} $\pm 0.740 \times 10^{-6}$
$t = 15$	-1.572×10^{-5} $\pm 0.260 \times 10^{-5}$	-2.791×10^{-5} $\pm 0.216 \times 10^{-5}$	-3.394×10^{-5} $\pm 0.524 \times 10^{-5}$	-1.777×10^{-5} $\pm 0.329 \times 10^{-5}$	-3.155×10^{-5} $\pm 0.277 \times 10^{-5}$	-3.804×10^{-5} $\pm 0.678 \times 10^{-5}$
$t = 16$	-2.925×10^{-4} $\pm 0.368 \times 10^{-4}$	-3.792×10^{-4} $\pm 0.300 \times 10^{-4}$	-4.001×10^{-4} $\pm 0.449 \times 10^{-4}$	-3.904×10^{-4} $\pm 0.553 \times 10^{-4}$	-5.184×10^{-4} $\pm 0.456 \times 10^{-4}$	-5.435×10^{-4} $\pm 0.710 \times 10^{-4}$
$t = 17$	-7.116×10^{-3} $\pm 0.366 \times 10^{-3}$	-7.963×10^{-3} $\pm 0.401 \times 10^{-3}$	-8.541×10^{-3} $\pm 0.559 \times 10^{-3}$	-1.113×10^{-2} $\pm 0.063 \times 10^{-2}$	-1.266×10^{-2} $\pm 0.069 \times 10^{-2}$	-1.357×10^{-2} $\pm 0.098 \times 10^{-2}$
$K = 0.162$						
	$\Delta\tau = 0.02$	π 0.01	0.005	$\Delta\tau = 0.02$	ρ 0.01	0.005
$t = 0$		1.635×10 $\pm 0.011 \times 10$			1.236×10 $\pm 0.012 \times 10$	
$t = 1$		2.431 ± 0.048			1.275 ± 0.010	
$t = 2$		7.345×10^{-1} $\pm 0.328 \times 10^{-1}$			2.596×10^{-1} $\pm 0.050 \times 10^{-1}$	
$t = 3$		3.151×10^{-1} $\pm 0.207 \times 10^{-1}$			7.407×10^{-2} $\pm 0.265 \times 10^{-2}$	
$t = 4$		1.662×10^{-1} $\pm 0.141 \times 10^{-1}$			2.753×10^{-2} $\pm 0.141 \times 10^{-2}$	
$t = 5$		9.958×10^{-2} $\pm 1.129 \times 10^{-2}$			1.203×10^{-2} $\pm 0.083 \times 10^{-2}$	
$t = 6$		6.605×10^{-2} $\pm 1.013 \times 10^{-2}$			5.916×10^{-3} $\pm 0.503 \times 10^{-3}$	
$t = 7$		4.739×10^{-2} $\pm 0.932 \times 10^{-2}$			3.285×10^{-3} $\pm 0.411 \times 10^{-3}$	
$t = 8$		3.724×10^{-2} $\pm 0.836 \times 10^{-2}$			2.091×10^{-3} $\pm 0.371 \times 10^{-3}$	
$t = 9$		3.368×10^{-2} $\pm 0.780 \times 10^{-2}$			1.711×10^{-3} $\pm 0.355 \times 10^{-3}$	
$\langle \bar{\psi}\psi \rangle$		0.9023 ± 0.0045				
	$\Delta\tau = 0.02$	N 0.01	0.005	$\Delta\tau = 0.02$	Δ 0.01	0.005
$t = 0$		1.296 ± 0.020			3.049 ± 0.046	
$t = 1$		3.204×10^{-2} $\pm 0.058 \times 10^{-2}$			7.622×10^{-2} $\pm 0.143 \times 10^{-2}$	
$t = 2$		1.737×10^{-3} $\pm 0.059 \times 10^{-3}$			3.767×10^{-3} $\pm 0.116 \times 10^{-3}$	

TABLE V. (Continued).

	$K=0.162$				
	$\Delta\tau=0.02$	N 0.01	0.005	Δ 0.01	0.005
$t=3$		1.457×10^{-4} $\pm 0.094 \times 10^{-4}$		2.634×10^{-4} $\pm 0.143 \times 10^{-4}$	
$t=4$		2.167×10^{-5} $\pm 0.245 \times 10^{-5}$		3.069×10^{-5} $\pm 0.287 \times 10^{-5}$	
$t=5$		4.638×10^{-6} $\pm 0.745 \times 10^{-6}$		5.329×10^{-6} $\pm 0.767 \times 10^{-6}$	
$t=6$		1.198×10^{-6} $\pm 0.228 \times 10^{-6}$		1.199×10^{-6} $\pm 0.212 \times 10^{-6}$	
$t=7$		3.218×10^{-7} $\pm 0.792 \times 10^{-7}$		3.016×10^{-7} $\pm 0.598 \times 10^{-7}$	
$t=8$		7.474×10^{-8} $\pm 4.948 \times 10^{-8}$		6.971×10^{-8} $\pm 2.106 \times 10^{-8}$	
$t=9$		-0.483×10^{-8} $\pm 5.218 \times 10^{-8}$		0.708×10^{-8} $\pm 1.861 \times 10^{-8}$	
$t=10$		-4.576×10^{-8} $\pm 8.564 \times 10^{-8}$		-1.613×10^{-8} $\pm 2.147 \times 10^{-8}$	
$t=11$		-1.102×10^{-7} $\pm 1.328 \times 10^{-7}$		-5.168×10^{-8} $\pm 3.918 \times 10^{-8}$	
$t=12$		-3.086×10^{-7} $\pm 2.075 \times 10^{-7}$		-1.760×10^{-7} $\pm 0.847 \times 10^{-7}$	
$t=13$		-1.141×10^{-6} $\pm 0.312 \times 10^{-6}$		-8.297×10^{-7} $\pm 2.058 \times 10^{-7}$	
$t=14$		-5.882×10^{-6} $\pm 0.685 \times 10^{-6}$		-5.456×10^{-6} $\pm 0.655 \times 10^{-6}$	
$t=15$		-4.384×10^{-5} $\pm 0.324 \times 10^{-5}$		-5.058×10^{-5} $\pm 0.387 \times 10^{-5}$	
$t=16$		-5.121×10^{-4} $\pm 0.334 \times 10^{-4}$		-7.131×10^{-4} $\pm 0.539 \times 10^{-4}$	
$t=17$		-1.003×10^{-2} $\pm 0.050 \times 10^{-2}$		-1.621×10^{-2} $\pm 0.091 \times 10^{-2}$	

$$\begin{aligned} \Lambda_{\text{MOM}} &= 340 \pm 15 \text{ MeV} \quad (N_f=0) \\ &= 270 \pm 25 \text{ MeV} \quad (N_f=2) . \end{aligned} \quad (43)$$

In Table VII we see that m_N/m_ρ and m_Δ/m_N became closer to the experimental values:

$$m_N^{\text{expt}}/m_\rho^{\text{expt}} = 1.22, \quad m_\Delta^{\text{expt}}/m_N^{\text{expt}} = 1.31 .$$

This better agreement is caused by a steeper slope of the $\Delta\tau$ extrapolation curve for nucleon (slightly less steep for Δ) as observed in Fig. 12. We cannot conclude, however, whether this is a real physical effect or merely represents either a size effect that the baryons are not contained in the lattice or an artifact due to our extrapolation procedure combined with large statistical errors. In any case, an analysis at a larger value of β should be made before drawing conclusions on its physical significance.

The critical hopping parameter shifts from $K_c = 0.1844 \pm 0.0012$ to $K_c = 0.1611 \pm 0.0002$ with the inclusion of vacuum quark loops. A finite $\Delta\tau$ makes the effective hopping parameter effectively smaller than its input value. For example, our largest hopping parameter $K = 0.162$, which apparently exceeds K_c , corresponds to the real hopping parameter around $K = 0.16$ due to the finite Langevin time step $\Delta\tau = 0.01$, as may be seen from a comparison of values of $m_\pi a$ and m_ρ/m_π .

The definition of quark mass is somewhat ambiguous with the Wilson action. We conventionally define it using the relation suggested from the free field

$$m_q = \frac{1}{2a} (K^{-1} - K_c^{-1}) . \quad (44)$$

We then obtain for full QCD

$$m_q a = 0.00128 \pm 0.00026 \quad \text{or} \quad (45a)$$

$$m_q = 2.1 \pm 0.4 \text{ MeV}$$

using (39), and for quenched QCD

$$m_q a = 0.00569 \pm 0.00057 \quad \text{or} \quad (45b)$$

$$m_q = 5.6 \pm 0.6 \text{ MeV} .$$

These m_q 's differ approximately by a factor of 2–3. If we form the ratio to Λ_L we obtain

$$\begin{aligned} m_q/\Lambda_L &= 1.4 \pm 0.2 \quad \text{for } N_f=0 , \\ m_q/\Lambda_L &= 0.8 \pm 0.2 \quad \text{for } N_f=2 . \end{aligned} \quad (46)$$

Let us now examine the question of whether the spatial

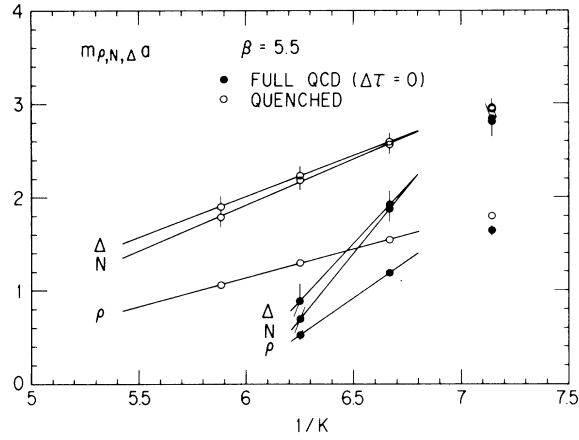


FIG. 14. Comparison of the ρ , N , and Δ masses as a function of $1/K$. The data for full QCD represent the value at $\Delta\tau=0$. Errors shown are statistical only.

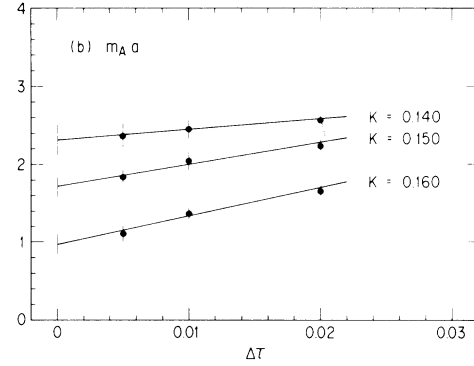
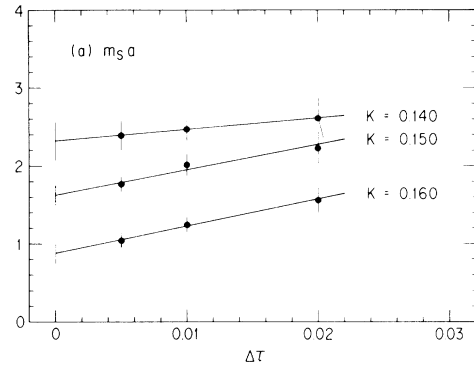


FIG. 16. (a) Scalar- and (b) axial-vector-meson masses as a function of $\Delta\tau$ with lines of $\Delta\tau$ extrapolation.

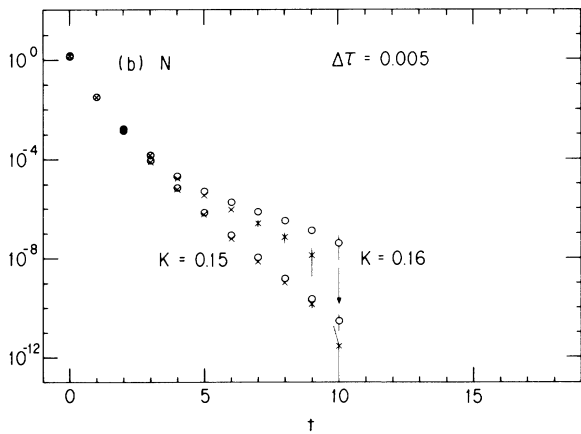
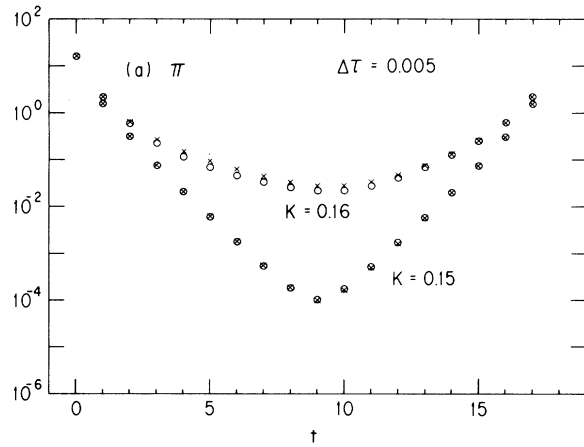


FIG. 15. Test of the finite-size effect at $K=0.15$ and at $K=0.16$. Circles (crosses) represent propagators solved with the periodic (antiperiodic) boundary condition in the spatial directions for quarks on the gauge configuration generated imposing the periodic boundary condition with $\Delta\tau=0.005$. (a) π ; (b) N .

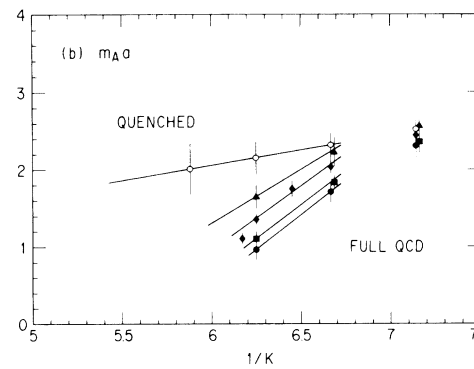
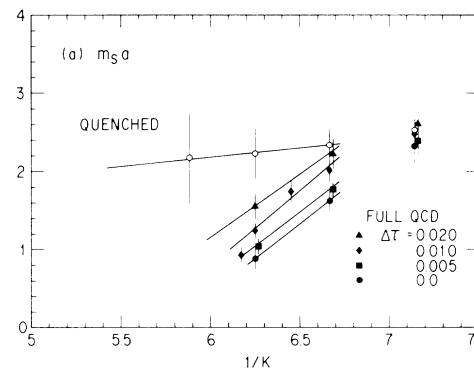


FIG. 17. (a) Scalar- and (b) axial-vector-meson masses as a function of $1/K$ for various values of $\Delta\tau$.

TABLE VI. Hadron mass for full QCD (A) and quenched QCD (B). A fit is made to the propagator for the range $t = 5-13$ (π, ρ), $t = 3-7$ and $11-15$ (S, A), and $t = 6-9$ (N, Δ).

$\Delta\tau$	A. Full QCD			
	0.02	(a) m_π 0.01	0.005	0
K				
0.14	1.736 ± 0.033	1.670 ± 0.020	1.650 ± 0.033	1.614 ± 0.037
0.15	1.366 ± 0.028	1.261 ± 0.021	1.195 ± 0.022	1.142 ± 0.028
0.155		0.984 ± 0.023		
0.16	0.856 ± 0.023	0.631 ± 0.023	0.458 ± 0.026	0.348 ± 0.030
0.162		0.436 ± 0.057		
		(b) m_ρ		
0.14	1.764 ± 0.038	1.698 ± 0.022	1.678 ± 0.037	1.642 ± 0.041
0.15	1.419 ± 0.032	1.313 ± 0.024	1.244 ± 0.025	1.190 ± 0.032
0.155		1.050 ± 0.031		
0.16	0.959 ± 0.030	0.767 ± 0.022	0.602 ± 0.041	0.532 ± 0.040
0.162		0.665 ± 0.042		
		(c) m_S		
0.14	2.612 ± 0.272	2.474 ± 0.147	2.393 ± 0.186	2.324 ± 0.244
0.15	2.233 ± 0.205	2.019 ± 0.142	1.772 ± 0.092	1.628 ± 0.139
0.155		1.749 ± 0.126		
0.16	1.561 ± 0.158	1.250 ± 0.093	1.046 ± 0.098	0.886 ± 0.133
0.162		0.934 ± 0.098		
		(d) m_A		
0.14	2.571 ± 0.219	2.454 ± 0.121	2.367 ± 0.150	2.308 ± 0.195
0.15	2.235 ± 0.193	2.045 ± 0.114	1.836 ± 0.090	1.715 ± 0.135
0.155		1.759 ± 0.109		
0.16	1.654 ± 0.149	1.363 ± 0.069	1.106 ± 0.101	0.966 ± 0.130
0.162		1.110 ± 0.071		
		(e) m_N		
0.14	2.898 ± 0.154	2.849 ± 0.105	2.836 ± 0.130	2.811 ± 0.160
0.15	2.327 ± 0.132	2.124 ± 0.122	1.978 ± 0.116	1.875 ± 0.146
0.155		1.736 ± 0.126		
0.16	1.596 ± 0.143	1.256 ± 0.108	0.863 ± 0.117	0.692 ± 0.148

TABLE VI. (Continued).

$\Delta\tau$		A. Full QCD					
		0.02	0.01	0.005	0		
K							
0.162			(e) m_N 1.376 ± 0.263				
0.14		2.907 ± 0.158	(f) m_Δ 2.872 ± 0.114	2.856 ± 0.144	2.839 ± 0.172		
0.15		2.352 ± 0.137	2.164 ± 0.125	2.014 ± 0.117	1.918 ± 0.150		
0.155			1.773 ± 0.137				
0.16		1.671 ± 0.154	1.348 ± 0.104	0.994 ± 0.176	0.886 ± 0.186		
0.162			1.440 ± 0.169				
		B. Quenched QCD					
β	K	m_π	m_ρ	m_S	m_A	m_N	m_Δ
5.5	0.14	1.770 ± 0.016	1.797 ± 0.018	2.532 ± 0.153	2.529 ± 0.130	2.947 ± 0.089	2.961 ± 0.098
5.5	0.15	1.496 ± 0.017	1.541 ± 0.019	2.342 ± 0.201	2.322 ± 0.159	2.561 ± 0.097	2.588 ± 0.103
5.5	0.16	1.214 ± 0.017	1.293 ± 0.020	2.229 ± 0.319	2.156 ± 0.217	2.176 ± 0.099	2.229 ± 0.107
5.5	0.17	0.910 ± 0.019	1.057 ± 0.022	2.178 ± 0.578	2.015 ± 0.330	1.786 ± 0.107	1.897 ± 0.116
5.62	0.15	1.250 ± 0.015	1.303 ± 0.020	2.066 ± 0.141	2.089 ± 0.119	2.168 ± 0.098	2.209 ± 0.105
5.65	0.15	1.199 ± 0.021	1.252 ± 0.023	1.929 ± 0.110	1.975 ± 0.097	2.131 ± 0.097	2.171 ± 0.104
5.73	0.16	0.631 ± 0.029	0.760 ± 0.037	1.584 ± 0.389	1.385 ± 0.173	1.133 ± 0.212	1.191 ± 0.186
5.75	0.16	0.576 ± 0.041	0.736 ± 0.038	1.172 ± 0.127	1.345 ± 0.110	1.174 ± 0.208	1.253 ± 0.156
5.79	0.16	0.448 ± 0.036	0.602 ± 0.048	1.613 ± 0.601	1.264 ± 0.117	0.935 ± 0.201	1.145 ± 0.217

extent of our lattice is large enough to contain hadrons. In Fig. 15 we compare the π and N propagators obtained with periodic and antiperiodic spatial boundary conditions for the quark propagator at $K=0.15$ and $K=0.16$ on the configurations generated with the periodic boundary condition at $\beta=5.5$, $\Delta\tau=0.01$. (The behavior of ρ and Δ propagators are similar to that of π and N , respectively.) The extracted mass is tabulated in Table VIII. For mesons the difference is small and within statistical errors (except for a somewhat larger deviation at $K=0.16$ and $\Delta\tau=0.01$ which, however, is not seen at $\Delta\tau=0.005$ with an effectively smaller lattice size). For baryons, however, the difference is noticeable at $K=0.16$. This could be counted as a possible finite-size effect arising from the increase of baryon size for smaller quark masses, and also from an effective shrinking of the lattice spacing with increasing K and decreasing $\Delta\tau$ (recall that decreasing $\Delta\tau$ means an effective increase of K). It is possible that the difference might also come from the nonvanishing

momentum of baryons for the antiperiodic boundary condition [see Eq. (36)]. To ensure the absence of the finite-size effect, we perhaps need a spatial extent of 12^3 or larger for our parameters.

We now consider the scalar- and axial-vector-meson masses. As seen in Fig. 11(b), statistical errors are large for $t=7-11$, and reliable mass values could not be obtained by the fit to $t=5-13$. We, therefore, attempted at extracting scalar and axial-vector masses by the fit to the propagator data for $t=3-7$ and $11-15$. Fortunately, the scalar and axial-vector propagators show a better exponential falloff from small t values as compared with the case for π and ρ , and the increase of masses caused by this change of time intervals is probably less than 20%.

The scalar- and axial-vector-meson masses are shown in Fig. 16 as a function of $\Delta\tau$, and then in Fig. 17 as a function of $1/K$. The spectroscopic parameters, which are obtained by applying the second equation of (38) are given in Table VII, together with the quenched values. Statistical

TABLE VII. Summary of spectroscopic parameters.

	Full QCD					Quenched
	$\Delta\tau=0.02$	$\Delta\tau=0.01$	$\Delta\tau=0.005$	$\Delta\tau=0$		
A_π	2.718 ± 0.205	2.854 ± 0.139	2.924 ± 0.136	2.838 ± 0.161	1.795 ± 0.076	
A_ρ	1.105 ± 0.106	1.312 ± 0.078	1.541 ± 0.116	1.579 ± 0.124	0.615 ± 0.037	
B_ρ	0.661 ± 0.054	0.588 ± 0.029	0.491 ± 0.049	0.465 ± 0.045	0.779 ± 0.035	
A_N	1.756 ± 0.467	2.091 ± 0.391	2.675 ± 0.395	2.838 ± 0.499	0.984 ± 0.183	
B_N	1.122 ± 0.251	0.981 ± 0.145	0.672 ± 0.139	0.570 ± 0.164	1.345 ± 0.169	
A_Δ	1.635 ± 0.495	1.963 ± 0.389	2.449 ± 0.506	2.476 ± 0.574	0.879 ± 0.197	
B_Δ	1.230 ± 0.269	1.081 ± 0.142	0.818 ± 0.207	0.780 ± 0.206	1.497 ± 0.183	
A_S	1.611 ± 0.621	1.916 ± 0.400	1.744 ± 0.322	1.782 ± 0.462	0.235 ± 0.640	
B_S	1.126 ± 0.292	1.007 ± 0.132	0.921 ± 0.116	0.809 ± 0.147	2.047 ± 0.705	
A_A	1.395 ± 0.585	1.674 ± 0.311	1.751 ± 0.326	1.797 ± 0.450	0.394 ± 0.420	
B_A	1.277 ± 0.276	1.140 ± 0.099	0.981 ± 0.120	0.889 ± 0.144	1.832 ± 0.442	
K_c	0.1672 ± 0.0009	0.1636 ± 0.0004	0.1619 ± 0.0003	0.1611 ± 0.0002	0.1844 ± 0.0012	
$K_{\text{phys}}^{-1} - K_c^{-1}$	0.0054 ± 0.0009	0.0041 ± 0.0005	0.0028 ± 0.0006	0.0026 ± 0.0005	0.0114 ± 0.0011	
a^{-1} (GeV)	1.15 ± 0.10	1.30 ± 0.06	1.56 ± 0.16	1.64 ± 0.16	0.98 ± 0.04	
m_N/m_ρ	1.69 ± 0.40	1.67 ± 0.26	1.37 ± 0.31	1.23 ± 0.37	1.73 ± 0.23	
m_Δ/m_N	1.10 ± 0.24	1.10 ± 0.16	1.22 ± 0.28	1.36 ± 0.37	1.11 ± 0.13	
m_S/m_ρ	1.70 ± 0.46	1.71 ± 0.24	1.88 ± 0.30	1.74 ± 0.36	2.63 ± 0.91	
m_A/m_ρ	1.93 ± 0.45	1.94 ± 0.19	2.00 ± 0.32	1.91 ± 0.36	2.35 ± 0.57	

errors are about 3 to 5 times larger than those for π and ρ due to smaller amplitudes of the propagator. (For the quenched case errors are even larger because of the small value of $\beta=5.5$.) From this table we quote the scalar- and axial-vector-meson masses to be $m_S/m_\rho \simeq 1.7 \pm 0.4$, $m_A/m_\rho \simeq 1.9 \pm 0.4$. These values appear to be quite reasonable, if we recall the possible +20% bias which we mentioned above.

C. Chiral order parameter

The $\Delta\tau$ dependence of the chiral order parameter $\langle \bar{\psi}\psi \rangle = \frac{1}{12} \text{tr} G_{00}$ (where $G = D^{-1}$) is shown in Fig. 18 and the value extrapolated to $\Delta\tau=0$ is given in Fig. 19 (see also Table V for numerical values) as a function of $1/K$ together with the data for the quenched case.

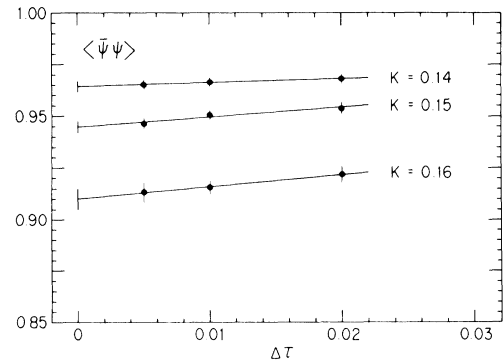


FIG. 18. The chiral order parameter $\langle \bar{\psi}\psi \rangle$ as a function of $\Delta\tau$, together with lines for the $\Delta\tau$ extrapolation.

TABLE VIII. Selected data of the hadron mass for full QCD with the antiperiodic boundary condition imposed for solving quark propagators. This table should be compared with Table VII, where the periodic boundary condition is imposed, to see the finite-size effect. The periodic boundary condition is used when gauge configurations are generated.

$K \backslash \Delta\tau$	0.02	(a) m_π 0.01	0.005	0
0.14	1.735 ± 0.032	1.669 ± 0.021	1.648 ± 0.033	1.612 ± 0.036
0.15	1.368 ± 0.028	1.256 ± 0.020	1.198 ± 0.021	1.141 ± 0.027
0.16	0.854 ± 0.023	0.568 ± 0.026	0.452 ± 0.048	0.297 ± 0.044
(b) m_ρ				
0.14	1.763 ± 0.036	1.697 ± 0.023	1.675 ± 0.037	1.639 ± 0.041
0.15	1.420 ± 0.031	1.306 ± 0.024	1.249 ± 0.022	1.192 ± 0.030
0.16	0.964 ± 0.027	0.698 ± 0.029	0.614 ± 0.047	0.464 ± 0.046
(c) m_N				
0.14	2.934 ± 0.156	2.898 ± 0.107	2.872 ± 0.139	2.854 ± 0.168
0.15	2.370 ± 0.129	2.175 ± 0.122	2.046 ± 0.114	1.947 ± 0.144
0.16	1.663 ± 0.120	1.387 ± 0.102	1.325 ± 0.193	1.156 ± 0.182
(d) m_Δ				
0.14	2.942 ± 0.167	2.919 ± 0.116	2.890 ± 0.151	2.881 ± 0.182
0.15	2.393 ± 0.135	2.208 ± 0.123	2.081 ± 0.114	1.986 ± 0.147
0.16	1.743 ± 0.135	1.483 ± 0.106	1.428 ± 0.153	1.283 ± 0.171

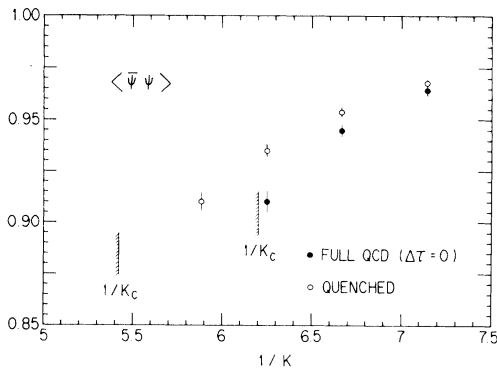


FIG. 19. The chiral order parameter $\langle \bar{\psi}\psi \rangle$ for full QCD ($\Delta\tau=0$) and quenched QCD as a function of $1/K$.

We have also measured the double quark loop average $G_{\eta-\pi}(t=0) = \langle [\text{tr}(\gamma_5 G_{00})]^2 \rangle$, which gives rise to the difference of π and η propagators at $t=0$. As is seen in Fig. 20 the value for full QCD does not differ much from that for the quenched case, and the ratio $G_{\eta-\pi}(0)/G_\pi(0) \sim 10^{-4}$ is quite small at $K=0.16$. Therefore the effect of vacuum quark loop is not likely to enhance the π - η mass difference over that in the quenched case. Recently it has been pointed out³⁸ within the quenched approximation that $G_{\eta-\pi}(t)$ becomes comparable to $G_\pi(t)$ if $K_c - K \lesssim 10^{-5}$ and if the gauge configuration is topologically nontrivial. It is very important to study whether this phenomenon is modified by the vacuum quark loops. Full QCD simulation at such a small quark mass, however, is beyond the capacity of the current computing power.

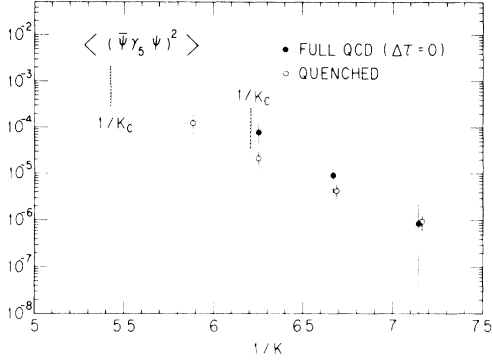


FIG. 20. Double quark loop propagator for the pseudoscalar at $t=0$, as defined by $G_{\eta-\pi}(t=0) = \langle (\text{tr} \gamma_5 D^{-1})^2 \rangle$. Solid and open circles represent full ($\Delta\tau=0$) and quenched QCD values, respectively.

D. The line of critical hopping parameter on (β, K) plane

To study the general structure of lattice QCD with the Wilson fermion it is necessary to know the position of the critical hopping parameters $K_c(\beta)$ as a function of β and N_f . We extended our spectroscopic analysis employing a smaller lattice $6^3 \times 12$ to find $K_c(\beta)$ for $\beta=4.0$ and 5.0 ($N_f=2$ and/or 4). The resulting pion mass is given in Fig. 21(a) for $\beta=5.0$ and 21(b) for $\beta=4.0$ both for full

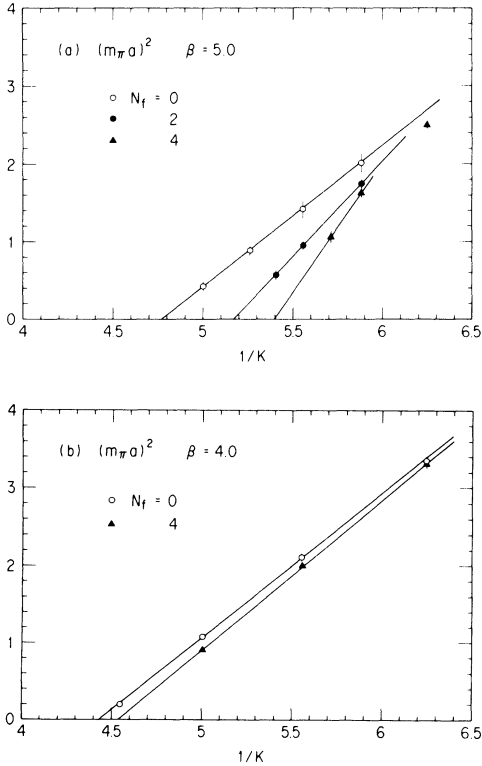


FIG. 21. Pion mass squared as a function of $1/K$. Simulations are made with $\Delta\tau=0.01$. (a) $\beta=5.0$ ($N_f=0,2,4$) and (b) $\beta=4.0$ ($N_f=0,4$).

and quenched QCD (the mass data is given in Table IX). These analyses are of a more qualitative character and we did not carry out the $\Delta\tau$ extrapolation. We present $K_c(\beta)$ in Table X and in Fig. 22. The typical error due to the finite $\Delta\tau(=0.01)$ is $\delta K_c \simeq 0.002$. In Fig. 22 we have also shown the curve for $m_\pi a = 1$ (dashed line).

V. PHYSICAL IMPLICATIONS

It is quite conceivable that a part of the vacuum-polarization effect can be absorbed into a shift of the gauge coupling constant β . To investigate this point we estimate the magnitude of the shift of β by matching the Wilson loop of full QCD at given values of K and $\Delta\tau$ with that for the pure gauge system at a shifted coupling $\beta + \Delta\beta$. (The value of Wilson loop for the pure gauge system is taken from Ref. 39. We also generated new data for $\beta=5.0-5.5$ on 6^4 and 8^4 lattices using the standard Monte Carlo algorithm. Our data smoothly continue to those of Ref. 39 within the accuracy required for our purpose.) The result is shown in Table XI and also in Fig. 23. The dependence of $\Delta\beta$ on the loop size is modest; $\Delta\beta$ for various sizes agrees within 20% even at $K=0.16$. A trend is observed, however, that a larger Wilson loop gives slightly a larger shift. We may estimate $\Delta\beta$ at $K=K_c$ by extrapolating the curve ($\Delta\tau=0$) of Fig. 23 to K_c , which gives

$$\Delta\beta(K=K_c) \simeq 0.34 - 0.36. \quad (47a)$$

For a consistency check one may alternatively measure the distance in β between K_c ($\beta=5.5$, $K_c=0.1611$) and the critical line $K=K_c(\beta)$ for quenched ($N_f=0$) QCD (see Fig. 22). This gives also

$$\Delta\beta(K=K_c) \simeq 0.35 - 0.39, \quad (47b)$$

in good agreement.

Let us compare $\Delta\beta$ for the 1×1 Wilson loop with that predicted in an effective hopping-parameter expansion.⁴⁰ To order K^{12} this expansion predicts $\Delta\beta \simeq 0.061$ for $K=0.14$, $\Delta\beta \simeq 0.089$ for $K=0.15$, and $\Delta\beta \simeq 0.13$ for $K=0.16$. The value for $K=0.14$ almost agrees with our measurement, but that for $K=0.16$ is a factor 2 smaller than the estimation from the simulation.

At $\beta=5.0$ ($\Delta\tau=0.01$) we found that the magnitude of the shift $\Delta\beta$ at $K=K_c$ estimated from the Wilson loop ($\Delta\beta=0.42-0.46$) is appreciably different from that obtained from the distance measurement in the (β, K) plane ($\Delta\beta=0.32-0.37$) in the manner described above for $\beta=5.5$.

We think that this is a remnant of the behavior in the strong-coupling limit where the shift $\Delta\beta$ shows a marked increase with the size and the effect of vacuum quark loops cannot be absorbed into the shift of β . In fact one can readily see in the hopping-parameter expansion that, at $\beta=0$,

$$\Delta\beta \sim K^{P/A}, \quad (48)$$

with P the perimeter and A the area of the Wilson loop, e.g., $\Delta\beta = 48N_f K^4$ from $W(1 \times 1)$, $\Delta\beta = 72(2N_f/3)^{1/2} K^3$

TABLE IX. Hadron mass at $\beta=5.0$ and 4.0 with $\Delta\tau=0.01$. Numbers of gauge configurations used in the analysis are presented in B. The periodic boundary condition is used throughout.

A. Hadron mass		
K	(a) $\beta=5.0, N_f=0$ ($8^3 \times 16$)	
	m_π	m_ρ
0.15	1.860 ± 0.041	1.903 ± 0.045
0.17	1.419 ± 0.045	1.520 ± 0.051
0.18	1.190 ± 0.044	1.346 ± 0.054
0.19	0.943 ± 0.037	1.192 ± 0.058
0.20	0.649 ± 0.041	1.080 ± 0.117
(b) $\beta=5.0, N_f=2$ ($6^3 \times 12$)		
0.17	1.323 ± 0.022	1.424 ± 0.026
0.18	0.979 ± 0.031	1.151 ± 0.042
0.185	0.758 ± 0.042	1.029 ± 0.042
(c) $\beta=5.0, N_f=4$ ($6^3 \times 12$)		
0.16	1.578 ± 0.020	1.649 ± 0.024
0.17	1.273 ± 0.023	1.389 ± 0.027
0.175	1.029 ± 0.041	1.207 ± 0.043
(d) $\beta=4.0, N_f=0$ ($6^3 \times 12$)		
0.16	1.830 ± 0.018	1.871 ± 0.020
0.18	1.453 ± 0.017	1.542 ± 0.021
0.20	1.043 ± 0.017	1.238 ± 0.024
0.22	0.444 ± 0.041	0.965 ± 0.067
(e) $\beta=4.0, N_f=4$ ($6^3 \times 12$)		
0.16	1.819 ± 0.016	1.860 ± 0.019
0.18	1.417 ± 0.013	1.512 ± 0.017
0.20	0.952 ± 0.019	1.185 ± 0.027

B. Number of gauge configurations			
β	$N_f=0$	2	4
4.0	30 ($\tau=20-50$)		30 ($\tau=20-50$)
5.0	5 ($\tau=5-10$)	20 ($\tau=20-40$)	20 ($\tau=20-40$)

TABLE X. Critical hopping parameter K_c .

β	$N_f=0$	2	4	
4.0	0.226 ± 0.001		0.221 ± 0.001	$6^3 \times 12$ ($\Delta\tau=0.01$)
5.0	0.210 ± 0.002			$8^3 \times 16$ ($\Delta\tau=0.01$)
		0.193 ± 0.001	0.185 ± 0.003	$6^3 \times 12$ ($\Delta\tau=0.01$)
5.5	0.1844 ± 0.0012	0.1637 ± 0.0004		$9^3 \times 18$ ($\Delta\tau=0.01$)
		0.1611 ± 0.0002		$9^3 \times 18$ ($\Delta\tau=0$)

from $W(1 \times 2)$, and $\Delta\beta=72 (N_f/6)^{1/4} K^2$ from $W(2 \times 2)$, etc.

It is a nontrivial question whether the shift estimated from the Wilson loop could also account for the magnitude of decrease of hadron masses in full QCD. We then calculated hadron propagators in the quenched approximation at $\beta'=\beta+\Delta\beta(K, \Delta\tau)$. We took $\Delta\beta$ for the large Wilson loop ($3 \times 3-4 \times 4$), because hadron masses are controlled by the large-distance behavior of propagators. In Figs. 24(a)–24(d) and Table XII the masses for full QCD are compared with those in the quenched approximation with the shifted β . The agreement between the two cases is very good for every K and $\Delta\tau$, and no appreciable deviation can be seen within our statistics.

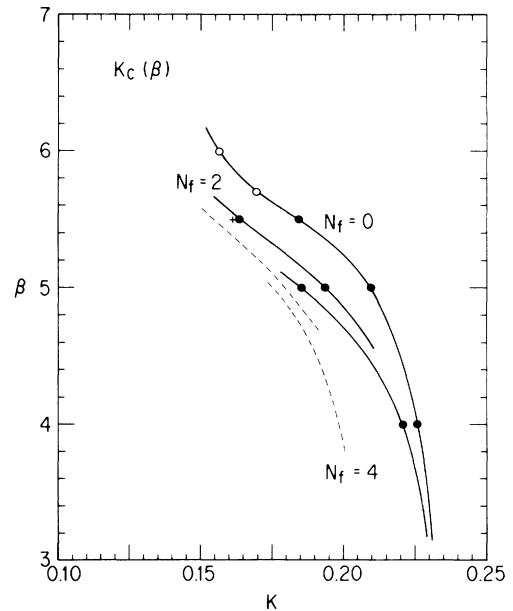


FIG. 22. Critical hopping parameters $K=K_c(\beta)$ ($\Delta\tau=0.01$) for $N_f=0$ (quenched), 2, and 4. Open circles are taken from Ref. 41. Lines interpolate measured points to guide the eyes. Dashed lines show the hopping parameter for which $m_\pi a=1$. The cross for the $\Delta\tau=0$ point is added to demonstrate the typical error induced by finite time step $\Delta\tau$.

TABLE XI. Effective shift of the gauge coupling $\Delta\beta$ from the Wilson loop matching.

	$\Delta\tau=0.02$	$K=0.14$		
		0.01	0.005	0
1×1	0.01 ± 0.00	0.06 ± 0.01	0.07 ± 0.01	0.09 ± 0.01
2×2	0.01 ± 0.00	0.06 ± 0.01	0.08 ± 0.01	0.10 ± 0.01
3×3	0.01 ± 0.01	0.06 ± 0.01	0.08 ± 0.01	0.10 ± 0.01
4×4	0.02 ± 0.07	0.09 ± 0.03	0.11 ± 0.03	0.13 ± 0.03
$K=0.15$				
1×1	0.06 ± 0.01	0.10 ± 0.01	0.13 ± 0.01	0.15 ± 0.01
2×2	0.06 ± 0.01	0.11 ± 0.01	0.14 ± 0.01	0.17 ± 0.01
3×3	0.06 ± 0.01	0.12 ± 0.01	0.15 ± 0.01	0.17 ± 0.01
4×4	0.08 ± 0.05	0.13 ± 0.02	0.16 ± 0.03	0.17 ± 0.03
$K=0.155$				
1×1		0.14 ± 0.01		
2×2		0.16 ± 0.01		
3×3		0.17 ± 0.01		
4×4		0.16 ± 0.02		
$K=0.16$				
1×1	0.12 ± 0.01	0.19 ± 0.01	0.23 ± 0.01	0.28 ± 0.01
2×2	0.14 ± 0.01	0.22 ± 0.01	0.26 ± 0.01	0.32 ± 0.01
3×3	0.15 ± 0.01	0.24 ± 0.01	0.29 ± 0.01	0.32 ± 0.01
4×4	0.15 ± 0.03	0.25 ± 0.01	0.29 ± 0.01	0.32 ± 0.02
$K=0.162$				
1×1		0.23 ± 0.01		
2×2		0.26 ± 0.01		
3×3		0.28 ± 0.01		
4×4		0.30 ± 0.02		

TABLE XII. Comparison of hadron masses at $K=0.16$ for full QCD ($\beta=5.5$, $\Delta\tau=0.005$) with those for quenched at shifted β 's. $\beta=5.79$ and $\beta=5.73$ correspond to those which match the large ($4\times 4-3\times 3$) and the small (1×1) Wilson loops, respectively. For a similar comparison at other values of K and $\Delta\tau$ consult Table VII.

	Quenched			Full QCD $\beta=5.5$
	$\beta=5.5$	5.73	5.79	
m_π	1.214 ± 0.017	0.631 ± 0.029	<u>0.448</u> ± 0.036	<u>0.458</u> ± 0.026
m_ρ	1.293 ± 0.020	0.760 ± 0.037	<u>0.602</u> ± 0.048	<u>0.602</u> ± 0.041
m_N	2.176 ± 0.099	1.133 ± 0.212	<u>0.935</u> ± 0.201	<u>0.863</u> ± 0.117
m_Δ	2.229 ± 0.107	1.191 ± 0.186	<u>1.145</u> ± 0.217	<u>0.994</u> ± 0.176
$\langle \bar{\psi}\psi \rangle$	0.9350 ± 0.0031	0.9165 ± 0.0034	0.9099 ± 0.0029	0.9135 ± 0.0048

A similar comparison was also made for the chiral order parameter $\langle \bar{\psi}\psi \rangle$. Since this is a local quantity we may expect a better agreement with $\Delta\beta$ corresponding to smaller Wilson loops. This in fact was found to be the case (see Table XII).

From this analysis we conclude that a bulk of the quark-vacuum-polarization effect can be absorbed into a shift of the gauge coupling constant. At a more precise level, however, the shift seems to depend slightly on length. In other words, the gauge field fluctuation of a given length scale in full QCD is very similar to that of the pure gauge system with a shifted effective coupling whose magnitude varies slightly with the length scale. A good agreement of the full QCD and the quenched case at any $\Delta\tau$ also suggests that most of the effect of finite $\Delta\tau$ may also be absorbed effectively into a shift of β .

Let us note here that, while the hadron masses extracted from the full QCD and quenched QCD with a shifted β agree, the value of propagators are different between the

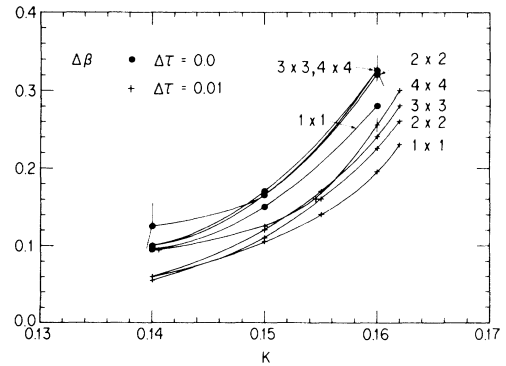


FIG. 23. The effective shift of β determined by matching the Wilson loop data of size from 1×1 to 4×4 . The values for $\Delta\tau=0.01$ and those extrapolated to $\Delta\tau=0$ are shown as a function of K . The lines drawn are guides to the eyes.

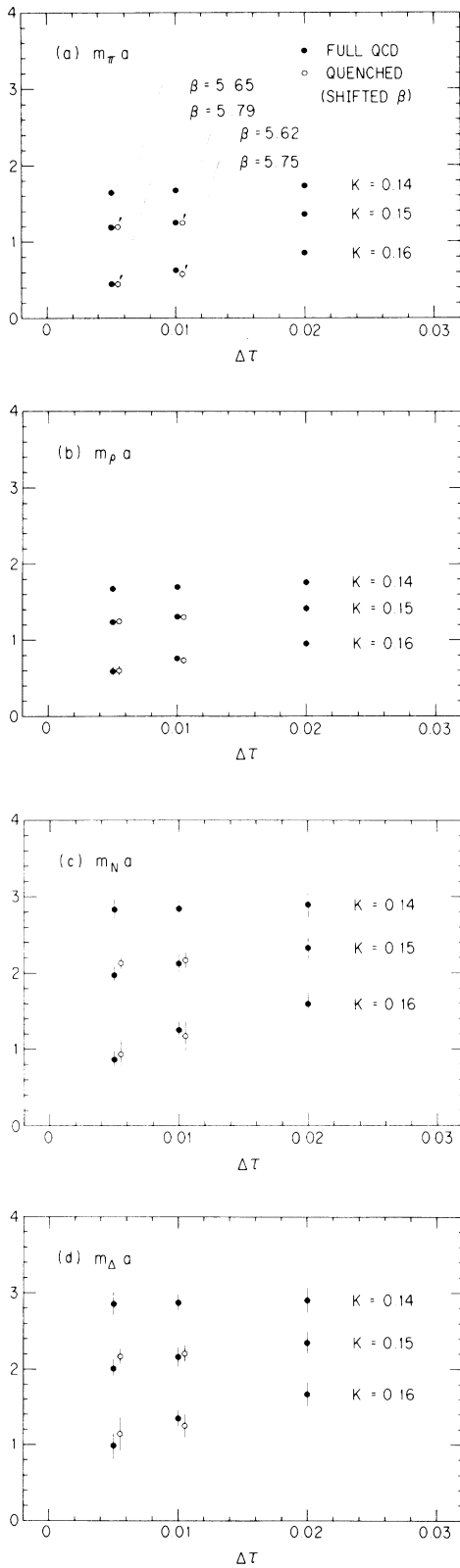


FIG. 24. Hadron masses for full QCD with a given $\Delta\tau$ (solid circle), as compared with those for the quenched case with a shifted β obtained from the large Wilson loops ($3 \times 3-4 \times 4$) (open circle). (a) π ; (b) ρ ; (c) N ; (d) Δ .

two (the ratio to the value for full QCD is presented in Fig. 25). The propagator of full QCD falls off more rapidly at a small distance and gradually becomes parallel to the quenched one at large distances.

At this point we recall the interesting feature of the recent quenched calculations⁴¹ that the results for masses are not too far from the experimental values. In fact if π and ρ masses are used as input the nucleon and Δ masses are higher than the experimental values by only 10–15%. Our finding on the effect of quark vacuum polarization shows that this is not an accident; since the bulk of the quark loop effect is absorbable into a shift of the coupling, the hadron masses in quenched QCD should not be very different from those of full QCD.

It is an interesting question to ask where one can see a clear physical effect of the quark vacuum loops. One obvious place will be the opening of the decay channels such as $\rho \rightarrow \pi\pi$ and $\Delta \rightarrow N\pi$. To examine this phenomenon, we have to explore the region where $m_\pi a \lesssim 0.2$. Such a simulation will be extremely time consuming not only because of the slower rate of convergence of ILUCR [see (35)] but also due to the possibility of critical slowing down and the need for a larger lattice to avoid finite-size effects.

Another possible place is the slight dependence of the shift $\Delta\beta$ on the length scale. To examine this point fur-

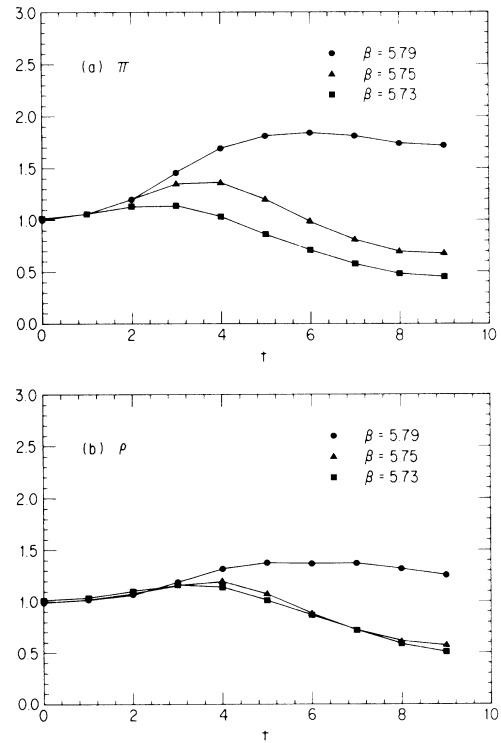


FIG. 25. Ratio of (a) the π and (b) the ρ propagators for quenched QCD with shifted β 's to those for full QCD ($K=0.16$, $\Delta\tau=0.005$). $\beta=5.79$ is the coupling constant obtained by matching the large Wilson loop ($3 \times 3-4 \times 4$), and $\beta=5.73$ the 1×1 Wilson loop.

ther we have calculated the static quark-antiquark potential $V(r)$ by fitting⁴² the timelike Wilson loop $W(r \times t)$ to the form $A \exp[-tV(r)]$ over the time interval $t=2-6$ at each spatial separation r in the range $1 \leq r \leq 4$. The potential $V(r)$ thus determined reflects the variation of the Wilson loop with respect to its size and hence is a quantity sensitive to the size dependence of the shift $\Delta\beta$. The full QCD potential at $K=0.16$ and $\beta=5.5$ with $\Delta\tau=0.005$ is presented in Fig. 26 together with the pure gauge potential at $\beta=5.79$. We observe a good agreement between the two in the inner part, whereas they start to differ in the outer region; the potential for full QCD increases more slowly than the pure gauge case. This trend agrees with the naive expectation that in full QCD the string between a quark-antiquark pair will split at a large separation.

The agreement of masses between the full and quenched QCD calculations found for the ground-state hadrons shows that these hadrons are confined in the inner region of the potential for which vacuum quark loop effects can be absorbed into a shift of β (Ref. 43). On the other hand, this suggests that the physical effect of the quark vacuum polarization may be more visible with the excited hadrons since their wave functions should spread over larger distances (e.g., in a charmonium model⁴⁴ $\langle r^2 \rangle_{2S}^{1/2} / \langle r^2 \rangle_{1S}^{1/2} \simeq 1.8$). We have noted that the rate of decrease of the propagator in full and quenched QCD differ at small temporal distances (Fig. 25), where one expects a substantial contribution from the excited states. The difference might therefore be ascribed to the net physical effect of quark vacuum loops. Unfortunately our lat-

tice size is not large enough to examine quantitatively the excited hadrons both in its spatial and temporal extents.

One of the pressing issues of full QCD simulation is to examine whether the physical quantities obey the scaling law predicted by the renormalization-group equation for full QCD. A direct check will be provided if one carries out another simulation at a larger β . Unfortunately, this seems to be beyond the computing power available to us at present. We therefore provisionally made use of the data at $\beta=5.5$ and $\beta=5.0$ to detect the effect of the vacuum quark loops in the following way. The renormalization-group equation predicts that the two length scales a_1 and a_0 at the two different β 's, β_1 and β_0 , should be connected by

$$\delta\beta \equiv \beta_1 - \beta_0 = \int da \frac{d\beta}{da} = -b_0 \ln a_1/a_0 + \dots \quad (49)$$

with $b_0 = (33 - 2N_f)/4\pi^2$ the coefficient of one-loop β function. Since we have seen that the physics of full QCD at β is well approximated by that of quenched QCD at $\beta + \Delta\beta$, the effective difference of the β values should be given by

$$\begin{aligned} \delta\beta' &\equiv (\beta_1 + \Delta\beta_1) - (\beta_0 + \Delta\beta_0) \\ &= -b'_0 \ln a_1/a_0 + \dots, \end{aligned} \quad (50)$$

where $b'_0 = 33/4\pi^2$ is the β -function coefficient for the pure gauge system and a_1/a_0 the same as in (49). Hence we expect

$$\frac{\delta\beta'}{\delta\beta} = \frac{33}{29} \quad (51)$$

for $N_f=2$. In our case $\delta\beta = 5.5 - 5.0 = 0.5$ and we can estimate $\delta\beta'$ from the effective shift at $K=K_c$ to be $\delta\beta' = (5.5 + 0.37 \pm 0.02) - (5.0 + 0.34 \pm 0.02) \sim 0.53$ [see the estimation for (47b)], i.e.,

$$\delta\beta' / \delta\beta |_{\text{measured}} = 1.0 - 1.1. \quad (52)$$

This is suggestive of the reduction of the one-loop β -function coefficient by an amount anticipated in the presence of dynamical quarks.

VI. CONCLUSION

In this work we have carried out a Langevin simulation of the full QCD hadron mass spectrum. We have shown that the Langevin simulation is practically feasible and works well for full QCD. At the same time we have shown that an extrapolation procedure is necessary to remove the effect of finite time-step size for a quantitative analysis. An important point, however, is that systematic errors seem to be controllable to a desired accuracy.

We have seen that the inclusion of quark vacuum polarization induces a significant shift in the hadron masses in lattice units, but it is mostly absorbed into a shift of the gauge coupling constant at least for the ground-state hadrons above the decay threshold. Probably this is also true for other static quantities of the ground-state hadrons, as may be anticipated from the shape of the static potential, which hardly differs in those parts relevant for such hadrons from that in quenched approximation. A physical

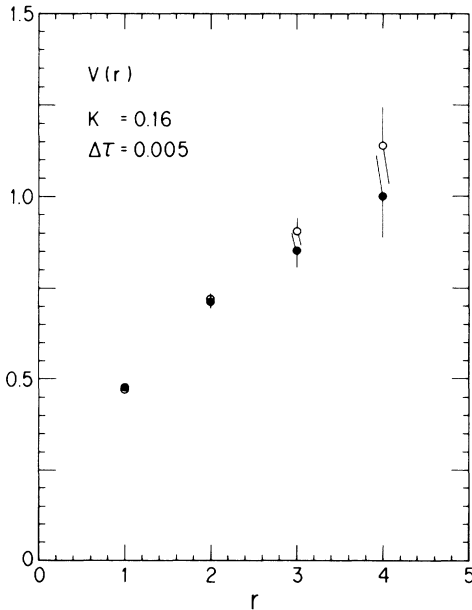


FIG. 26. Static potential estimated from rectangular Wilson loops. Solid circle stands for full QCD with $\beta=5.5$, $K=0.16$, and $\Delta\tau=0.005$, and open circle for the pure gauge system with $\beta=5.79$.

effect should be more clearly visible with excited hadrons, and this is connected with the deviation of the potential from the linear form at large distances.

Our lattice size is probably too small for a realistic estimate of the spectroscopic quantities, as is indicated by an evidence for a finite-size effect for the baryon mass. The minimum momentum, if defined by $2\pi/(L_s a)$, is 1 GeV, considerably higher than the typical momentum carried by quarks. In addition to resolving these problems it is most desirable to carry out a simulation at a different value of β to find the full QCD β function and check the scaling. For these purposes a simulation with a larger lattice is urgently needed.

For the simulation reported in this article, we used about 1500 h of CPU time on HITAC S810/10 at KEK, 500 h for tests of the algorithms, and 1000 h for production runs. As a typical example we quote that collecting the full QCD data at $K=0.16$ with $\Delta\tau=0.01$ over $\tau=0-60$ took about 120 h. Our code required 67MB of central memory and runs at the speed of 100–150 Mflops on S810/10. With the Langevin simulation, the requirement of memory and CPU time grows with the lattice volume. For a simulation with a realistic predictive power, say on a $16^3 \times 32$ lattice, we therefore need a computer with the speed of a few Gflops or more. Computers of such a capacity seem within reach within the next few years and there is much hope that a first-principles calculation of the hadronic observables will become possible shortly.

ACKNOWLEDGMENTS

The numerical calculation was carried out on HITAC S810/10 at the National Laboratory for High Energy Physics (KEK). We are greatly indebted to S. Kabe, T. Kaneko, and R. Ogasawara for assistance in operating the computer, and to S. Ohta for his efficient help in carrying out our simulations. We are thankful to Y. Karita, K. Murata, and Y. Ushiro for their invaluable advice on the numerical algorithm. We also benefited from conversations with G. G. Batrouni, N. Christ, Ph. de Forcrand, Y. Iwasaki, J. Kogut, P. Lepage, O. Martin, M. Okawa, G. Parisi, J. Polonyi, I. O. Stamatescu, B. Svetitsky, and D. Weingarten at various stages of our work. We would like to thank Y. Banno, S. Hirobe, T. Ishikawa, and Y. Miura for kind advice on the computer code. Finally we should thank the Theory Division of KEK for its warm hospitality. We are particularly grateful to H. Sugawara and T. Yukawa for their strong support for our work. Our work was supported in part by the Grants-in-Aid for Scientific Research of the Ministry of Education (Nos. 60740133 and 61460019).

APPENDIX

In much of the literature, conjugate-gradient (CG) methods are used to solve the Dirac equation on the lattice

$$Dx = b. \quad (\text{A1})$$

Since the matrix D is not Hermitian, the CG method can-

not be directly applied to (A1). The equation should be modified as either

$$D^\dagger Dx = D^\dagger b \quad (\text{A2})$$

or

$$DD^\dagger u = b \quad (x = D^\dagger u). \quad (\text{A3})$$

We will refer to the CG method based on (A2) as the least-square (LS) type, since it minimizes $\|b - Dx\|$. The method⁴⁵ based on (A3) is called the least-norm (LN) type, since it minimizes $\|x - D^{-1}b\|$.

The conjugate-gradient method for

$$Ax = b, \quad (\text{A4})$$

where A is a positive-definite Hermitian matrix converges as⁴⁶

$$\frac{\|x_v - A^{-1}b\|}{\|x_0 - A^{-1}b\|} \leq 2 \left[\frac{\sqrt{c} - 1}{\sqrt{c} + 1} \right]^v, \quad (\text{A5})$$

where x_v is the v th approximation and c the condition number of A , i.e.,

$$c = \lambda_{\max}(A) / \lambda_{\min}(A). \quad (\text{A6})$$

The convergence of the LS-type CG method is estimated by

$$\frac{\|x_v - D^{-1}b\|}{\|x_0 - D^{-1}b\|} \leq 2 \left[\frac{\sigma - 1}{\sigma + 1} \right]^v \quad (\text{A7})$$

with σ the ratio of the largest and smallest singular values of D . Similar relation holds for the convergence of the LN-type CG method with an appropriate replacement in the norms.

We also tested the Gauss-Seidel and SOR methods, which are sometimes used in the literature.^{10,30} These algorithms can easily be vectorized by the hyperplane method.

The convergence properties of various algorithms are compared in Fig. 2 (Sec. II B) and more extensively in Fig. 27 for the same parameters as for Fig. 2: ILUCR

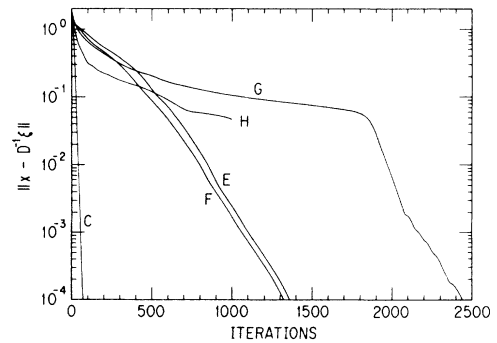


FIG. 27. Comparison of the behavior of the deviation from the true solution as a function of the number of iterations for various algorithms. The gauge configuration and the source vector are the same as in Fig. 2. The symbols denote: C (ILUCR with $c = 1.2$), E (LS type CG), F (LN type CG), G (CR), and H (SOR with $\omega = 0.7$).

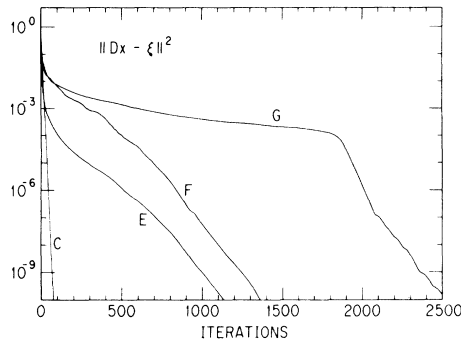


FIG. 28. The behavior of the residual norm squared as a function of the number of iterations for the examples shown in Fig. 27. The configuration and the symbols are the same as in Fig. 27. The residual in SOR method is not calculated.

($k=1$) with $c=1,2$, CG (LS type), CG (LN type), CR ($k=1$), and SOR ($\omega=0.7$). The “true” solution $D^{-1}b$ is obtained by the ILUCR method applying a more severe criterion. We see an excellent convergence of ILUCR with acceleration. Two CG methods behave almost similarly. The CR method without the ILU preconditioning has a long plateau up to around the 1800th iteration, and then suddenly accelerates its convergence. On the other hand, the Gauss-Seidel method diverges in this case. Even if we apply a deceleration ($\omega=0.7$), the approach to the solution is very slow. The CPU time for one iteration

is 1.23 sec for ILUCR, 0.66 sec for CG, and 0.39 sec for CR on HITAC S810/10. We note that one CR iteration costs 60% in time of one CG iteration, so that in this case both algorithms work almost equally to achieve an accuracy $\|x - A^{-1}b\| < 10^{-3}$, say. In less critical cases the number of iterations needed in the CR method is almost the same or only 20% larger than that in the CG method. We conclude that the CR method is generally more favorable than the CG method. This is the reason why we used the ILUCR rather than the ILUCG method.

In the actual computation we cannot monitor the error itself, since we do not know the true solution $D^{-1}b$. The criterion to terminate the iteration is the magnitude of the residual norm. We, therefore, checked the relation between the behaviors of the residuals and errors with various algorithms. In Fig. 28 we show the squared norm of the residual $\|b - Dx\|^2$ for the CG and CR methods and $\|(LU)^{-1}(b - Dx)\|^2$ for the ILUCR method.

The most notable feature in this analysis is the difference between the LN-type and LS-type CG methods. The norm of their residual differ in 2 orders of magnitude, though the error $\|x - D^{-1}b\|$ is almost the same with two methods. The difference is due to the fact that the LS-type algorithm searches the minimum of $\|b - Dx\|$. We presume the LN-type method is safer than the LS type; one has to choose the convergence criterion more carefully for the LS-type CG algorithm. Another noticeable feature is that, while the residual for the LS type decreases smoothly, the residual for the LN has many small plateaus. This is a usual feature characteristic of the CG method for a positive symmetric matrix.

- ¹K. G. Wilson, Phys. Rev. D **10**, 2445 (1974); A. M. Polyakov, Phys. Lett. **59B**, 82 (1975).
²H. Hamber and G. Parisi, Phys. Rev. Lett. **47**, 1792 (1981); E. Marinari, G. Parisi, and C. Rebbi, *ibid.* **47**, 1795 (1981); D. Weingarten, Phys. Lett. **109B**, 57 (1982).
³F. Fucito, E. Marinari, G. Parisi, and C. Rebbi, Nucl. Phys. **B180** [FS2], 369 (1981).
⁴J. Polonyi and H. W. Wyld, Phys. Rev. Lett. **51**, 2257 (1983).
⁵A. Ukawa and M. Fukugita, Phys. Rev. Lett. **55**, 1854 (1985).
⁶G. G. Batrouni, G. R. Katz, A. S. Kronfeld, G. P. Lepage, B. Svetitsky, and K. G. Wilson, Phys. Rev. D **32**, 2736 (1985).
⁷S. Duane, Nucl. Phys. **B257** [FS14], 652 (1985); S. Duane and J. B. Kogut, Phys. Rev. Lett. **55**, 2774 (1985); Nucl. Phys. **B275** [FS17], 398 (1986); S. Gottlieb, W. Liu, D. Toussaint, R. L. Renken, and R. L. Sugar, Santa Barbara report, 1986 (unpublished).
⁸D. J. Scalapino and R. L. Sugar, Phys. Rev. Lett. **46**, 519 (1981); A. Duncan and M. Furman, Nucl. Phys. **B190** [FS3], 767 (1981); D. H. Weingarten and D. N. Petcher, Phys. Lett. **99B**, 333 (1981); H. W. Hamber, Phys. Rev. D **24**, 951 (1981); J. Kuti, Phys. Rev. Lett. **49**, 183 (1982); A. Hasenfratz, Z. Kunszt, P. Hasenfratz, and C. B. Lang, Phys. Lett. **110B**, 289 (1982); D. Zwanziger, Phys. Rev. Lett. **50**, 1886 (1983); G. Bhanot, U. M. Heller, and I. Stamatescu, Phys. Lett. **129B**, 440 (1983); M. Fischler and R. Roskies, *ibid.* **145B**, 99 (1984); M. Grady, Phys. Rev. D **32**, 1496 (1985).
⁹G. Parisi and Y.-S. Wu, Sci. Sin. **24**, 483 (1981).

¹⁰Weingarten and Petcher (Ref. 8).

¹¹In the hybrid method with the time step h , the Langevin time step $\Delta\tau_L = h^2$ and the microcanonical time step $\Delta\tau_{MC} = h$. In order to ensure the ergodicity the condition $\Delta\tau_L N \gg 1$, with N the number of times that the random noise is applied to the system, should be satisfied. This practically requires a huge number $N > 10^5$ for a time step $h = 0.01$ chosen conventionally. This does not seem to be met in the simulations using the hybrid method presented so far (Ref. 7).

¹²An example is found in the results on the finite-temperature phase transition. When one compares the three analyses (i) by J. Polonyi *et al.* (microcanonical) [Phys. Rev. Lett. **53**, 644 (1984)], (ii) by R. V. Gavai (pseudofermion) [Nucl. Phys. **B269**, 530 (1986)], and (iii) by M. Fukugita and A. Ukawa (Langevin) [Phys. Rev. Lett. **57**, 503 (1986)], all three data on the Polyakov line and the chiral order parameter agree very well except for the transition region. While the position of the transition region agrees between (i) and (iii), it is shifted upward by $\Delta\beta = 0.06$ in the data of (ii).

¹³A. Guha and S.-C. Lee, Phys. Rev. D **27**, 2412 (1983); M. Falcioni, E. Marinari, M. L. Paciello, G. Parisi, B. Taglienti, and Y.-C. Zhang, Nucl. Phys. **B215** [FS7], 265 (1983); I. T. Drummond, S. Duane, and R. R. Horgan, *ibid.* **B220** [FS8], 119 (1983); M. B. Halpern, *ibid.* **B228**, 173 (1983); H. W. Hamber and U. M. Heller, Phys. Rev. D **29**, 928 (1984); M. Falcioni, M. L. Paciello, G. Parisi, and B. Taglienti, Nucl. Phys. **B251** [FS13], 624 (1985).

- ¹⁴E. Helfand, *Bell Syst. Tech. J.* **58**, 2289 (1979); H. S. Greenside and E. Helfand, *ibid.* **60**, 1927 (1981); W. Rümelin, *SIAM J. Numer. Anal.* **19**, 604 (1982).
- ¹⁵Drummond *et al.* (Ref. 13).
- ¹⁶M. R. Hestens and E. Stiefel, *J. Res. Nat. Bur. Standards* **49**, 409 (1952).
- ¹⁷J. A. Meijerink and H. A. van der Vorst, *Math. Comp.* **31**, 148 (1977); *J. Comp. Phys.* **44**, 134 (1981).
- ¹⁸Y. Oyanagi, *Computer Phys. Commun.* **42**, 338 (1986).
- ¹⁹P. Concus and G. H. Golub, in *Lecture Notes in Economics and Mathematical Systems*, edited by R. Glowinski and J. L. Lions (Springer, Berlin, 1976), Vol. 134, p. 56; Y. Saad, *SIAM J. Numer. Anal.* **19**, 485 (1982).
- ²⁰M. Fukugita, S. Ohta, and A. Ukawa, *Phys. Rev. Lett.* **57**, 1974 (1986).
- ²¹M. Fukugita, Y. Oyanagi, and A. Ukawa, *Phys. Rev. Lett.* **57**, 953 (1986).
- ²²For earlier attempts at full QCD simulation, see H. W. Hamber, E. Marinari, G. Parisi, and C. Rebbi, *Phys. Lett.* **124B**, 99 (1983); W. Langguth and I. Montvay, *ibid.* **145B**, 261 (1984); H. W. Hamber, *Nucl. Phys.* **B251** [FS13], 182 (1985). More recent attempts are seen in F. Fucito, K. J. M. Moriarty, C. Rebbi, and S. Solomon, *Phys. Lett.* **172B**, 235 (1986); R. V. Gavai and F. Karsch, *Phys. Rev. Lett.* **57**, 40 (1986).
- ²³Ph. de Forcrand and I. O. Stamatescu, *Nucl. Phys.* **B261**, 613 (1985); Freie Universität Berlin report, 1986 (unpublished).
- ²⁴O. C. Martin, S. W. Otto, and J. W. Flower, *Nucl. Phys.* **B264**, 89 (1986).
- ²⁵G. G. Batrouni, *Phys. Rev. D* **33**, 1815 (1986); A. S. Kronfeld, *Phys. Lett.* **172B**, 93 (1986).
- ²⁶S. C. Eisenstat, H. C. Elman, and M. H. Schultz, *SIAM J. Numer. Anal.* **20**, 345 (1983).
- ²⁷M. Fukugita, T. Kaneko, and A. Ukawa, *Phys. Rev. D* **28**, 2696 (1983); F. Gutbrod, P. Hasenfratz, Z. Kunszt, and I. Montvay, *Phys. Lett.* **128B**, 415 (1983).
- ²⁸T. G. Lewis and W. H. Payne, *J. Assoc. Comp. Mach.* **20**, 456 (1973).
- ²⁹G. E. P. Box and M. E. Muller, *Ann. Math. Stat.* **29**, 610 (1958).
- ³⁰D. Weingarten, *Nucl. Phys.* **B257** [FS14], 629 (1985).
- ³¹Y. Ushiro, M. Nishikata, and F. Nagahori, *Hitachi Hyoron* **65**, 557 (1983).
- ³²C. Lanczos, *J. Res. Nat. Bur. Standards* **45**, 255 (1950).
- ³³For related studies in the quenched calculation, see P. Hasenfratz and I. Montvay, *Phys. Rev. Lett.* **50**, 309 (1983); G. Martinelli, G. Parisi, R. Petronzio, and F. Rapuano, *Phys. Lett.* **122B**, 283 (1983); R. Gupta and A. Patel, *ibid.* **124B**, 94 (1983); M. Fukugita, T. Kaneko, and A. Ukawa, *Nucl. Phys.* **B230** [FS10], 62 (1984).
- ³⁴The extrapolated value of the Wilson loop agrees with that calculated by a different algorithm of Ref. 23 on $6^3 \times 16$ lattice with the antiperiodic boundary condition. The agreement is within 1–2% accuracy for any size L of the loop except at large L which suffers from large statistical errors. We acknowledge Philippe de Forcrand for providing the data.
- ³⁵A. Hasenfratz and P. Hasenfratz, *Phys. Lett.* **93B**, 165 (1980).
- ³⁶R. Dashen and D. J. Gross, *Phys. Rev. D* **23**, 2340 (1981).
- ³⁷H. Kawai, R. Nakayama, and K. Seo, *Nucl. Phys.* **B189**, 40 (1981).
- ³⁸S. Itoh, Y. Iwasaki, and T. Yoshié, *Phys. Lett.* **184B**, 375 (1987).
- ³⁹D. Barkai, K. J. M. Moriarty, and C. Rebbi, *Phys. Rev. D* **30**, 1293 (1984); J. Stack, *ibid.* **29**, 1213 (1984).
- ⁴⁰H. Joos and I. Montvay, *Nucl. Phys.* **B225** [FS9], 565 (1983); Langguth and Montvay (Ref. 22).
- ⁴¹For recent quenched calculations on a large lattice, see K. C. Bowler, D. L. Chalmers, A. Kenway, R. D. Kenway, G. S. Pawley, and D. J. Wallace, *Nucl. Phys.* **B240** [FS12], 213 (1984); J. P. Gilchrist, H. Schneider, G. Schierholz, and M. Teper, *Phys. Lett.* **136B**, 87 (1984); A. Billoire, E. Marinari, and R. Petronzio, *Nucl. Phys.* **B251** [FS13], 141 (1985); D. Barkai, K. J. M. Moriarty, and C. Rebbi, *Phys. Lett.* **156B**, 385 (1985); A. König, K. H. Mütter, K. Schilling, and J. Smit, *ibid.* **157B**, 421 (1985); H. W. Hamber, *ibid.* **178B**, 277 (1986); S. Itoh, Y. Iwasaki, and T. Yoshié, *ibid.* **167B**, 443 (1986); **183B**, 351 (1987); K. C. Bowler, C. B. Chalmers, R. D. Kenway, G. S. Pawley, and D. Roweth, *Nucl. Phys.* **B284**, 299 (1987).
- ⁴²J. D. Stack, *Phys. Rev. D* **27**, 412 (1983).
- ⁴³This has been speculated by Weingarten (Ref. 2).
- ⁴⁴E. Eichten, K. Gottfried, T. Kinoshita, J. Kogut, K. D. Lane, and T.-M. Yan, *Phys. Rev. Lett.* **34**, 369 (1975).
- ⁴⁵H. Takahasi and T. Nodera, in *Numerical Method for Engineering*, edited by E. Absi and R. Glowinski (Dunod, Paris, 1980), p. 209.
- ⁴⁶M. Engeli *et al.*, *Mitteilungen aus dem Institut für angewandte Mathematik* (Birkhäuser-Verlag, Berlin, 1959), Vol. 8, p. 79.